

# A cross-site comparison of ecosystem- and plot-scale methane fluxes across multiple timescales

5 Tiia Määttä<sup>1</sup>, Ankur R. Desai<sup>2</sup>, Masahito Ueyama<sup>3</sup>, Rodrigo Vargas<sup>4</sup>, Eric J. Ward<sup>5,6</sup>, Zhen Zhang<sup>7</sup>, Gil Bohrer<sup>8</sup>, Kyle Delwiche<sup>9</sup>, Etienne Fluets-Chouinard<sup>10</sup>, Järvi Järveoja<sup>11</sup>, Sara Knox<sup>12</sup>, Lulie Melling<sup>13</sup>, Mats B. Nilsson<sup>11</sup>, Matthias Peichl<sup>11</sup>, Angela Che Ing Tang<sup>14</sup>, Eeva-Stiina Tuittila<sup>15</sup>, Jinsong Wang<sup>16</sup>, Sheel Bansal<sup>17</sup>, Sarah Feron<sup>18</sup>, Manuel Helbig<sup>19</sup>, Aino Korrensalo<sup>20,21</sup>, Ken W. Krauss<sup>22</sup>, Gavin McNicol<sup>23</sup>, Shuli Niu<sup>16</sup>, Zutao Ouyang<sup>24</sup>, Kathleen Savage<sup>25</sup>, Oliver Sonnentag<sup>26</sup>, Robert Jackson<sup>27,28</sup>, and Avni Malhotra<sup>1,29</sup>

- 10 <sup>1</sup> Department of Geography, Faculty of Science, University of Zürich, Winterthurerstrasse 190, 8057 Zürich, Switzerland  
<sup>2</sup> Atmospheric and Oceanic Sciences, University of Wisconsin-Madison, Madison, WI, 53706, USA  
<sup>3</sup> Osaka Metropolitan University, Osaka, Japan  
<sup>4</sup> School of Life Sciences, Arizona State University, Tempe, AZ, 85287, USA  
<sup>5</sup> University of Maryland, Earth System Science Interdisciplinary Center, College Park MD, USA  
15 <sup>6</sup> NASA Goddard Space Flight Center, Biospheric Sciences Laboratory, Greenbelt MD, USA  
<sup>7</sup> National Tibetan Plateau Data Center (TPDC), State Key Laboratory of Tibetan Plateau Earth System, Environment and Resource (TPESER), Institute of Tibetan Plateau Research, Chinese Academy of Sciences, Beijing, 100101, China  
<sup>8</sup> Department of Civil, Environmental & Geodetic Engineering, The Ohio State University, Columbus, OH, 43210, USA  
<sup>9</sup> Department of Environmental Science, Policy & Management, UC Berkeley, Berkeley, California, USA  
20 <sup>10</sup> Earth System Sciences Division, Pacific Northwest National Laboratory, Richland, WA, USA  
<sup>11</sup> Department of Forest Ecology and Management, Swedish University of Agricultural Sciences, Umeå, Sweden  
<sup>12</sup> Department of Geography, McGill University, Montreal, Canada  
<sup>13</sup> UN Sustainable Development Solutions Network, Asia Headquarters, Sunway University, 47500 Bandar Sunway, Selangor, Malaysia  
25 <sup>14</sup> Department of Environmental Sciences, University of Toledo, Toledo, Ohio, USA  
<sup>15</sup> School of Forest Sciences, Joensuu campus, University of Eastern Finland, Joensuu, Finland  
<sup>16</sup> Key Laboratory of Ecosystem Network Observation and Modeling, Institute of Geographic Sciences and Natural Resources Research, Chinese Academy of Sciences, Beijing 100101, China  
<sup>17</sup> U.S. Geological Survey, Northern Prairie Wildlife Research Center, Jamestown, ND USA  
30 <sup>18</sup> University of Groningen, Leeuwarden, the Netherlands  
<sup>19</sup> GFZ Helmholtz Centre for Geosciences, Potsdam, Germany  
<sup>20</sup> Department of Environmental and Biological Sciences, University of Eastern Finland, Kuopio, Finland  
<sup>21</sup> Natural Resources Institute Finland, Joensuu, Finland  
<sup>22</sup> Louisiana Universities Marine Consortium (LUMCON), Chauvin, LA 70344, USA  
35 <sup>23</sup> Department of Earth and Environmental Sciences, University of Illinois Chicago, Chicago, IL, USA  
<sup>24</sup> College of Forestry, Wildlife and Environment, Auburn University, Auburn, AL, USA  
<sup>25</sup> Woodwell Climate Research Center, Falmouth, USA  
<sup>26</sup> Université de Montréal, Département de géographie, Montréal, QC, Canada  
<sup>27</sup> Department of Earth System Science, Stanford University, Stanford, 94305, USA  
40 <sup>28</sup> Woods Institute for the Environment and Precourt Institute for Energy, Stanford University, Stanford, 94305, USA  
<sup>29</sup> Biological Sciences Division, Pacific Northwest National Laboratory, 902 Battelle Boulevard, Richland, WA, USA

*Correspondence to:* Tiia Määttä ([tiia.maatta@geo.uzh.ch](mailto:tiia.maatta@geo.uzh.ch))

**Abstract.** Wetland and upland ecosystems play significant but opposing roles in the global methane (CH<sub>4</sub>) budget, acting as natural sources and sinks, respectively. Two of the most common approaches for measuring CH<sub>4</sub> fluxes (FCH<sub>4</sub>) are chambers,

45 which measure fluxes at fine spatial scales (ca. 1 m<sup>2</sup>), and eddy covariance (EC) towers, which integrate fluxes across larger  
footprints (ca. 100-10000 m<sup>2</sup>). Although chamber and EC observations have been combined in various syntheses and databases  
to estimate CH<sub>4</sub> budgets, a unified cross-site evaluation of FCH<sub>4</sub> estimates at plot and ecosystem scales is lacking. As a first  
step toward a systematic spatiotemporal scaling of EC tower and chamber footprints, we quantified differences in site-level  
50 aggregate FCH<sub>4</sub> between EC and chamber measurements ( $\Delta$ FCH<sub>4</sub>) across ten wetland and upland sites at half-hourly, hourly,  
daily, weekly, monthly, and annual timescales. We found that ecosystem-scale median FCH<sub>4</sub> was consistently higher than  
plot-scale FCH<sub>4</sub> at all temporal scales, with the smallest difference at the daily timescale (multi-site median  $\Delta$ FCH<sub>4</sub>: 1.36 nmol  
m<sup>-2</sup> s<sup>-1</sup>; median ecosystem-scale FCH<sub>4</sub> = 1.56 nmol m<sup>-2</sup> s<sup>-1</sup>, median plot-scale FCH<sub>4</sub> = 0.06 nmol m<sup>-2</sup> s<sup>-1</sup>) and the largest at  
annual scales (2.58 nmol m<sup>-2</sup> s<sup>-1</sup>; median ecosystem-scale FCH<sub>4</sub> = 25.91 nmol m<sup>-2</sup> s<sup>-1</sup>, median plot-scale FCH<sub>4</sub> = 6.55 nmol m<sup>-2</sup>  
s<sup>-1</sup>). In general, the agreement between ecosystem- and plot-scale FCH<sub>4</sub> decreased with finer temporal resolution (from  
55 Spearman  $\rho$  = 0.95 at the annual scale to  $\rho$  = 0.65 at the half-hourly scale), while  $\Delta$ FCH<sub>4</sub> variation was greatest at daily-to-  
annual scales. Key environmental predictors of  $\Delta$ FCH<sub>4</sub> across the ten sites included plot-scale spatial heterogeneity, dominant  
vegetation type, vapor pressure deficit, atmospheric pressure, and friction velocity at the daily and monthly scales. Wind  
direction was a significant predictor only at the monthly scale, suggesting EC footprint effects at these sites. These findings  
suggest that accounting for variability in EC footprint extent, chamber measurement placement, and measurement artifacts is  
60 key to reconciling multi-scale FCH<sub>4</sub> observations across diverse ecosystems and refining CH<sub>4</sub> budgets.

## 1 Introduction

Methane (CH<sub>4</sub>), a potent greenhouse gas, is produced in wetlands and consumed in upland soils- respectively the largest natural  
CH<sub>4</sub> sources and sinks globally. However, the magnitude of these fluxes remains highly uncertain (IPCC, 2023; Saunio et al.,  
2024). Field measurements of CH<sub>4</sub> fluxes (FCH<sub>4</sub>) are often conducted using enclosed chamber systems or eddy covariance  
65 (EC) towers (Bansal et al., 2023b). Chambers are typically deployed at point scale (< 1 m<sup>2</sup>) to capture plot-scale spatial  
heterogeneity in CH<sub>4</sub> source-sink dynamics within the study area (Livingston and Hutchinson, 1995; Morin et al., 2017;  
Virkkala et al., 2018). Chamber measurements can be manual or automated. Manual measurements are more labor-intensive  
and therefore result in a temporally sporadic sampling pattern (typically few per month). Automated chambers offer more  
consistent finer-scale temporal sampling (typically half-hourly over seasons) but high instrumentation cost can restrict their  
70 spatial coverage. Thus, chamber measurements generally involve a trade-off between temporal resolution and spatial  
representation of the ecosystem (Barba et al., 2018; McGuire et al., 2012; Morin et al., 2014, 2017).

In contrast, EC towers continuously measure FCH<sub>4</sub> with high temporal resolution (typically half-hourly) over seasons and  
years (Morin, 2019; Morin et al., 2017). The EC technique is based on the principle that the measured FCH<sub>4</sub> originating from  
75 the tower footprint area (100-10000 m<sup>2</sup>) is carried upwards and outward toward the sensor by turbulent diffusion (Aubinet et  
al., 2012; Morin et al., 2014). Therefore, a single half-hourly EC measurement represents a mixed observation at the ecosystem

scale located over a somewhat uncertain footprint area. The EC footprint changes from one observation to the other and may include a mixture of distinctly different ecosystem and hydrological patches, contributing to the EC FCH<sub>4</sub> uncertainties (Chu et al., 2021; Xu et al., 2018). At the ecosystem subtype scale (i.e., plot scale), chamber measurements represent fixed sampling  
80 points with well-defined spatial location but limited areal extent. Averaging multiple chamber observations from the same plot (defined as spatial replicates) increases the area representation of the chamber observation, but it is still several orders of magnitude smaller than EC measurements. While both approaches provide complementary perspectives on ecosystem FCH<sub>4</sub>, the data provided by each method pose different challenges for model parameterization or evaluation of relevant ecosystem FCH<sub>4</sub> processes across spatial and temporal scales.

85

Many global and regional FCH<sub>4</sub> models are parameterized using EC FCH<sub>4</sub> data because of its consistent temporal sampling and because the EC reporting standard include environmental covariates (e.g., McNicol et al., 2023; Oikawa et al., 2024; Peltola et al., 2019; Ueyama et al., 2023b). Community-contributed datasets, such as FLUXNET-CH<sub>4</sub> (Delwiche et al., 2021; Knox et al., 2019), offer unprecedented opportunity to access EC FCH<sub>4</sub> data from around the globe. However, even large  
90 collaborations such as FLUXNET-CH<sub>4</sub> only cover a relatively small number of locations globally and are missing important coverage in key ecosystems (e.g., tropics; Delwiche et al., 2021; Zhu et al., 2024). FCH<sub>4</sub> data from manual chamber campaigns are cheaper and simpler to deploy and are, therefore, implemented in a larger number of sites globally. Thus, sites with chambers provide a greater global measurement coverage than EC sites and could fill the missing data gaps. As a result, data from EC and chamber methods are sometimes compiled to augment syntheses and budget estimations (Hill and Vargas, 2022b;  
95 Kuhn et al., 2021; Yuan et al., 2024). Integration of plot-scale chamber FCH<sub>4</sub> data into ecosystem-scale EC datasets poses several challenges due to methodological differences (Hill and Vargas, 2022b). These challenges also apply to carbon dioxide (CO<sub>2</sub>) measurements: studies have noted significant discrepancy in CO<sub>2</sub> fluxes between EC and chambers, partly due to manual chambers (and sometimes EC) often lacking nighttime measurements (Barba et al., 2018; Phillips et al., 2017). Chamber and EC FCH<sub>4</sub> measurements also contain different uncertainties due to varying methods for measuring chamber gas concentration  
100 (e.g., gas chromatography vs high-precision CH<sub>4</sub> analyzers) and different EC and chamber instrument makes and models (Christiansen et al., 2015; Peltola et al., 2014; Pihlatie et al., 2013). To our knowledge, a systematic comparison of FCH<sub>4</sub> from these different scales across multiple sites, has not been conducted (but see Davidson et al. 2017).

Plot- and ecosystem-scale FCH<sub>4</sub> can differ due to different FCH<sub>4</sub> source areas, measurement artifacts, uncertainties of the  
105 chamber and EC methods, and differences in their response to environmental FCH<sub>4</sub> drivers. In many comparison studies conducted in wetland and upland ecosystems, chamber FCH<sub>4</sub> is higher than EC FCH<sub>4</sub> (Chaichana et al., 2018; Clement et al., 1995; Davidson et al., 2017; Krauss et al., 2016; Marushchak et al., 2016; Meijide et al., 2011; Morin et al., 2017; Riutta et al., 2007), although some studies report the opposite (Budishchev et al., 2014; Forbrich et al., 2011; Hill and Vargas, 2022b; Schrier-Uijl et al., 2010; Wang et al., 2013) and others find that the direction of the difference varies between years (Korrensalo  
110 et al., 2018). Since the attribution of surface cover type and location is better defined in chamber measurements, chamber

FCH<sub>4</sub> sampling can offer more representative estimates of FCH<sub>4</sub> variability within a site (Bansal et al., 2023a). However, chambers capture a small portion of the landscape, are often placed in high-emitting hotspots, do not sample over tall vegetation patches, and may incorporate sampling location biases (Bansal et al., 2023b). This can lead to higher observed fluxes at the sampled plots, than the mean ecosystem-scale FCH<sub>4</sub> as measured by EC (but see Voigt et al., 2023). For example, placing  
115 chambers over CH<sub>4</sub>-emitting hollows in a peatland could bias ecosystem FCH<sub>4</sub> estimates, as the lower FCH<sub>4</sub> in other peatland microtopographic forms and margins may not be captured (e.g., Bubier 1993; 1995; Juselius-Rajamäki et al., 2025; Waddington and Roulet, 2000).

The EC method integrates FCH<sub>4</sub> over the constantly moving and often spatially heterogeneous footprint, and the surface cover  
120 types within the footprint differ substantially in FCH<sub>4</sub>. For example, in wetlands, the EC footprint may include non-flooded areas where FCH<sub>4</sub> is expected to be near zero (Kutzbach et al., 2004; Riutta et al., 2007; Sha et al., 2011), which can also introduce significant bias to ecosystem FCH<sub>4</sub> estimates (Morin et al., 2017). Environmental variables that influence FCH<sub>4</sub> variability, such as soil temperature, water table level, and net ecosystem CO<sub>2</sub> exchange, could also predict cross-scale FCH<sub>4</sub> differences given the different processes influencing FCH<sub>4</sub> across spatial and temporal scales (Knox et al., 2021; Morin et al.,  
125 2014; Turetsky et al., 2014). EC observations are sensitive to environmental variables, such as wind speed and direction, that affect the extent and location of the observation footprint, while chamber measurements should likely be unaffected by these (Wang et al., 2013). While some studies have evaluated EC-chamber FCH<sub>4</sub> differences with spatially explicit FCH<sub>4</sub> upscaling or downscaling, many of these studies have been conducted in individual sites (e.g., Budishchev et al., 2014; Marushchak et al., 2016; Morin et al., 2017; Schrier-Uijl et al., 2010). Thus, an exploration of bulk-scale FCH<sub>4</sub> differences between ecosystem-  
130 and plot-scale FCH<sub>4</sub> (based on spatiotemporal aggregations) and their controls across multiple sites can help in directing future research efforts utilizing EC footprint modeling to reconcile cross-scale FCH<sub>4</sub> differences.

Here, we explore the differences between ecosystem and plot-scale FCH<sub>4</sub> ( $\Delta$ FCH<sub>4</sub>) measured by EC and chamber systems, respectively, and identify the time scales and environmental conditions at which the two data types agree best. We 1) compared  
135 co-located and contemporaneous EC and chamber FCH<sub>4</sub> rates across multiple sites and examined how the differences ranged across temporal scales (half-hourly to annual), and 2) investigated the potential predictors of  $\Delta$ FCH<sub>4</sub> at these sites. To achieve this, we utilized FCH<sub>4</sub> data commonly used by the FCH<sub>4</sub> community, i.e., gap-filled EC data and chamber data quality-controlled in different ways by data providers. We hypothesized that plot-scale FCH<sub>4</sub> would be higher than ecosystem-scale FCH<sub>4</sub> as chambers often selectively target FCH<sub>4</sub> hotspots and manual chamber measurements are often conducted at warmer  
140 daytime conditions. We also expected that  $\Delta$ FCH<sub>4</sub> is highest during daytime when most chamber measurements are conducted and plant activity is high, the latter of which is fully captured by towers but not always by manual chambers (Knox et al., 2021; Yu et al., 2013).

We hypothesized that larger variance (suggesting higher spatiotemporal heterogeneity) observed in chambers and EC  
145 measurements would increase  $\Delta FCH_4$ , and that the different temporal resolutions of manual and automated chambers would  
further contribute to  $\Delta FCH_4$ . Finally, we expected that the temporal scale of data aggregation could influence the magnitude  
of  $\Delta FCH_4$ , and we hypothesized that  $\Delta FCH_4$  would be lower at coarser (seasonal to annual) than at finer (hourly to daily)  
temporal aggregations. This comparison of bulk  $FCH_4$  rates is a key first step toward standardized harmonization of EC tower  
and chamber footprints to account for spatiotemporal heterogeneity across multiple sites.

## 150 **2 Methods**

### **2.1 Study sites**

We compiled ecosystem-scale (EC) and plot-scale (chamber)  $FCH_4$  data from ten sites, representing different climatic  
conditions and ecosystem types (two uplands and eight wetlands; Fig. 1, Table 1). Each site differed in the number of days  
with both chamber and EC measurements ( $n = 5-759$ ), the number of chambers used ( $n = 3-18$ ), the year of observations (range  
155 across sites: 2012-2020), and whether the chambers were automated or manual (Table C1 and Fig. B1). The site selection was  
based on the availability of coincident EC and chamber  $FCH_4$  data. EC data were obtained from the FLUXNET- $CH_4$  database  
(Delwiche et al., 2021; Knox et al., 2019) and chamber data were provided by site principal investigators in response to a call  
for data via the FLUXNET- $CH_4$  network. The sites are located in China, Finland, Sweden and the USA. Most sites have a  
humid continental ( $n = 3$ ) or subarctic climate ( $n = 3$ ), with others located in humid subtropical ( $n = 3$ ) and cold subtropical  
160 highland ( $n = 1$ ) regions (Table 1).

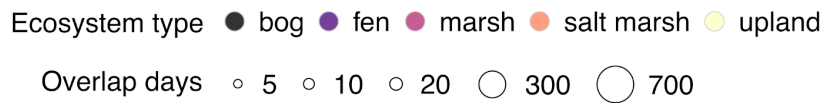
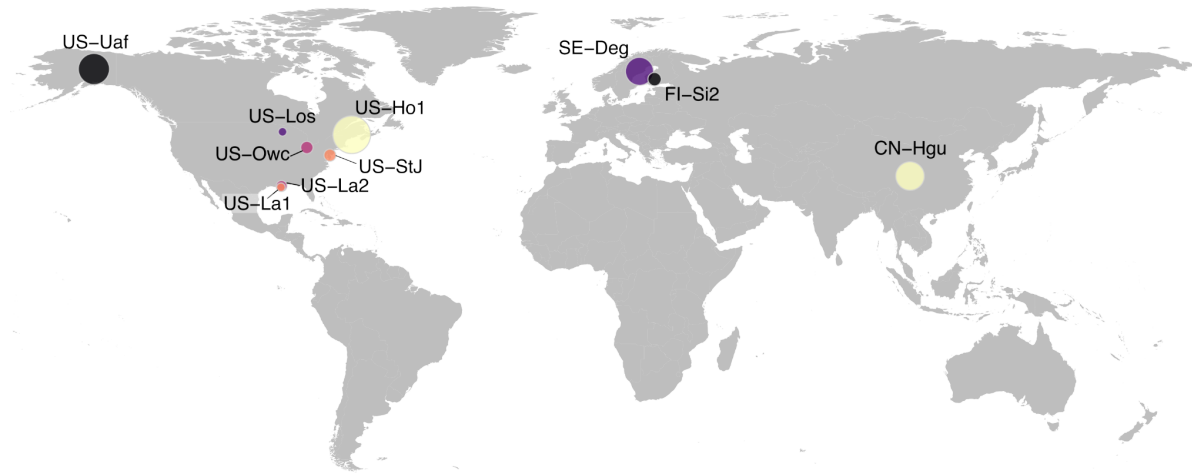


**Figure 1.** Map of study sites. Point colors indicate ecosystem type and point size reflects the number of overlap days between eddy covariance and chamber measurements (details in Table C1). Ecosystem type follows the site classification in the FLUXNET-CH<sub>4</sub> database (Delwiche et al., 2021; Knox et al., 2019). Base map: Natural Earth (1:50 m Cultural Vectors; 165 naturalearthdata.com), created with R package *maps* (Becker et al., 2023). Country abbreviations: CN = China, FI = Finland, SE = Sweden, US = The United States of America.

170

175

180 **Table 1.** Environmental characteristics of the study sites during the FCH<sub>4</sub> observation periods. Site classification, dominant  
vegetation, air temperature, precipitation, and water table level data were obtained from half-hourly FLUXNET-CH<sub>4</sub> and  
chamber datasets (Delwiche et al., 2021; Knox et al., 2019). Mean air temperature, total precipitation, and mean water table  
level were calculated over the EC-chamber overlap periods used in the analyses. Negative water table level indicates that water  
table level was below the soil surface. Köppen climate abbreviations: Cwc = cold subtropical highland, Dfc = subarctic, Dfb  
185 = warm-summer humid continental, Cfa = humid subtropical, Dwc = monsoon-influenced subarctic climate. Column  
abbreviations: TA = air temperature, P = total precipitation, WTL = water table level, Vegetation = site dominant vegetation  
type, Overlap days = number of days with both EC and chamber FCH<sub>4</sub> observations. In Overlap days, values marked with and  
without asterisk (\*) represent automated and manual chambers, respectively. Country abbreviations: CN = China, FI = Finland,  
SE = Sweden, US = The United States of America.

FLUXN ET-CH <sub>4</sub> ID	Site name	Climat		TA (° C)	P (m m)	WTL		Vegetatio n	Overla p days	Month covera ge	Chamber FCH <sub>4</sub> data ref.	EC FCH <sub>4</sub> data ref.
		e (Köppe n)	Site classificat ion			(min, max; cm)						
CN-Hgu	Hongyu an	Cwc	upland (alpine meadow)	2.6	386	-	Aerenchy matous	363*	Februar y- Novem ber	Wang et al. (2021)	Niu and Chen (2020)	
FI-Si2	Siikanev a-2 Bog	Dfc	bog	14. 6	14	-11.6 (-39, 15.2)	<i>Sphagnum</i> moss	26	May- October	Korrensalo et al. (2018)	Alekseyc hik et al. (2021); Vesala et al. (2020)	
SE-Deg	Degerö	Dfc	fen	4.7	394	-1.35 (- 10.2, 0.8)	<i>Sphagnum</i> moss	338*	May- October	Bond- Lamberty et al. (2020); Järveoja et al. (2018)	Nilsson and Peichl (2020)	

<b>US-Ho1</b>	Howland Forest	Dfb	upland (needleleaf forest)	6.9	838	-53.6 (-112, 8.19)	Tree	759*	April-November	Richardson et al. (2019)	Richardson and Hollinger (2020)
<b>US-La1</b>	Pointeaux-Chenes Brackish Marsh	Cfa	salt marsh	24.7	9	-0.99 (-13.3, 3.13)	Aerenchymatous	5	March-May, September-October	Krauss et al. (2016)	Holm et al. (2020a)
<b>US-La2</b>	Salvador WMA Freshwater Marsh	Cfa	marsh	26	15	1.33 (-8.79, 24.1)	Aerenchymatous	10	January, March-October	Krauss et al. (2016)	Holm et al. (2020b)
<b>US-Los</b>	Lost Creek	Dfb	fen	18.4	92	-11.2 (-16.1, -4.89)	Ericaceous shrub	5	June-August	Desai (2025b)	Desai (2025a); Desai and Thom (2020)
<b>US-Owc</b>	Old Woman Creek	Dfb	marsh	15.2	468	73.9 (35, 120)	Aerenchymatous	18	June-October	Bohrer et al. (2019)	Bohrer et al. (2020)
<b>US-StJ</b>	St Jones Reserve	Cfa	salt marsh	20	520	30.1 (-39, 102)	Aerenchymatous	16	May-December	Hill and Vargas (2022a)	Hill and Vargas (2022b); Vázquez-Lule and Vargas (2021)

---

	Universi										
	ty of										
US-Uaf	Alaska,	Dwc	bog	-	262	-12.5	<i>Sphagnum</i>	458*	May-	Ueyama et	Iwata et
	Fairban			0.2		37.8,	moss		October	al. (2022)	al.
	ks					12.9)					(2020)

---

## 190 2.2 Datasets and data compilation

### 2.2.1 Chamber and EC CH<sub>4</sub> flux data

The FCH<sub>4</sub> data were selected based on coincident plot- and ecosystem-scale FCH<sub>4</sub> observations. The plot-scale chamber FCH<sub>4</sub> data for each site were obtained from the site principal investigators. Each dataset included FCH<sub>4</sub> (varying units) and additional environmental variables, such as soil temperature and water table level. Chamber datasets comprised measurements from both manual (n = 6 sites; taken 1-3 times per month) and automated chamber methods (n = 4 sites; taken at half-hourly or hourly intervals, see Table C1; Subke et al., 2021). Chamber fluxes for all sites were calculated by the data providers using linear regression of change in CH<sub>4</sub> concentration over time. None of the chamber FCH<sub>4</sub> data were gap-filled, and in some cases (n = 4 sites), ebullition events had been filtered out by the data providers (Table C2). The decision to utilize chamber FCH<sub>4</sub> data with differing ebullition removal protocols across data providers was intended to reflect the way ebullition data are dropped in chamber studies. Typically, FCH<sub>4</sub> measurements are excluded from analyses when linear regressions between timepoints fall below a user-defined R<sup>2</sup> threshold (Jentsch et al., 2025). These data exclusions may contribute to differences between bulk ecosystem- and plot-scale FCH<sub>4</sub> estimates. We designated CH<sub>4</sub> emission with positive, and CH<sub>4</sub> uptake with negative signs.

The ecosystem-scale EC datasets for each site (except US-StJ, see below) were obtained from the FLUXNET-CH<sub>4</sub> database (Delwiche et al., 2021; Knox et al., 2019). These data include both gap-filled and non-gap-filled FCH<sub>4</sub> values (nmol m<sup>-2</sup> s<sup>-1</sup>) at a half-hourly resolution along with various meteorological and environmental variables. We used gap-filled EC FCH<sub>4</sub> in the analyses but excluded data during long data gaps (> 2 months) when the gap-filled values may be a significant source of uncertainty (Delwiche et al., 2021). Gap-filling was performed using artificial neural networks (ANN; Knox et al. 2019) which have shown good performance for FCH<sub>4</sub> data gap-filling (Irvin et al., 2021; Knox et al., 2016, 2019).

CN-Hgu EC FCH<sub>4</sub> data showed anomalous extreme CH<sub>4</sub> uptake and isolated extreme positive FCH<sub>4</sub> spikes. Therefore, we filtered out EC FCH<sub>4</sub> values where 1) CH<sub>4</sub> uptake exceeded -100 nmol m<sup>-2</sup> s<sup>-1</sup> (empirically determined threshold; Chen et al., 2019, 2020), 2) nighttime (incoming shortwave radiation < 10 W m<sup>-2</sup>; Morin et al., 2014) friction velocity (u\*) < 0.1 m s<sup>-1</sup> (Chen et al., 2019, 2020), and 3) single extreme positive FCH<sub>4</sub> spikes occurred beyond the monthly 99.5th FCH<sub>4</sub> percentile where nighttime air temperature was within 1 °C of its dew point (calculated with Magnus formula and Alduchov & Eskridge constants; Alduchov and Eskridge, 1996; Lawrence, 2005) and the open-path gas analyzer may have had condensation

215 (Heusinkveld et al., 2008). Additional extreme FCH<sub>4</sub> (FCH<sub>4</sub> = 862 nmol m<sup>-2</sup> s<sup>-1</sup>) associated with friction velocity = 0.93 m s<sup>-1</sup> and wind speed = 0.05 m s<sup>-1</sup> was removed as an outlier. After filtering, the CN-Hgu dataset was 70% of the original.

For US-StJ, we obtained EC FCH<sub>4</sub> data from the data providers (Hill and Vargas, 2022b; Vázquez-Lule and Vargas, 2021). As ANN-gap-filled EC FCH<sub>4</sub> values were not available at US-StJ, we used only non-gap-filled EC FCH<sub>4</sub>. EC FCH<sub>4</sub> were processed by the data providers following AmeriFlux protocols (Chu et al., 2023; Hill and Vargas, 2022b; Vázquez-Lule and  
220 Vargas, 2021).

### 2.2.2 Environmental data

For all sites (except US-StJ), environmental data were obtained from the FLUXNET-CH<sub>4</sub> EC data product, including ANN-gap-filled net ecosystem CO<sub>2</sub> exchange (NEE), friction velocity (u\*), wind direction (WD), gap-filled wind speed, gap-filled vapor pressure deficit (VPD), and gap-filled air pressure (PA) (Delwiche et al. 2021; Knox et al. 2019). Soil temperature (TS;  
225 topmost 2-10 cm depth) data was obtained from FLUXNET-CH<sub>4</sub> and site-specific chamber datasets when available. If a site had TS observations from both chamber and FLUXNET-CH<sub>4</sub> datasets, a mean of both was taken to obtain a site-level TS. Similarly, site-level water table level (WTL) was obtained by utilizing either FLUXNET-CH<sub>4</sub> or chamber-associated WTL measurements, or by taking their mean.

Environmental data for US-StJ were obtained from the data providers (Hill and Vargas, 2022b; Vázquez-Lule and Vargas,  
230 2021). PA, VPD, wind speed, WD, and u\* were not gap-filled, while TS and WTL were gap-filled based on their linear relationships with water temperature and water table level, respectively (Hill and Vargas, 2022b). NEE was gap-filled using marginal distribution sampling moving look-up tables (Hill and Vargas, 2022b).

See a summary of environmental data in Table C3.

### 2.3 Data processing and harmonization

235 The chamber datasets were harmonized to a similar structure, and FCH<sub>4</sub> units were standardized to nmol m<sup>-2</sup> s<sup>-1</sup>, matching the units used in the FLUXNET-CH<sub>4</sub> EC FCH<sub>4</sub> data. Then, EC and chamber datasets were combined using common timestamps (Fig. 2). To evaluate differences across temporal aggregations, we aggregated data at six temporal scales: 1. half-hourly (automated chamber data only; CN-Hgu, SE-Deg, US-Ho1, US-Uaf; n = 4 sites), 2. hourly (CN-Hgu, SE-Deg, US-Ho1, US-Uaf; n = 4 sites), 3. daily (all sites, n = 10 sites), 4. weekly (n = 10 sites), 5. monthly (n = 10 sites), and 6. annual (n = 10 sites)  
240 (Fig. 2). Note that most sites did not include snow-covered periods, and the datasets primarily represent the snow-free season.

The data were aggregated from the timestamp-aligned data by taking the median of FCH<sub>4</sub> measurements (non-normally distributed), mean of NEE (normally distributed) and wind *u* and *v* components (see 2.4.2), and median of the rest of the environment and meteorological variables (non-normally distributed). Half-hourly aggregation was created by taking the median of chamber measurements for each EC timestamp. To check for robustness of our results from the median-based

245 temporal aggregations, we also created temporal aggregations based on FCH<sub>4</sub> means. In addition, we calculated cumulative sums (mg CH<sub>4</sub> m<sup>-2</sup>) of chamber and EC FCH<sub>4</sub> at daily, weekly, monthly, and annual scales to see how EC-chamber differences scale up to ecosystem CH<sub>4</sub> budgets. As the chamber FCH<sub>4</sub> data from FI-Si2, US-La1, and US-La2 lacked hourly timestamps, we estimated daily cumulative FCH<sub>4</sub> for these sites by using the daily median or mean chamber FCH<sub>4</sub> and multiplied it by 48 while EC cumulative FCH<sub>4</sub> was calculated based on half-hourly EC FCH<sub>4</sub> from FLUXNET-CH<sub>4</sub>. As this is not an accurate  
250 estimate of daily cumulative chamber FCH<sub>4</sub> for EC-chamber FCH<sub>4</sub> comparisons, we included these sites only in site-specific analyses and excluded them from cross-site analyses.

The difference between ecosystem and plot-scale FCH<sub>4</sub> was calculated as the row-wise difference between instantaneous EC FCH<sub>4</sub> and chamber FCH<sub>4</sub> ( $\Delta$ FCH<sub>4</sub>) in each aggregated dataset by subtracting chamber FCH<sub>4</sub> from the corresponding EC FCH<sub>4</sub> on the same timestamp. For supplementary analyses, we calculated the difference between cumulative EC FCH<sub>4</sub> and chamber  
255 FCH<sub>4</sub> at daily, weekly, monthly, and annual scales.

## 2.4 Statistical analyses

### 2.4.1 Differences between ecosystem and plot-scale FCH<sub>4</sub> observations

We used non-parametric statistics to analyze the FCH<sub>4</sub> data (EC, chamber and  $\Delta$ FCH<sub>4</sub>), because the data were skewed and non-normal. To test the statistical significance ( $\alpha = 0.05$ ) of  $\Delta$ FCH<sub>4</sub> and to assess  $\Delta$ FCH<sub>4</sub> differences between chamber types  
260 at different temporal scales, we used Wilcoxon-Mann-Whitney tests (*wilcox.test* from *stats*; R Core Team 2024). Since the mean-based temporal aggregations were used as a sensitivity check, only descriptive statistics and Wilcoxon-Mann-Whitney tests were conducted for the mean-based aggregations (results in Table C4). Similarly, cumulative FCH<sub>4</sub> were analyzed with descriptive statistics and Wilcoxon-Mann-Whitney tests (results in Table C5). The rest of the methods described here were conducted on the median-based temporal aggregations of instantaneous FCH<sub>4</sub>.

265 To estimate the slopes of the EC FCH<sub>4</sub> - chamber FCH<sub>4</sub> relationship, we built simple linear mixed effects models with site as the random effect using function *lme* from package *nlme* (Pinheiro et al., 2000, 2023). For better interpretability of model slopes (in contrast to Yeo-Johnson-transformed values, see 2.4.2) and to meet the residual normality assumptions of linear mixed modeling, we transformed EC FCH<sub>4</sub> with inverse hyperbolic sine (Table C6). Due to non-convergence and residual non-normality, half-hourly and hourly scales were not assessed for EC-chamber FCH<sub>4</sub> slopes. As the data were non-normally  
270 distributed and did not meet the assumptions of linear regression, we used Spearman correlations together with normalized root mean square error (using the standard deviation of pooled EC and chamber FCH<sub>4</sub> as the denominator at each temporal scale) to assess the direction and strength of the relationship between EC FCH<sub>4</sub> and chamber FCH<sub>4</sub>, manual and automated chamber FCH<sub>4</sub>, as well as FCH<sub>4</sub> magnitude (row-wise mean of EC and chamber FCH<sub>4</sub>) and absolute  $\Delta$ FCH<sub>4</sub>.

We used Kruskal-Wallis tests (*kruskal.test* from *stats*; R Core Team 2024) to test for differences in  $\Delta$ FCH<sub>4</sub> across hours and  
275 months (treated as categorical variables) within each temporal aggregation (half-hourly, hourly, daily, weekly, monthly, and

annual). Then, we identified the significantly differing groups using the Conover-Iman post hoc test (function *conover.test* from package *conover.test*; Dinno, 2024).

#### 2.4.2 Predictors of FCH<sub>4</sub> differences between ecosystem and plot scales

We built linear mixed models to estimate the predictors of  $\Delta\text{FCH}_4$ . The aim was to explore how the predictors influence the direction of  $\Delta\text{FCH}_4$  (i.e., more positive or negative  $\Delta\text{FCH}_4$  or, in other words, increase ecosystem-scale FCH<sub>4</sub> in relation to plot-scale FCH<sub>4</sub> or vice versa) at the ten sites. To meet the assumptions of linear mixed modeling and to improve residual diagnostics (normality and homoscedasticity of residuals) for model inference, we applied Yeo-Johnson power transformation (Yeo and Johnson, 2000) to absolute  $\Delta\text{FCH}_4$  values using the function *yeojohnson* from *bestNormalize* (Peterson, 2021). This transformation can be applied to zero values, and it improved our residual diagnostics, which were important for model inference. Acknowledging the difficulty to interpret the precise effect sizes after this transformation, we used this model only to investigate the directionality of  $\Delta\text{FCH}_4$ . All models were built with the function *lme* from *nlme* (Pinheiro et al., 2000, 2023).

To evaluate potential predictors of  $\Delta\text{FCH}_4$ , we included environmental and temporal variables available in the FLUXNET-CH<sub>4</sub> and chamber datasets in the models. The predictor selection was based on literature. They included: TS (°C), WTL (cm), PA (kPa),  $u^*$  ( $\text{m s}^{-1}$ ), WD (degrees), VPD (hPa), NEE ( $\mu\text{mol CO}_2 \text{ m}^{-2} \text{ s}^{-1}$ ), month (categorical), site dominant vegetation (VEG; categorical; “tree”, “ericaceous shrub”, “aerenchymatous”, “brown moss”, and “*Sphagnum* moss”; taken from Delwiche et al., 2021), and hour (categorical; only with half-hourly and hourly datasets). We included EC-specific variables, such as  $u^*$  and WD, as proxies for EC footprint to assess how variables contributing to the EC footprint may affect  $\Delta\text{FCH}_4$ . While two of the VEG classes (tree and ericaceous shrub) were only represented in one site, preliminary linear regression model comparisons showed that VEG explained a large proportion of the  $\Delta\text{FCH}_4$  variance ( $R^2 = 0.4\text{-}0.7$ ), and its inclusion in linear mixed models substantially improved model fit. Therefore, we included VEG as a fixed effect, while acknowledging that for tree and ericaceous shrub classes, the estimated effect may be related to the site rather than vegetation.

For all models, the reference level in VEG was *Sphagnum* moss, 0 in Hour, and May in Month. As WD is a circular variable ( $0^\circ = 360^\circ$ ), we represented WD as a continuous function of wind direction and speed by separating WD into orthogonal  $u$  and  $v$  wind components ( $u\text{WD}$  and  $v\text{WD}$ , respectively), which were averaged from the half-hourly EC datasets in hourly, daily, weekly, monthly, and annual aggregations (Supplementary Methods A1). As a result,  $u\text{WD}$  represents the strength of west-east wind while  $v\text{WD}$  represents the strength of north-south wind. This representation avoided discontinuity at  $360^\circ/0^\circ$  and potential multicollinearity between model predictors.

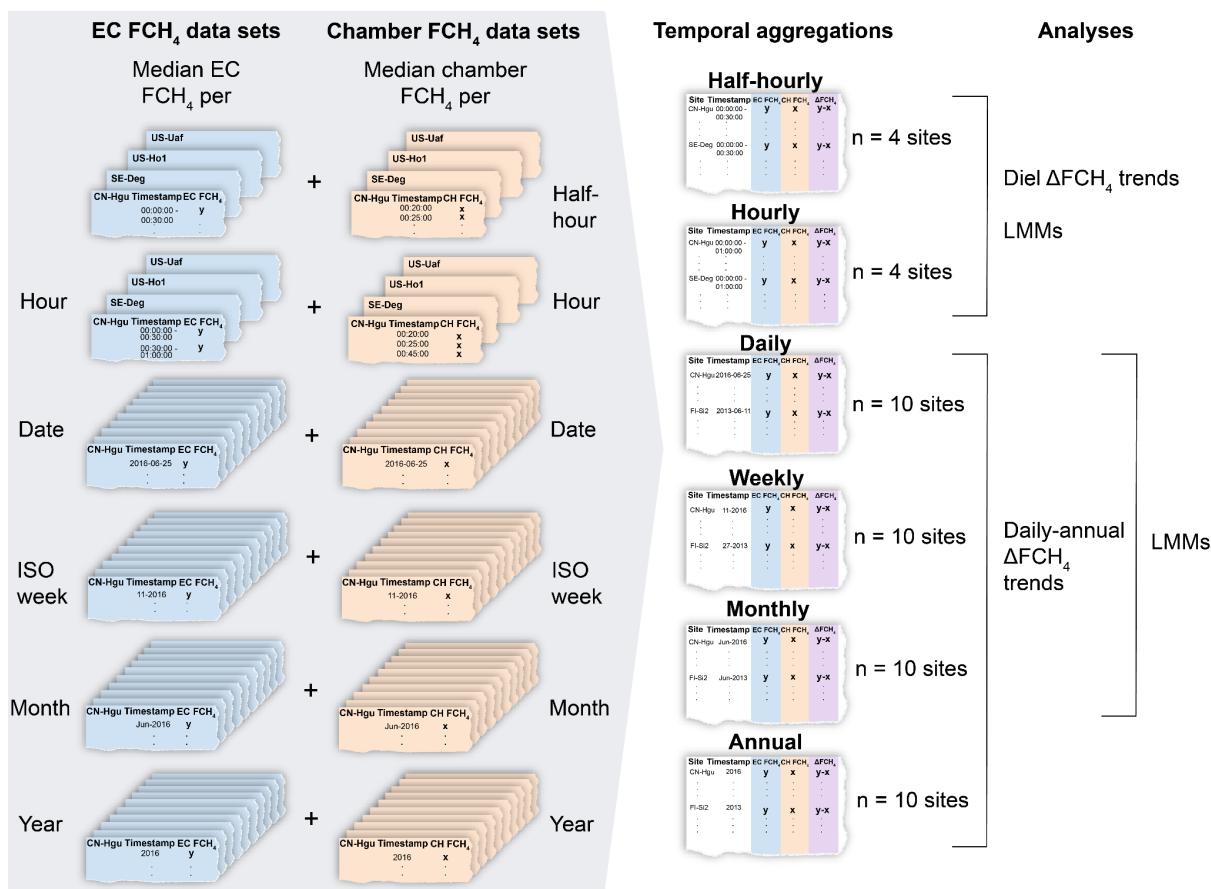
For improved model convergence and  $\beta$ -coefficient calculations, Yeo-Johnson-transformed absolute  $\Delta\text{FCH}_4$  and all predictors were centered and scaled, except hour, month and VEG, which were categorical variables and were included without centering and scaling. To account for multicollinearity, we chose predictors based on Pearson correlation matrices (threshold  $|r| < 0.7$ ) and checked variance inflation factors (VIF; threshold  $\leq 3$ ) using the function *vif* from *car* (Fox and Weisberg, 2018). Due to

multicollinearity ( $VIF > 3$ ), we built two separate half-hourly models containing either month or TS, two weekly models without NEE or VPD, and a monthly model without VPD and TS. WTL data was not available for CN-Hgu, and thus, this site was excluded from the models.

310 After accounting for temporal autocorrelation and residual variance (Supplementary Methods A2), we used backward variable selection based on likelihood ratio tests (AIC and  $p$ -values) together with type I ANOVA tests to determine significant predictors of Yeo-Johnson-transformed absolute  $\Delta FCH_4$ . During variable selection, the models were fitted with maximum likelihood, and the final models were refitted with restricted maximum likelihood for statistical inference. Model marginal and conditional  $R^2$  were calculated with the function *r.squaredGLMM* from package *MuMin* (Bartoń, 2024). To test how well the  
315 models generalize to other sites, we validated the models with leave-one-site-out cross validation and evaluated model performance with  $R^2$ , mean absolute error (MAE) and root mean square error (RMSE) between observed and predicted values. To allow for predictions to new sites with the training data, the fixed effect VEG had to be removed from the models, as some of the VEG classes (tree and ericaceous shrub) were represented only by a single site and the effect of these classes cannot be estimated when they are withheld in the test data. Similarly, due to uneven temporal coverage across sites, observations (e.g.,  
320 date or year-month) included in the test data but not present in the training data were excluded from evaluation.

We built linear mixed effects models to investigate the effect of spatiotemporal  $FCH_4$  variation on  $\Delta FCH_4$ . To represent the  $FCH_4$  variation between individual chambers within each site, we calculated the interquartile range (IQR) of chamber  $FCH_4$  from an unaggregated dataset per each site and temporal scale unit (i.e., per day, week, month, or year). To see whether temporal variation within each temporal scale unit in EC  $FCH_4$  may affect absolute  $\Delta FCH_4$ , we also calculated EC  $FCH_4$  IQR  
325 per each site and temporal scale unit. In the models, log-transformed absolute  $\Delta FCH_4$  was the response variable, and either log (+0.01)-transformed chamber IQR or log (+0.01)-transformed EC IQR was the explanatory variable, or both were included as explanatory variables to assess their relative effects on absolute  $\Delta FCH_4$ .

All data processing and statistical analyses were carried out using R v4.3.3 (R Core Team, 2024).



330

335

340

**Figure 2.** Overview of the main data aggregation workflow. Site-specific eddy covariance (EC) methane (CH<sub>4</sub>) flux (FCH<sub>4</sub>; blue) and chamber FCH<sub>4</sub> (orange) datasets were combined by taking the median FCH<sub>4</sub> per timestamp (half-hour to annual scale). ISO week is the week number according to the ISO-8601 standard. Then, site-level datasets were combined into multi-site datasets at six temporal scales: half-hourly, hourly, daily, weekly, monthly, and annual. Half-hourly EC FCH<sub>4</sub> data was not aggregated as it was already in half-hourly scale. ΔFCH<sub>4</sub> (purple) was calculated by subtracting median chamber instantaneous FCH<sub>4</sub> from median EC instantaneous FCH<sub>4</sub> per timestamp per site, and this measure was used in all analyses and linear mixed effects models (LMMs). Note that we also created temporal aggregations by taking the mean of EC and chamber FCH<sub>4</sub>, and these data sets were used as a sensitivity check with descriptive statistics and pairwise comparisons.

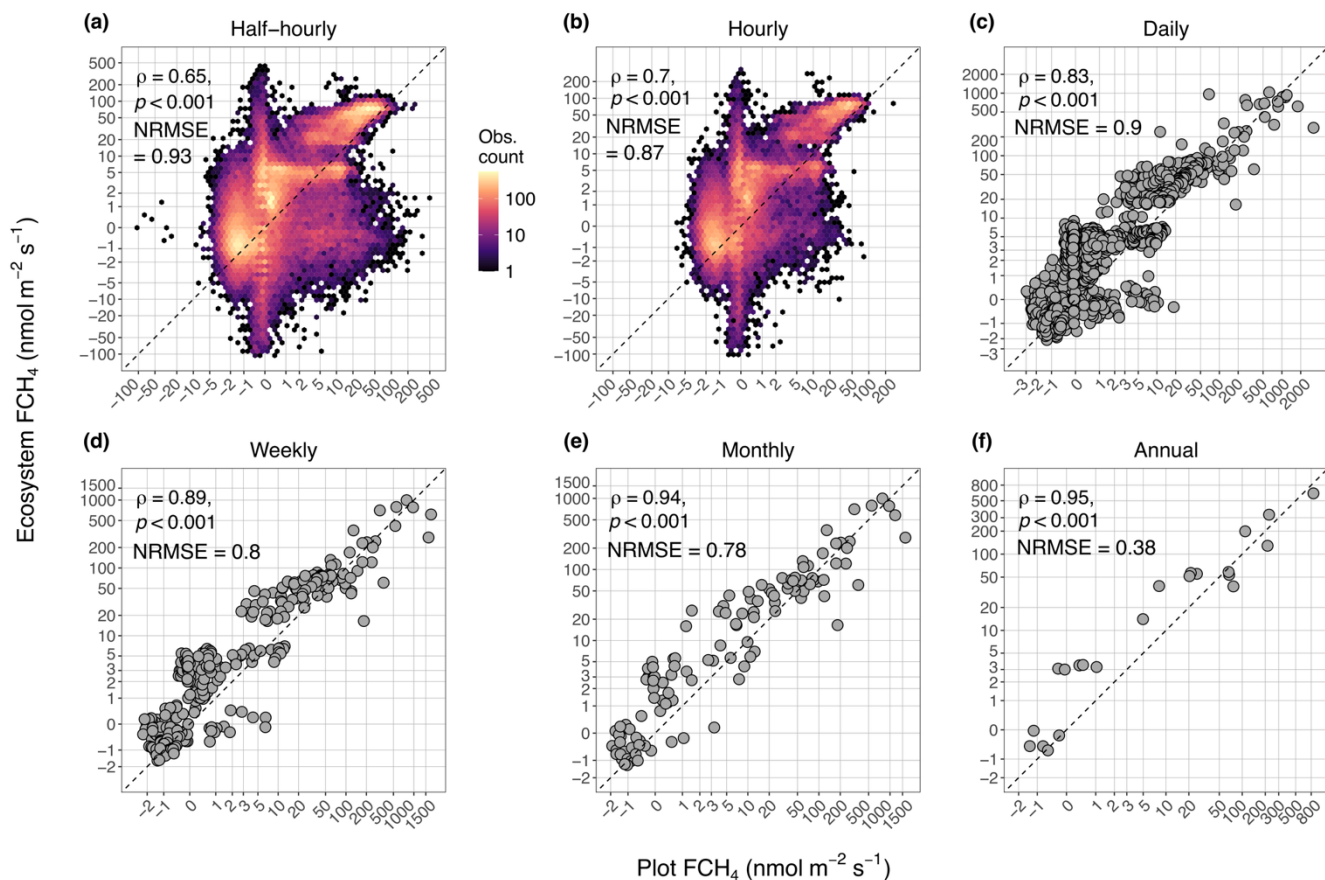
### 3 Results

#### 3.1 Ecosystem and plot-scale FCH<sub>4</sub> differ most at finer temporal scales

Ecosystem- (EC) and plot-scale (chamber) FCH<sub>4</sub> differed significantly at half-hourly to weekly scales (Table 2). Median ecosystem FCH<sub>4</sub> was higher than plot-scale FCH<sub>4</sub> at all temporal aggregations (half-hourly to annual: 102%, 109%, 104%, 345 90%, 58%, and 87% higher, respectively). However, the coefficient of variation (CV, %) for  $\Delta$ FCH<sub>4</sub> was large, particularly in daily (674%) and weekly (467%) aggregations (Table 2). Across temporal aggregations and site-years, CH<sub>4</sub> emissions (FCH<sub>4</sub> > 0) above the 90<sup>th</sup> percentile contributed a larger share of total (sum) plot-scale FCH<sub>4</sub> than ecosystem-scale FCH<sub>4</sub> (mean-based aggregations; Table 2, Fig. B2), possibly indicating more CH<sub>4</sub> emission hot spots and hot moments at the plot scale. Our observed trend persisted when we aggregated chamber and EC FCH<sub>4</sub> data with means instead of medians (Table C4 and C5). 350 In the mean-based aggregations, median  $\Delta$ FCH<sub>4</sub> ranged between 0.28 nmol m<sup>-2</sup> s<sup>-1</sup> (annual) and 1.23 nmol m<sup>-2</sup> s<sup>-1</sup> (half-hourly) but mean  $\Delta$ FCH<sub>4</sub> turned increasingly negative from daily (-1.16 nmol m<sup>-2</sup> s<sup>-1</sup>) to annual (-70.94 nmol m<sup>-2</sup> s<sup>-1</sup>) scales, highlighting plot-scale CH<sub>4</sub> emission hotspots and hot moments as possible  $\Delta$ FCH<sub>4</sub> drivers. Ecosystem- and plot-scale FCH<sub>4</sub> were positively correlated across temporal aggregations, with annual aggregation having the best agreement, while the worst agreements were in half-hourly and hourly aggregations (Fig. 3). Using linear mixed models, we showed that an increase of 1 nmol m<sup>-2</sup> s<sup>-1</sup> in 355 plot-scale FCH<sub>4</sub> was associated with an ecosystem-scale FCH<sub>4</sub> increase of 0.007 nmol m<sup>-2</sup> s<sup>-1</sup> ( $p = 0.03$ ) at daily plot-scale FCH<sub>4</sub> median (0.06 nmol m<sup>-2</sup> s<sup>-1</sup>), 0.01 nmol m<sup>-2</sup> s<sup>-1</sup> ( $p = 0.066$ ) at weekly plot-scale FCH<sub>4</sub> median (0.51 nmol m<sup>-2</sup> s<sup>-1</sup>), 0.009 nmol m<sup>-2</sup> s<sup>-1</sup> ( $p = 0.183$ ) at monthly plot-scale FCH<sub>4</sub> median (4.07 nmol m<sup>-2</sup> s<sup>-1</sup>), and 0.019 ( $p = 0.044$ ) at annual plot-scale FCH<sub>4</sub> median (6.55 nmol m<sup>-2</sup> s<sup>-1</sup>; see Table C6 for details).

360 **Table 1.** Ecosystem- (eddy covariance; EC) and plot-scale (chamber) methane (CH<sub>4</sub>) flux (FCH<sub>4</sub>) difference ( $\Delta$ FCH<sub>4</sub>) at different temporal aggregations. A positive  $\Delta$ FCH<sub>4</sub> indicates a higher ecosystem- than plot-scale FCH<sub>4</sub> and vice versa. The EC and chamber data sample sizes in Wilcoxon-Mann-Whitney tests are reported as  $n_{EC}$  and  $n_{CH}$ , respectively. The 90th percentiles (p90, without parentheses) and proportion (% , in parentheses) of chamber and EC CH<sub>4</sub> emission observations (where FCH<sub>4</sub> > p90 and FCH<sub>4</sub> > 0) of the total chamber or EC FCH<sub>4</sub> sum show the contribution of high CH<sub>4</sub> emissions to total CH<sub>4</sub> emissions 365 (see site-specific trends in the unaggregated dataset in Fig. B2). Abbreviations: IQR = interquartile range, SD = standard deviation, CV = coefficient of variation.

Aggregation				Chamber	EC	Chamber	EC			Wilcoxon-Mann-Whitney test
	$\Delta\text{FCH}_4$ median (IQR), $\text{nmol m}^{-2} \text{s}^{-1}$	$\Delta\text{FCH}_4$ mean (SD), $\text{nmol m}^{-2} \text{s}^{-1}$	$\Delta\text{FCH}_4$ CV (%)	$\text{FCH}_4$ median (IQR), $\text{nmol m}^{-2} \text{s}^{-1}$	$\text{FCH}_4$ median (IQR), $\text{nmol m}^{-2} \text{s}^{-1}$	$\text{FCH}_4$ mean (SD), $\text{nmol m}^{-2} \text{s}^{-1}$	$\text{FCH}_4$ mean (SD), $\text{nmol m}^{-2} \text{s}^{-1}$	Chamber $\text{FCH}_4$ p90, $\text{nmol m}^2 \text{s}^{-1}$ (% of total $\text{FCH}_4$ )	EC $\text{FCH}_4$ p90, $\text{nmol m}^2 \text{s}^{-1}$ (% of total $\text{FCH}_4$ )	
Half-hourly	1.4 (5.67)	5.61 (17.71)	196	0.27 (5.79)	1.55 (6.97)	5.88 (14.07)	11.49 (24.25)	33.44 (46)	64.31 (44)	$p < 0.001$ ( $n_{\text{EC}} = 74482$ , $n_{\text{CH}} = 74482$ )
Hourly	1.41 (5.28)	6.08 (15.34)	191	0.15 (4.07)	1.39 (6.68)	4.98 (12.36)	11.05 (23.59)	45.76 (47)	63.92 (44)	$p < 0.001$ ( $n_{\text{EC}} = 40072$ , $n_{\text{CH}} = 40072$ )
Daily	1.36 (4.27)	4.01 (81.49)	674	0.06 (4.79)	1.53 (6.27)	13.98 (106.34)	18.0 (69.09)	43.18 (75)	68.5 (60)	$p < 0.001$ ( $n_{\text{EC}} = 1879$ , $n_{\text{CH}} = 1879$ )
Weekly	1.44 (5.29)	-0.62 (105.8)	467	0.51 (11.9)	3.0 (31.19)	34.28 (155.8)	33.66 (103.49)	112.64 (76)	78.08 (63)	$p < 0.001$ ( $n_{\text{EC}} = 349$ , $n_{\text{CH}} = 349$ )
Monthly	1.46 (14.82)	-8.14 (151.18)	350	4.07 (46.41)	5.88 (60.3)	75.55 (223.01)	67.42 (161.75)	247.77 (69)	219.98 (64)	$p = 0.082$ ( $n_{\text{EC}} = 121$ , $n_{\text{CH}} = 121$ )
Annual	2.58 (24.59)	-1.37 (63.6)	194	6.55 (67.22)	25.91 (53.29)	76.84 (185.83)	75.47 (145.95)	220.35 (64)	250.78 (57)	$p = 0.507$ ( $n_{\text{EC}} = 22$ , $n_{\text{CH}} = 22$ )



370 **Figure 3.** Results of correlation test (Spearman rank correlation coefficient,  $\rho$ , its significance level,  $p$ , and the normalized root mean square error, NRMSE) between plot-scale (chamber) methane (CH<sub>4</sub>) flux (FCH<sub>4</sub>) and ecosystem-scale (eddy covariance; EC) FCH<sub>4</sub> at half hourly (a), hourly (b), daily (c), weekly (d), monthly (e), and annual scales (f). For visualization, the plot axes (a-f) were transformed with inverse hyperbolic sine to spread out points in the low FCH<sub>4</sub> range and retain negative values (see untransformed plots in Fig. B3). Spearman  $\rho$  was calculated with untransformed data. NRMSE was calculated by dividing

375 RMSE by the standard deviation of untransformed ecosystem- and plot-scale FCH<sub>4</sub> at each temporal aggregation. In a) and b) the points for half-hourly ( $n = 74482$ ) and hourly ( $n = 40072$ ) aggregations are shown in hexagonal density clouds with log<sub>10</sub>-transformed color range to highlight trends in high point density areas (colors represent number of observations per hexagon). Agreement between chamber and EC FCH<sub>4</sub> improves from finer to coarser temporal aggregations (a-f), as indicated by  $\rho$ . The high observation densities in a) and b) reveal site-specific trends in the discrepancy between ecosystem and plot scales (e.g.,

380 at  $x = 0$  and  $y = 5$ ). For daily (c), weekly (d), monthly (e), and annual (f) aggregations, sample sizes were  $n = 1879, 349, 121,$  and  $22,$  respectively. The dashed line represents 1:1 line.

Ecosystem- and plot-scale FCH<sub>4</sub> differed between hours, months, and sites. In support of our hypotheses, the highest  $\Delta$ FCH<sub>4</sub> occurred between 5 AM and 3 PM ( $p < 0.001$ ; Fig. B4-B7), with maximum median  $\Delta$ FCH<sub>4</sub> at 9 AM (2.01 nmol m<sup>-2</sup> s<sup>-1</sup>, IQR:

6.16; half-hourly scale) and minimum at 8 PM (0.9 nmol m<sup>-2</sup> s<sup>-1</sup>, IQR: 4.16; half-hourly scale). However, the diel  $\Delta\text{FCH}_4$  trends  
385 varied between sites and months ( $p < 0.001$ ; Fig. B8-B12). The highest absolute  $\Delta\text{FCH}_4$  (with observations from all sites) was  
in August, September, and October (half-hourly to daily  $p < 0.001$ ; Fig. B13). In addition,  $\Delta\text{FCH}_4$  varied in both magnitude  
and direction within and between sites (Kruskal-Wallis  $p < 0.001$ ; half-hourly to monthly scale), with most medians being  
positive (Tables C6-C11 and B14-B15). The difference between cumulative sums of ecosystem- and plot-scale  $\text{FCH}_4$  increased  
390 from daily to annual scales but the seasonal and inter-annual trends varied between sites (Table B4, Fig. B16). The largest  
absolute  $\Delta\text{FCH}_4$  medians and CVs were consistently found in US-Owc (median: -108.22 nmol m<sup>-2</sup> s<sup>-1</sup>, CV: 169%; daily scale),  
while the lowest absolute  $\Delta\text{FCH}_4$  and  $\text{FCH}_4$  were consistently found in US-Ho1 (median  $\Delta\text{FCH}_4 < 1$  nmol m<sup>-2</sup> s<sup>-1</sup>; Tables C6-  
C11).

Flux magnitude, measured as the mean between EC and chamber  $\text{FCH}_4$  ( $\text{FCH}_{4\_mean}$ ), was generally positively related to  $\Delta\text{FCH}_4$   
395 but negative relationships existed when  $\text{FCH}_{4\_mean} < 0$  (i.e., net uptake). The positive  $\text{FCH}_4$  magnitude and absolute  $\Delta\text{FCH}_4$   
relationship became stronger at coarser temporal resolutions (Spearman  $p < 0.001$ ; Fig. 4). In all aggregations, the higher  
 $\Delta\text{FCH}_4$  came from a higher ecosystem-scale  $\text{FCH}_4$  than from a higher plot-scale  $\text{FCH}_4$  ( $\geq 70\%$  of all observations when  
 $\text{FCH}_{4\_mean} > 0$ ; result not shown). In half-hourly and hourly aggregations,  $\Delta\text{FCH}_4$  and  $\text{FCH}_{4\_mean}$  were negatively or positively  
related when  $\text{FCH}_{4\_mean}$  suggested net uptake or emission, respectively (Fig. 4a and b). When  $\text{FCH}_{4\_mean} < 0$ , ecosystem-scale  
400  $\text{FCH}_4$  was generally higher than plot-scale  $\text{FCH}_4$  (57% and 58% of all observations when  $\text{FCH}_{4\_mean} < 0$  in half-hourly and  
hourly aggregations, respectively; result not shown). However, most of the highest observations originate from CN-Hgu. Sites  
also differed in whether the trends in negative  $\text{FCH}_4$  came from higher plot or ecosystem-scale  $\text{FCH}_4$ : for example, at US-Uaf  
and CN-Hgu, 100% and 91% of  $\Delta\text{FCH}_4$  observations at  $\text{FCH}_{4\_mean} < 0$ , respectively, consisted of higher plot-scale  $\text{FCH}_4$  while  
ca. 66% of hourly and half-hourly observations ( $\text{FCH}_{4\_mean} < 0$ ) in US-Ho1 came from higher ecosystem-scale  $\text{FCH}_4$ .

405

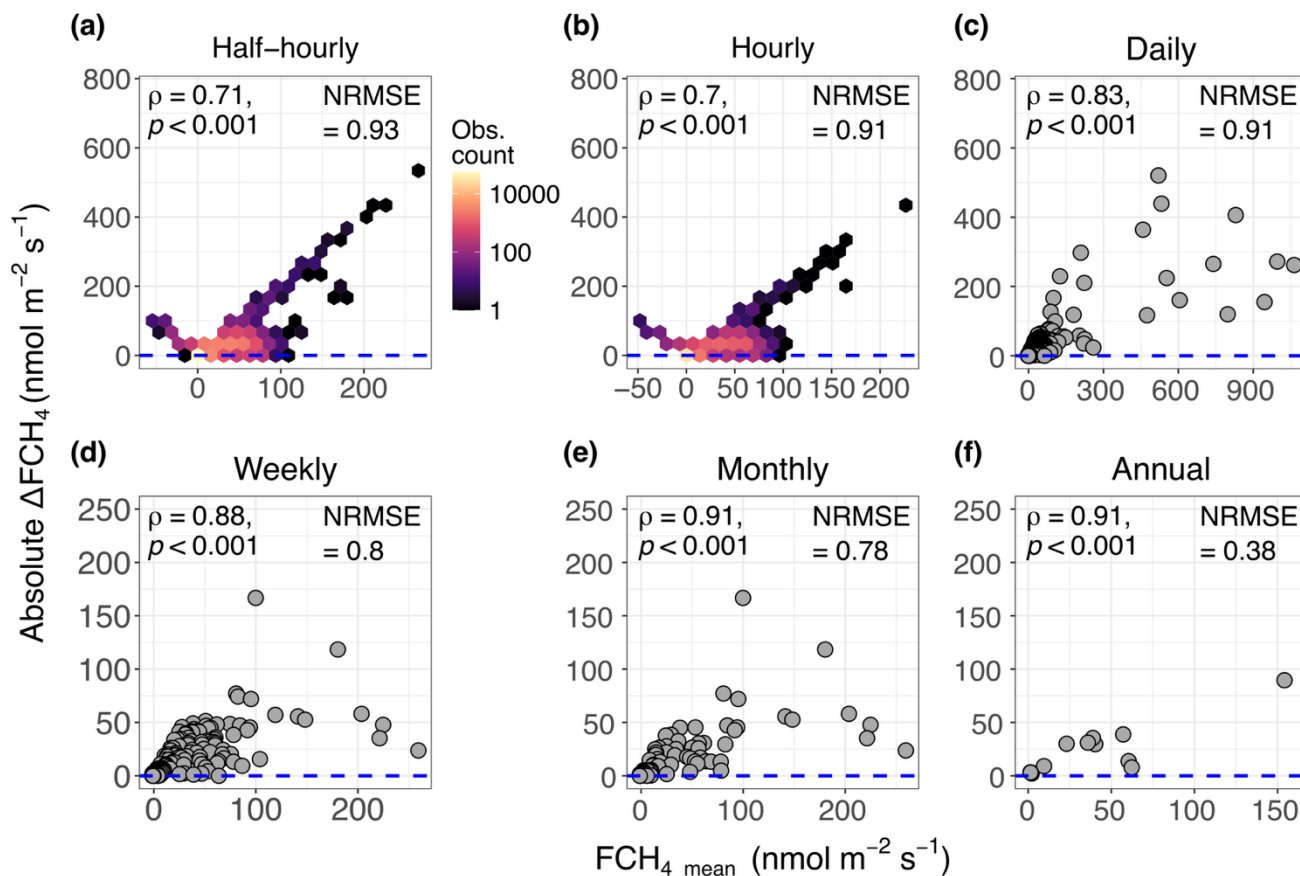


**Figure 4.** The relationship between methane ( $\text{CH}_4$ ) flux ( $\text{FCH}_4$ ) magnitude ( $\text{FCH}_{4\_mean}$ ) and absolute difference between ecosystem-scale (eddy covariance; EC) and plot-scale  $\text{FCH}_4$  ( $\Delta\text{FCH}_4$ ) from half-hourly (a) to annual (f) scales, represented by Spearman correlation coefficient, ( $\rho$ ), its significance, ( $p$ ), and normalized root mean square error of  $\Delta\text{FCH}_4$  (NRMSE).  $\text{FCH}_{4\_mean}$  is the row-wise mean of EC  $\text{FCH}_4$  and chamber  $\text{FCH}_4$ . In a) and b) half-hourly and hourly points are shown in hexagonal density clouds with a log-transformed color range to highlight trends in high point density areas (colors represent number of observations per hexagon). Plots c-f show daily, weekly, monthly and annual aggregations, respectively. The blue dashed line represents  $\Delta\text{FCH}_4 = 0$  meaning complete agreement between ecosystem and plot-scale  $\text{FCH}_4$ . Higher Spearman correlation coefficient ( $\alpha = 0.05$ ) represents stronger deviation from  $\Delta\text{FCH}_4 = 0$ . NRMSE was calculated by dividing RMSE (of  $\Delta\text{FCH}_4$ ) by the standard deviation of ecosystem- and plot-scale  $\text{FCH}_4$  at each temporal aggregation. For visualization, outliers were removed from daily ( $n = 3$ ), weekly ( $n = 10$ ), monthly ( $n = 8$ ) and annual ( $n = 1$ ) plots but the Spearman correlations and NRMSE are based on original data. See plots with outliers in Fig. B17 and a figure showing how high  $\text{CH}_4$  emissions from ecosystem and plot scales contribute to annual  $\text{CH}_4$  emissions per site in Fig. B2.

### 3.2 Predictors of ecosystem and plot-scale FCH<sub>4</sub> differences

#### 420 3.2.1 Atmospheric pressure, friction velocity and wind direction drive daily-to-monthly FCH<sub>4</sub> differences between ecosystem and plot scales

The significance and effect size of  $\Delta$ FCH<sub>4</sub> predictors varied across temporal aggregations, with site dominant vegetation type having the highest effect sizes at the daily-to-monthly scale (Table 3). Dominance of aerenchymatous vegetation had relatively high effect sizes ( $|\beta$ -coefficient| > 0.68). However, only one site was classified as tree-dominated (US-Ho1) and ericaceous shrub-dominated (US-Los), while three were aerenchymatous and two were *Sphagnum*-moss dominated. Thus, we were unable to separate true vegetation-related effects from site effects.

PA and  $u^*$  were significant  $\Delta$ FCH<sub>4</sub> predictors at the daily and monthly scales (but weekly PA  $p = 0.057$ ), while VPD was significant only at the daily scale. However, the effect sizes were relatively low ( $\beta$ -coefficient  $\leq 0.25$ ; Table 3). Wind direction (uWD) was a significant  $\Delta$ FCH<sub>4</sub> predictor only in the monthly scale. Month was a significant predictor only in the final half-hourly-daily models, where August and July had the highest effect sizes ( $\beta$ -coefficient > 0.41). Morning hours, particularly 5 AM, were most important in the half-hourly models (5 AM  $\beta$ -coefficient > 0.08). However, the fixed effects in the final half-hourly and hourly models explained a very small proportion of the total variation (marginal  $R^2 < 0.05$ , Tables S12-S13). In addition, the high conditional  $R^2$  and high negative LOOCV  $R^2$ , high MAE and RMSE showed that the  $\Delta$ FCH<sub>4</sub> predictors are specific to the sites included in this study (Table 3).

435 **Table 2.** Linear mixed effects model results identifying environmental predictors of ecosystem- and plot-scale methane (CH<sub>4</sub>) flux (FCH<sub>4</sub>) difference ( $\Delta$ FCH<sub>4</sub>) at different temporal scales. Fixed effects are listed in decreasing order based on their  $\beta$ -coefficients. Significant predictors are highlighted in bold. Half-hourly and hourly models had very low marginal  $R^2$  (<0.05) and were excluded from this table. See half-hourly and hourly models in Table C14 and full models in Table C15. Abbreviations: SE = standard error, Df = degrees of freedom, LOOCV = leave-one-out cross validation, MAE = mean absolute error, RMSE = root mean square error, VEG = site dominant vegetation, PA = air pressure (kPa),  $u^*$  = friction velocity ( $m s^{-1}$ ), WTL = water table level (cm), TS = soil temperature ( $^{\circ}C$ ), NEE = net ecosystem CO<sub>2</sub> exchange ( $\mu mol CO_2 m^{-2} s^{-1}$ ), VPD = vapor pressure deficit (hPa), vWD =  $v$  wind component ( $m s^{-1}$ ), uWD =  $u$  wind component ( $m s^{-1}$ ).

Dataset	Predictors	$\beta$ -coefficient	SE	$p$ -value (t-test)	Marginal $R^2$	Conditional $R^2$	Df	LOOCV		
								Random effect variation explained, %	$R^2$	MAE
Daily (n=9 sites)	Intercept	0.4867	0.361	0.1779	0.5346	0.9265	1363	-1.65	1.48	1.76
	<b>Fixed effects</b>									
	VEG									
	- Tree	-1.4718	0.6767	0.0816			5			
	- Aerenchymatous	1.0111	0.4723	0.0852			5			
	Month									

- Jul	0.4939	0.1685	<b>0.0043</b>	87
- Aug	0.4577	0.1696	<b>0.0084</b>	87
VEG				
-Ericaceous shrub	0.4333	0.7104	0.5686	5
Month				
- Sep	0.2851	0.1656	0.0886	87
- Apr	0.234	0.3683	0.5269	87
- Dec	0.2281	0.5059	0.6533	87
- Oct	0.1884	0.1689	0.2677	87
- Jun	0.1595	0.1658	0.3389	87
- Nov	0.1118	0.2356	0.6363	87
- Mar	-0.0735	0.5003	0.8835	87
TS	-0.0525	0.0269	0.051	1371
<b>VPD</b>	-0.0457	0.0109	<b>0</b>	1371
<b>u*</b>	0.0342	0.0076	<b>0</b>	1371
<b>PA</b>	-0.0259	0.0072	<b>0</b>	1371
uWD	0.0052	0.0066	0.4305	1371
vWD	0.0043	0.007	0.5423	1371
NEE	0.0017	0.0104	0.8679	1371
WTL	0.0012	0.0376	0.9745	1371

### Random effects

Site	59.59
Year-month	24.62

<b>Weekly</b>	Intercept	0.5066	0.3402	0.1381	0.5554	0.8351	178	-0.82	1.25	1.46
---------------	-----------	--------	--------	--------	--------	--------	-----	-------	------	------

### Fixed effects

(n=9 sites)

VEG										
- Tree	-1.3455	0.6772	0.1036	3						
- Aerenchymatous	0.8552	0.4642	0.1248	3						
-Ericaceous shrub	0.5256	0.6837	0.4767	3						
PA	-0.0716	0.0374	0.0572	178						

### Random effects

Site	62.91
Year-month	1.03e <sup>-05</sup>

<b>Monthly</b>	Intercept	-0.2243	0.3145	0.4778	0.6599	0.8788	80	-0.57	1.04	1.25
----------------	-----------	---------	--------	--------	--------	--------	----	-------	------	------

### Fixed effects

(n=9 sites)

Month										
- Mar	1.4967	1.4236	0.2962	80						
VEG										
-Aerenchymatous	1.2901	0.4307	<b>0.0303</b>	5						
-Ericaceous shrub	0.7673	0.6684	0.3029	5						

Month				
- Apr	0.6774	0.2947	<b>0.0241</b>	80
VEG				
- Tree	-0.5482	0.5955	0.3995	5
PA	-0.2535	0.1046	<b>0.0177</b>	80
uWD	0.2322	0.0666	<b>0.0008</b>	80
u*	-0.1875	0.0774	<b>0.0176</b>	80
Month				
- Oct	-0.1805	0.1432	0.2111	80
WTL	0.1375	0.0809	0.0931	80
Month				
- Dec	0.1258	0.3948	0.7509	80
NEE	0.1069	0.0664	0.1114	80
Month				
- Sep	0.0963	0.1475	0.5158	80
vWD	0.0686	0.0501	0.1747	80
Month				
- Jul	0.0608	0.1465	0.6789	80
- Jun	0.0461	0.1408	0.7442	80
- Nov	-0.0404	0.2062	0.8453	80
- Aug	0.021	0.1456	0.8857	80

### **Random effects**

Site

64.35

### **3.2.2 Spatial FCH<sub>4</sub> variation increases ecosystem and plot-scale FCH<sub>4</sub> difference**

445 Spatial variation between FCH<sub>4</sub> measurements by individual chambers increased absolute  $\Delta$ FCH<sub>4</sub> (Fig. 5). The increasing trend between chamber IQR (log +0.01) and absolute  $\Delta$ FCH<sub>4</sub> (log) became clearer in coarser temporal scales, where a unit (*e*-fold; ca. 2.7x) increase in monthly and annual chamber FCH<sub>4</sub> variation (IQR +0.01) was associated with ca. 51% and 63% increase in absolute  $\Delta$ FCH<sub>4</sub>, respectively (marginal  $R^2 \geq 0.31$ ,  $p \leq 0.01$ ). Temporal EC FCH<sub>4</sub> variation (e.g., within date at the daily scale) did not lead to strong increases in absolute  $\Delta$ FCH<sub>4</sub> at daily-to-monthly aggregations (marginal  $R^2 < 0.01$ ), but the

450 annual mixed effects model showed a ca. 198% increase in absolute  $\Delta$ FCH<sub>4</sub> with a unit increase in EC FCH<sub>4</sub> IQR (+0.01; marginal  $R^2 = 0.82$ ). Models with both chamber and EC IQR (log +0.01) as explanatory variables showed significant chamber IQR at daily-to-monthly aggregations ( $p < 0.001$ , marginal  $R^2 = 0.06$ -0.31) and significant EC IQR at daily scale ( $p = 0.005$ ). In contrast, the annual model had a nonsignificant chamber IQR and significant EC IQR ( $p = 0.001$ , marginal  $R^2 = 0.81$ ). The sites also differed in the strength and direction of the relationship between chamber and EC FCH<sub>4</sub> variation and  $\Delta$ FCH<sub>4</sub> (Fig.

455 5).

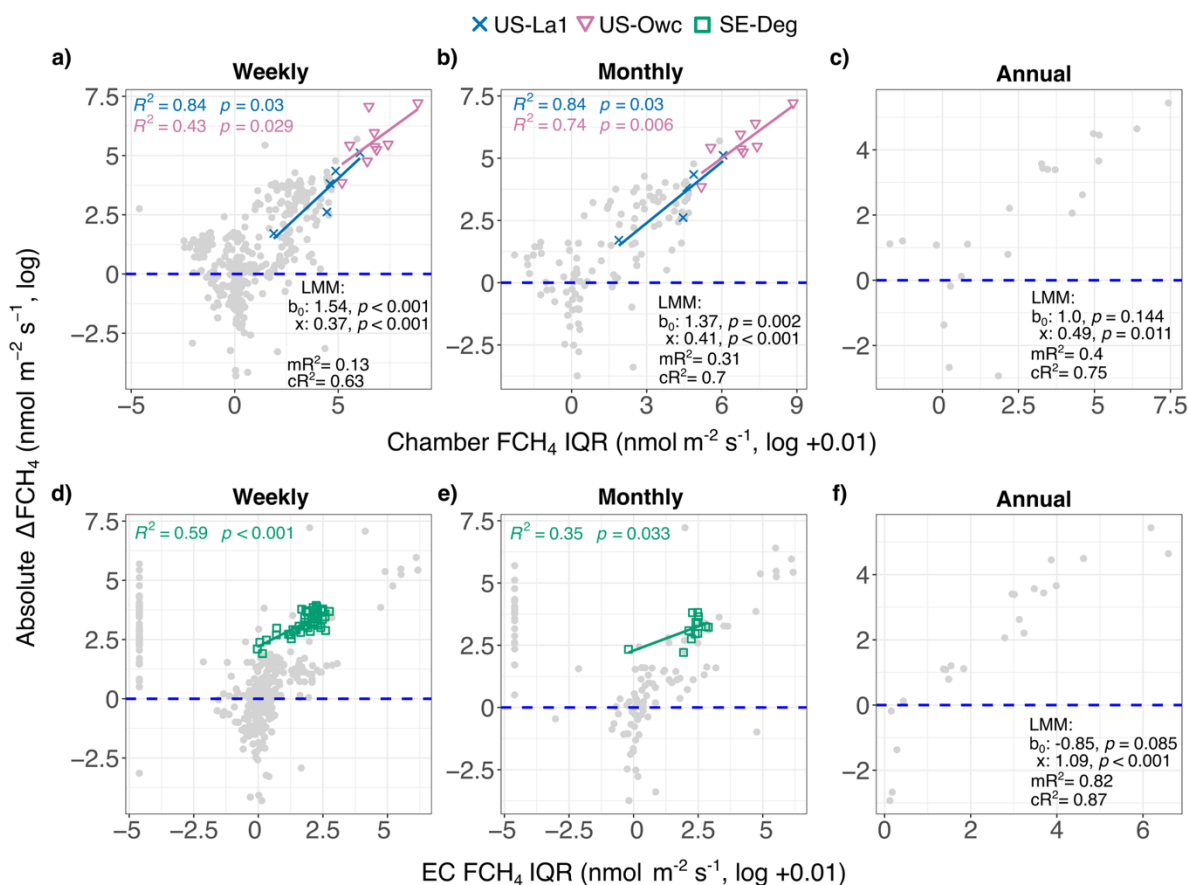


**Figure 5.** Variation in methane ( $CH_4$ ) flux ( $FCH_4$ ) between individual chambers and eddy covariance (EC) timestamps increases absolute  $\Delta FCH_4$ . a-c) Relationship between chamber  $FCH_4$  variation (variation between individual chambers per aggregation timestamp, represented by interquartile range; IQR) and absolute  $\Delta FCH_4$  at weekly (a), monthly (b) and annual (c) scales. d-f) Relationship between EC timestamp  $FCH_4$  variation (represented by IQR) and absolute  $\Delta FCH_4$  at weekly (d), monthly (e) and annual (f) scales. Linear mixed effects model (LMM) results:  $b_0$  = model intercept,  $x$  = predictor (chamber or EC  $FCH_4$  log IQR +0.01) of log absolute  $\Delta FCH_4$ ,  $p$  = predictor significance (preceded by model coefficient estimates),  $mR^2$  and  $cR^2$  = marginal and conditional  $R^2$ , respectively. In d) and e) LMM results are not shown due to low marginal  $R^2$  ( $mR^2 \leq 0.06$ ). In e) linear regression results for SE-Deg without data point where  $x < 0$ :  $R^2 = 0.62$ ,  $p = 0.002$ . Daily scale is not shown due to the low number ( $n=1$ ) of sites with significant relationships and low marginal  $R^2$  ( $mR^2 \leq 0.06$ ). Linear regressions,  $R^2$ s and  $p$ -values are only shown for sites with significant IQR predictor and  $R^2 > 0.2$  and are shown in different colors and shapes (gray points: nonsignificant and  $R^2 \leq 0.2$  sites). The dashed blue line indicates  $\Delta FCH_4 = 0$ . See version with untransformed data in Fig. B18.

### 3.2.3 Ecosystem and plot-scale FCH<sub>4</sub> difference does not significantly vary among chamber types

We did not find significant differences in  $\Delta\text{FCH}_4$  between automated and manual chambers at all aggregations (Wilcoxon-Mann-Whitney; daily  $p = 0.948$ , weekly  $p = 0.361$ , monthly  $p = 0.565$ , annual  $p = 0.722$ ). However,  $\Delta\text{FCH}_4$  in manual chambers had higher variation than automated chambers at the daily ( $\text{CV}_{\text{manual}} = 284\%$ ,  $\text{CV}_{\text{automated}} = 181\%$ ), weekly ( $\text{CV}_{\text{manual}} = 262\%$ ,  $\text{CV}_{\text{automated}} = 181\%$ ), and monthly ( $\text{CV}_{\text{manual}} = 240\%$ ,  $\text{CV}_{\text{automated}} = 182\%$ ) scales. The correlations between chamber FCH<sub>4</sub> and EC FCH<sub>4</sub> for both automated and manual chambers were strong at the daily-to-annual scales ( $\rho > 0.7$ , Fig. B19).

## 4 Discussion

### 4.1 Ecosystem-scale FCH<sub>4</sub> is higher than plot-scale FCH<sub>4</sub> at all temporal scales

As a first step to reconcile the discrepancies in FCH<sub>4</sub> data obtained from ecosystem-scale EC and plot-scale chamber measurements, we explored the cross-scale differences across ten sites and six temporal aggregations. Across all temporal scales, ecosystem-scale (EC) FCH<sub>4</sub> was higher than at the plot scale (chamber). Supporting these results, higher EC FCH<sub>4</sub> than chamber FCH<sub>4</sub> have been observed in an arctic peatland with area-weighted chamber FCH<sub>4</sub> (Budishchev et al., 2014), a managed peat meadow with upscaled chamber FCH<sub>4</sub> (Schrier-Uijl et al., 2010), a peatland with down-scaled EC FCH<sub>4</sub> (Forbrich et al., 2011), a temperate forest with spatial chamber FCH<sub>4</sub> averages (Wang et al., 2013), and a temperate salt marsh with spatio-temporal chamber and EC FCH<sub>4</sub> averages (Hill and Vargas, 2022b). Other studies at individual sites have observed higher chamber FCH<sub>4</sub> (upscaled to ecosystem-level with different methods) than EC FCH<sub>4</sub> (Chaichana et al., 2018; Clement et al., 1995; Davidson et al., 2017; Krauss et al., 2016; Marushchak et al., 2016; Mejjide et al., 2011; Morin et al., 2017; Riutta et al., 2007). Nonetheless, the median difference was relatively low across sites and temporal aggregations (min 1.36 daily, max 2.58 nmol m<sup>-2</sup> s<sup>-1</sup> annual), with CV ranging from a minimum of 191% (hourly) to a maximum of 674% (daily; Table 2), indicating relatively good agreement between ecosystem and plot-scale FCH<sub>4</sub> across sites despite high variability. While our higher ecosystem- than plot-scale FCH<sub>4</sub> trend was robust across temporal scales, due to the limited data availability ( $n = 10$  sites), our results reflect site differences and generalizations should be tested when more data become available.

We found the best general agreement between instantaneous ecosystem- and plot-scale FCH<sub>4</sub> at the monthly and annual aggregations, with the agreement improving from fine to coarse temporal resolutions. The improved agreement is likely a result of the data aggregation, which reduces the influence of inter-daily FCH<sub>4</sub> variability and inflates correlation coefficients (e.g., Clark and Avery, 1976; Pollet et al., 2015). In addition, mean  $\Delta\text{FCH}_4$  at the weekly, monthly, and annual scales was negative (i.e., higher plot-scale than ecosystem-scale FCH<sub>4</sub>; Table 2), and the CV for the weekly aggregation in particular was large (467%) (Table 2). These results indicate that high CH<sub>4</sub> emissions and FCH<sub>4</sub> variability in plot-scale measurements are associated with more negative  $\Delta\text{FCH}_4$ , particularly at time scales longer than daily (Table 2 and Fig. B2). This suggests that combining plot- and ecosystem-scale bulk FCH<sub>4</sub> at heterogeneous sites is particularly problematic at coarse temporal scales.

However, footprint-aware comparisons between upscaled chamber or downscaled EC FCH<sub>4</sub> could show better agreement between ecosystem and plot scales (e.g., Schrier-Uijl et al., 2010) (see 4.6). Nonetheless, these results highlight the practice of selective chamber placement on high-emitting locations and time periods (Hill and Vargas 2022b; Vargas and Le 2023). However, our results based on cumulative FCH<sub>4</sub> (Table C5) also show that ecosystem-scale cumulative FCH<sub>4</sub> are generally higher than at plot scale. Therefore, site-level CH<sub>4</sub> budgets calculated with ecosystem-scale FCH<sub>4</sub> data can exceed plot-scale estimates despite localized plot-scale CH<sub>4</sub> emission peaks (with site-specific variation; Fig. B16).

Mismatches in capturing site FCH<sub>4</sub> heterogeneity, and chamber measurement artifacts may have contributed to the higher ecosystem-scale FCH<sub>4</sub> and  $\Delta$ FCH<sub>4</sub> variation. Chamber measurements are challenged by tall vegetation and ebullition events are often discarded, which could artificially bias chamber FCH<sub>4</sub> estimates. The EC footprints may have covered high-CH<sub>4</sub>-emitting areas (i.e., CH<sub>4</sub> emission hot spots) and ebullition events (i.e., CH<sub>4</sub> emission hot moments) more often than chambers, increasing  $\Delta$ FCH<sub>4</sub>. Although ebullition can also be triggered by chamber placement onto waterlogged soil surface (e.g., Jentsch et al., 2025), ebullition events were removed from some of the chamber FCH<sub>4</sub> data (see 2.2.1 and Table C2), so this was unlikely to contribute to the general  $\Delta$ FCH<sub>4</sub> trends. Indeed, in spatially heterogeneous areas, CH<sub>4</sub> emission hot spots within EC footprints can be important  $\Delta$ FCH<sub>4</sub> drivers (Desai et al., 2015; Rey-Sanchez et al., 2025; Xu et al., 2018), and at some sites, the majority of FCH<sub>4</sub> is contributed through ebullition (Männistö et al., 2019; Ueyama et al., 2023b; Villa et al., 2021). FCH<sub>4</sub> hot spots and hot moments can also vary in space and time, which manual chamber FCH<sub>4</sub> measurements (n = 6 sites) may not capture due to sporadic daytime measurements in weekly or monthly intervals (Anthony and Silver, 2021, 2023; Vargas and Le, 2023). This may result in uncertainties in spatio-temporal FCH<sub>4</sub> and  $\Delta$ FCH<sub>4</sub> variation across temporal scales (Anthony and Silver, 2021, 2023; Vargas and Le, 2023). The EC footprint effects could be further highlighted by the increasing  $\Delta$ FCH<sub>4</sub> with greater FCH<sub>4</sub> (Fig. 4), and similar trends were observed in a rice paddy where plot-scale FCH<sub>4</sub> was higher than at ecosystem scale (Meijide et al., 2011). In addition, high CH<sub>4</sub> uptake at the plot scale increased  $\Delta$ FCH<sub>4</sub> particularly at CN-Hgu (see 3.1), highlighting selective chamber placement on CH<sub>4</sub>-consuming areas (Table C2). However,  $\Delta$ FCH<sub>4</sub> in low FCH<sub>4</sub> is uncertain due to EC and chamber detection limits, the reported ranges of which cover the minimum absolute  $\Delta$ FCH<sub>4</sub> of 0-0.05 nmol m<sup>-2</sup> s<sup>-1</sup> (Desai et al., 2015; Erkkilä et al., 2018; Kroon et al., 2007, 2010; Richardson et al., 2019; Smeets et al., 2009). Altogether, the mismatch in EC and chamber footprint coverages, as well as chamber CH<sub>4</sub> ebullition removal, could be important  $\Delta$ FCH<sub>4</sub> drivers. This highlights the importance of accounting for EC and chamber footprint representativeness as well as chamber data quality control when combining plot- and ecosystem-scale FCH<sub>4</sub> data, particularly at high-FCH<sub>4</sub> sites and time periods (Fig. 4).

#### 4.2 Atmospheric pressure, friction velocity and vapor pressure deficit predict daily and weekly FCH<sub>4</sub> difference between ecosystem and plot scales

PA, u\* and VPD were important daily and weekly-scale  $\Delta$ FCH<sub>4</sub> predictors. PA is a strong predictor of daily and multiday (ca. 3-21 days) FCH<sub>4</sub> (Knox et al., 2021), and  $\Delta$ FCH<sub>4</sub> decreased with higher PA (Table 3). Drops in PA have been associated with ebullitive FCH<sub>4</sub> in wetlands (Knox et al., 2021; Nadeau et al., 2013; Sachs et al., 2008; Tokida et al., 2007) and unvented

closed chambers can alter chamber air pressure (Jentsch et al., 2025). Together with chamber CH<sub>4</sub> ebullition filtering (Table 2), this may have led to EC capturing FCH<sub>4</sub> pulses that chamber data did not include. As ebullition events are often removed from chamber FCH<sub>4</sub> data, these results suggest that the large variation in chamber FCH<sub>4</sub> data processing protocols could increase  $\Delta$ FCH<sub>4</sub> and uncertainty in multi-site syntheses utilizing cross-scale FCH<sub>4</sub> data (e.g., Jentsch et al., 2025; Levy et al., 2011). Friction velocity likely increased  $\Delta$ FCH<sub>4</sub> mainly via effects on CH<sub>4</sub> ebullition in open water (Wille et al., 2008), which EC detected but chambers excluded. EC FCH<sub>4</sub> can be underestimated in low  $u^*$ , decreasing  $\Delta$ FCH<sub>4</sub>. However, EC FCH<sub>4</sub> under low  $u^*$  were filtered out by the FLUXNET-CH<sub>4</sub> team, so low  $u^*$  was unlikely to influence the observed  $\Delta$ FCH<sub>4</sub> trends (Aubinet, 2008; Baldocchi, 2003; Knox et al., 2019; Delwiche et al., 2021). The strong effect size of site dominant vegetation and the negative VPD effect can reflect species- and site-specific stomatal conductance and CH<sub>4</sub> transport (Cernusak et al., 2018; Grossiord et al., 2020). For example, at US-Owc (dominated by aerenchymatous vegetation), plant CH<sub>4</sub> conductance varies spatially and temporally between *Nelumbo lutea*, *Nymphaeae odorata*, and *Typha angustifolia*, which may have been covered differently by chamber and EC FCH<sub>4</sub> footprints (Villa et al., 2020). The importance of plant activity is further supported by the marginally-significant TS (Table 3), a possible proxy for increased plant activity in the peak growing season months in the northern hemisphere (July and August; Table 3). Chamber artifacts could have also contributed to the  $u^*$  and VPD effects: short chamber deployments in high  $u^*$  and low WTL can underestimate chamber FCH<sub>4</sub> (Lai et al., 2012), while longer measurements (e.g., FI-Si2, US-La1 and US-La2: >30 min) in high WTL can keep stomata open and increase CH<sub>4</sub> transport and chamber FCH<sub>4</sub> (Knapp and Yavitt, 1992; Langensiepen et al., 2012). However, given the limited sample size in the models (n = 9 sites) and the low model performance based on leave-one-site-out analyses (Table 3), these results are influenced by site selection and generalizations to other sites are not possible.

As hypothesized, greater variation in FCH<sub>4</sub> between chambers led to higher  $\Delta$ FCH<sub>4</sub> especially at the weekly to annual scales. Chamber FCH<sub>4</sub> can vary strongly between individual chambers (Davidson et al., 2002) but FCH<sub>4</sub> variation can be even stronger between chamber patches (due to differences in vegetation and microtopography) than within them (Stewart et al., 2024), a factor which was not included in our analyses. Similar to CH<sub>4</sub>, spatial variation in soil CO<sub>2</sub> respiration measurements has been an important driver of the discrepancies between ecosystem and soil CO<sub>2</sub> respiration observations, indicating that chambers may weigh soil respiration hot spots and moments more heavily than the larger EC footprints where CO<sub>2</sub> fluxes are averaged out (Phillips et al., 2017). While CH<sub>4</sub> cycling is driven by different controls than CO<sub>2</sub>, chambers capturing CH<sub>4</sub> emission hot spots and hot moments may have similarly led to the large  $\Delta$ FCH<sub>4</sub> CVs and negative mean  $\Delta$ FCH<sub>4</sub>, particularly at the daily and weekly scales in both median and mean-based temporal aggregations (Table 2 and Table C4). The spatial variation between chambers could have also contributed to chamber FCH<sub>4</sub> random errors and  $\Delta$ FCH<sub>4</sub> patterns in Fig. 4 (Levy et al., 2011). Nevertheless, despite the possible importance of chamber CH<sub>4</sub> emission hot spots and moments in driving  $\Delta$ FCH<sub>4</sub>, cumulative plot-scale FCH<sub>4</sub> is increasingly exceeded by higher ecosystem-scale FCH<sub>4</sub> at coarser temporal scales (albeit with site-specific trends; Table C5, Fig. B16).

The FCH<sub>4</sub> variation between chambers and its influence on  $\Delta$ FCH<sub>4</sub> differed between sites. Between-chamber variation explained  $\Delta$ FCH<sub>4</sub> best at US-La1 (but n = 5) and US-Owc where plot-scale FCH<sub>4</sub> were also higher (Table C9-C12). At US-Owc, these trends are likely related to spatial FCH<sub>4</sub> heterogeneity: the daily mean FCH<sub>4</sub> range from 500 nmol m<sup>-2</sup> s<sup>-1</sup> in open water areas to 21 000 nmol m<sup>-2</sup> s<sup>-1</sup> in mud flats, and CH<sub>4</sub> ebullition, diffusion, and plant-mediated CH<sub>4</sub> transport rates are highest at and differ between the *Nelumbo lutea* and *Typha angustifolia*-dominated vegetation patches (Rey-Sanchez et al., 2018; Villa et al., 2020, 2021). In contrast, SE-Deg has a relatively homogeneous vegetation composition dominated by *Sphagnum* spp. mosses, *Eriophorum vaginatum*, and *Andromeda polifolia* (Järveoja et al., 2018), which may explain why EC FCH<sub>4</sub> variation had a better fit than between-chamber FCH<sub>4</sub> variation (Fig. 5). Across sites, the increasing absolute  $\Delta$ FCH<sub>4</sub> with between-chamber FCH<sub>4</sub> variation may result from the EC footprint capturing patches that only a portion of the chamber measurements may represent. This may be highlighted in sites with manual chamber measurements which were conducted 1-3 times a month and during daytime when FCH<sub>4</sub> are often higher than at nighttime (Koebsch et al., 2015; Long et al., 2010; Parmentier et al., 2011) (e.g., US-La1; Fig. 5). However, at some sites median plot-scale FCH<sub>4</sub> was higher than at the ecosystem scale and very high plot-scale FCH<sub>4</sub> contributed more to annual FCH<sub>4</sub> than ecosystem-scale FCH<sub>4</sub>, (e.g., US-Owc), highlighting the ability of chambers to capture fine-scale spatial FCH<sub>4</sub> heterogeneity as a  $\Delta$ FCH<sub>4</sub> driver (Tables C9-C12). Therefore, using representative chamber patches and measurement times to upscale chamber FCH<sub>4</sub> to the EC footprint could potentially decrease  $\Delta$ FCH<sub>4</sub> (Schrier-Uijl et al., 2010; Vargas and Le, 2023). This could be achieved for example by utilizing statistical optimization for temporal sampling (Vargas and Le, 2023) and matching the chamber, EC and site spatial heterogeneity by surveying the vegetation, hydrological and edaphic properties of the study site, EC footprint, and the surrounding area/region that the footprint represents (e.g., Chu et al., 2021; Schrier-Uijl et al., 2010, Riutta et al., 2007) (see also 4.6).

#### **4.3 Wind direction, atmospheric pressure and friction velocity drive monthly ecosystem- and plot-scale FCH<sub>4</sub> differences**

At the monthly scale  $\Delta$ FCH<sub>4</sub> was best explained by wind direction (uWD), PA and u\*. Wind direction has been an important EC FCH<sub>4</sub> predictor in wetlands similar to the sites of this study in multiday (ca. 3-21 days) and seasonal (ca. 43-341 days) scales (Knox et al., 2021). The significant effect of uWD may indicate monthly-scale variation in EC footprint and the possibly systematically different land cover coverage than that of chambers, but footprint-aware analyses with a larger sample size are required to confirm these hypotheses. PA and u\* are also considered to be more influential FCH<sub>4</sub> drivers at the diel to multiday scales, which potentially represent  $\Delta$ FCH<sub>4</sub> seasonality, driven by continental-scale air pressure systems or regional land-sea winds (Griebel et al., 2016; Montaldo and Oren, 2016; Rebmann et al., 2005). The significant and positive effect of aerenchymatous vegetation may further suggest a role of seasonal plant activity with higher CH<sub>4</sub>-emitting or -consuming aerenchymatous plant biomass in growing season months (Knox et al., 2021; Niu et al., 2011). The significant effect of April in the monthly model (Table 3) was likely influenced by site-specificity, as only three out of ten sites had observations in that

month (Fig. B1, Table 1). Thus, more sites with year-round FCH<sub>4</sub> observations should aid in confirming the significance of, and the possible  $\Delta$ FCH<sub>4</sub> drivers in, April.

600 Monthly and annual  $\Delta$ FCH<sub>4</sub> trends may have also reflected seasonal snow and ice thaw dynamics, as well as changes in the chamber measurement system. The higher ecosystem-scale FCH<sub>4</sub> at CN-Hgu in cooler months (February-April, Fig. B15) may have resulted from spring snowmelt releasing stored CH<sub>4</sub> below the ice and snow cover (Hargreaves et al., 2001; Morin et al., 2017; Rinne et al., 2007; Zhang et al., 2012). These fluxes may be captured by EC but not by chambers since chamber placement in frozen conditions tends to be located further from ice cracks and fissures. Furthermore, due to the practical  
605 difficulties with sampling in frozen conditions, FCH<sub>4</sub> data from winter months was limited (Fig. B1, Table 1) and full year co-occurring chamber and EC FCH<sub>4</sub> coverage would allow further investigation of seasonal  $\Delta$ FCH<sub>4</sub> dynamics. Changes in the chamber measurement system also likely contributed to monthly and interannual  $\Delta$ FCH<sub>4</sub>. In US-Ho1 and US-Uaf, the number of chambers per chamber surface cover class varied between years and months: due to instrument malfunction or chamber replacements, in some timestamps spatial chamber medians did not include CH<sub>4</sub>-emitting or -consuming patches while EC  
610 did, leading to a large monthly- and annual-scale  $\Delta$ FCH<sub>4</sub> variation (Richardson et al., 2019; Ueyama et al., 2023a). The chamber footprint variations likely influenced  $\Delta$ FCH<sub>4</sub> particularly at US-Ho1, where the EC footprint often covers both CH<sub>4</sub>-consuming upland forest and CH<sub>4</sub>-emitting wetland areas. In contrast, chamber FCH<sub>4</sub> measurements did not always include wetland areas, increasing  $\Delta$ FCH<sub>4</sub> (Richardson et al., 2019). This further highlights the influence of selective site-specific chamber and EC tower placement and the development of methods for plot selection over time on  $\Delta$ FCH<sub>4</sub>.

#### 615 **4.4 FCH<sub>4</sub> difference between ecosystem and plot scales is highest in the morning and at noon**

Our diel analyses revealed that  $\Delta$ FCH<sub>4</sub> and ecosystem-scale FCH<sub>4</sub> are higher from morning to noon (max  $\Delta$ FCH<sub>4</sub> at 9 AM) and lower in the evening and at night (min  $\Delta$ FCH<sub>4</sub> at 8 PM). Higher daytime FCH<sub>4</sub> has been observed particularly during growing seasons (Koebsch et al., 2015; Long et al., 2010; Parmentier et al., 2011), and higher daytime EC FCH<sub>4</sub> than chamber FCH<sub>4</sub> also by Yu et al. (2013). Ecosystem-scale FCH<sub>4</sub> seemed to be driving the monthly diel  $\Delta$ FCH<sub>4</sub> particularly in July with  
620 noon and August with morning FCH<sub>4</sub> peaks, while plot-scale FCH<sub>4</sub> showed less diel variation (Fig. B8-B12). The lack of diel variation in plot-scale FCH<sub>4</sub> possibly resulted from the spatial aggregation of chamber measurements across ecohydrological patches that differ in FCH<sub>4</sub> (e.g., from wet *Carex* sp. to dry lichen in US-Uaf; Ueyama et al., 2023a). Our findings of increasing absolute  $\Delta$ FCH<sub>4</sub> with FCH<sub>4</sub> (Fig. 4) may reflect these differences, as EC and chamber FCH<sub>4</sub> random error can increase with flux magnitude (Hollinger and Richardson, 2005; Knox et al., 2019; Richardson et al., 2006, 2008), and may also be associated  
625 with diel variation in turbulence, EC footprint, and spatial FCH<sub>4</sub> heterogeneity (Hollinger & Richardson, 2005; Knox et al., 2021; Levy et al., 2011), and vary between sites (Delwiche et al., 2021; Richardson et al., 2006). The diel-scale mixed models also had very low explanatory power and high site-specificity (conditional R<sup>2</sup> > 0.79), making it difficult to identify drivers for the observed  $\Delta$ FCH<sub>4</sub> trends. Thus, more sites with hourly chamber FCH<sub>4</sub> measurements could help disentangle the diel  $\Delta$ FCH<sub>4</sub> predictors.

630 The high daytime  $\Delta FCH_4$  (CN-Hgu, SE-Deg, US-Ho1) could have resulted from diel variation in  $u^*$  and VPD. High daytime  
 $u^*$  can enhance ebullition,  $CH_4$  volatilization and release of stored  $CH_4$  from nocturnal boundary layer (Baldocchi, 2003; Long  
et al., 2010; Morin et al., 2014; Sachs et al., 2008; Wille et al., 2008). Related to VPD, pressurized plant-mediated  $CH_4$  transport  
peaks from late morning to afternoon, as temperature and humidity gradients between cooler belowground tissues and warmer,  
635 et al., 2021; Morin et al., 2014; Vroom et al., 2022; Whiting and Chanton, 1996). However, very high VPD can induce stomatal  
closure, thereby reducing  $CH_4$  transport (Grossiord et al., 2020). Enhanced stomatal conductance under high solar radiation  
may have also increased diffusive plant-mediated  $CH_4$  transport (van der Nat et al., 1998), leading to higher daytime  
ecosystem-scale  $FCH_4$  than plot-scale  $FCH_4$  as dark chambers possibly closed the stomata. However, longer chamber  
deployment can decrease VPD within the chamber, and re-open the stomata (Knapp and Yavitt, 1992; Langensiepen et al.,  
640 2012). In addition, the lower plot- than ecosystem-scale diel  $FCH_4$  at CN-Hgu (e.g., Fig. B9) likely reflected the selective  
chamber placement at  $CH_4$ -consuming areas whereas the EC footprint captured  $CH_4$  emission events more often (Table C2).  
The high nighttime  $\Delta FCH_4$  (US-Uaf) could have been driven by  $u^*$ : the nighttime EC footprint may have covered high- $CH_4$ -  
emitting areas when  $u^*$  was low and EC footprint larger (Baldocchi et al., 2012; Chu et al., 2021; Vesala et al., 2008). Deeply-  
rooted aerenchymatous vegetation (e.g., *Carex* sp.) may have also decreased daytime ecosystem-scale  $FCH_4$  by increasing  
645 rhizospheric oxidation and  $CH_4$  consumption under high solar radiation, VPD, and soil temperature (Cho et al., 2012; Zhao et  
al., 2021, Ueyama et al., 2023a). However, these hypotheses and diel  $\Delta FCH_4$  patterns should be explored further with footprint-  
aware methods (see 4.6).

#### 4.5 Plot-scale $FCH_4$ may have been underestimated

EC and chamber techniques fundamentally differ in how ecosystem  $FCH_4$  is measured, which could influence  $\Delta FCH_4$ . Gas  
650 analyzers used for EC can be either open- or closed-path analyzers, the former of which is more sensitive to weather conditions,  
while the latter is influenced by the choice of the air pump and time lags between sonic anemometer and the gas analyzer  
(Baldocchi, 2003; Detto et al., 2011). The specific EC  $CH_4$  analyzers can also differ in signal noise (Peltola et al. 2014).  
However, the random and systematic errors associated with open- and closed-path EC gas analyzers do not contribute  
significantly to the total EC  $FCH_4$  random error, which may be more affected by the movement of EC footprint and turbulence  
655 (Deventer et al., 2019; Knox et al., 2019; Peltola et al., 2014). Thus, the two analyzers agree relatively well in practice and  
they can be combined in multi-site syntheses (Detto et al., 2011; Deventer et al., 2019; Peltola et al., 2014). However, detecting  
upland  $CH_4$  uptake rates accurately with open-path analyzers is challenging due to uptake rates often falling within the  
instrument's detection limits (Chamberlain et al., 2017; Iwata et al., 2014). Of the two upland sites included in this study, these  
artifacts may have affected the results from CN-Hgu where EC  $FCH_4$  were measured with an open-path gas analyzer.

660 As manual and automated chambers differ in temporal representation, the similarity in  $\Delta FCH_4$  between automated and manual  
chambers was surprising. The similarity was also reflected in the strong correlations between automated and manual chamber

FCH<sub>4</sub> and EC FCH<sub>4</sub> (Fig. B19), which have been observed previously in a Tibetan wetland (Yu et al., 2013). While manual chambers allow researchers to capture higher spatial FCH<sub>4</sub> variation than automated chambers (e.g., Vargas and Le, 2023), the use of spatial medians for chamber FCH<sub>4</sub> may have reduced manual chamber FCH<sub>4</sub> variation so that the resulting median FCH<sub>4</sub> was similar to the FCH<sub>4</sub> measured by automated chambers. However, the higher  $\Delta$ FCH<sub>4</sub> variation of manual chambers could have also resulted from chamber measurements being conducted 1-3 times a month leading to data gaps (Morin et al., 2014, 2017). Thus, care should be taken when combining manual chamber FCH<sub>4</sub> data with EC FCH<sub>4</sub> data in multi-site syntheses.

Chamber FCH<sub>4</sub> measurement and calculation methodology may have contributed to the generally lower plot-scale FCH<sub>4</sub>. As previously discussed (see 4.1 and 4.2), plot-scale FCH<sub>4</sub> could have been generally underestimated due to the removal of ebullition events from some of the chamber FCH<sub>4</sub> data (Table C2), calling for standardization of chamber-based ebullition measurements and data processing (Jentzsch et al., 2025). In addition, all chamber FCH<sub>4</sub> data was calculated using linear regression which may underestimate FCH<sub>4</sub> (Forbrich et al., 2010; Korhonen et al., 2017; Levy et al., 2011; Nakano, 2004; Pihlatie et al., 2013). High-precision CH<sub>4</sub> analyzers, such as cavity ring-down spectrometers and near-infrared laser gas analyzers, could capture nonlinear CH<sub>4</sub> concentration gradients which linear regression fails to do (Forbrich et al., 2010). With gas chromatography, the underestimation and related uncertainties may become even greater due to smaller sample sizes and difficulty in detecting low-quality FCH<sub>4</sub> measurements during chamber measurements (Christiansen et al., 2015; Levy et al., 2011). In sites which used gas chromatography, the number of samples was 4-7 per chamber deployment (e.g., FI-Si2, US-Owc), while sites that used high-precision CH<sub>4</sub> analyzers (CN-Hgu, SE-Deg, US-Ho1, US-Uaf) had ca. 1 Hz sampling interval, resulting in vastly different sample sizes per chamber deployment between sites, and thus higher uncertainties in chamber FCH<sub>4</sub>. However, linear regression can be statistically more robust for comparing chamber FCH<sub>4</sub> from different sites with varying soil properties (Venterea et al., 2009). Depending on chamber design, chambers can alter soil conditions (e.g., soil moisture) which may also contribute to  $\Delta$ FCH<sub>4</sub> (Bansal et al., 2023b; Subke et al., 2021). It may be valuable to compare chamber and EC FCH<sub>4</sub> using both linear and exponential fits for chamber FCH<sub>4</sub> (from both high-precision CH<sub>4</sub> analyzers and gas chromatography) to better understand  $\Delta$ FCH<sub>4</sub> trends across sites.

#### 685 **4.6 Limitations and uncertainties**

As we were able to include only ten sites in the analyses, our results are limited by the site-specific climate, vegetation, and methodology. Thus, in order to produce results that would be better generalizable to other sites and regions (e.g., tropics), future studies could include more sites from a variety of climates, ecosystem types, dominant vegetation types, and chamber measurement systems (i.e., automated and manual, gas chromatography and high-precision CH<sub>4</sub> analyzers) ( $n > 3$  sites per group to allow statistical inference). In addition, year-round FCH<sub>4</sub> observations were lacking, which introduced uncertainty, particularly into the annual  $\Delta$ FCH<sub>4</sub> trends. While challenging to measure, nongrowing season FCH<sub>4</sub> can be significant (Treat et al., 2018). Thus, future syntheses could include nongrowing season FCH<sub>4</sub> observations to improve annual  $\Delta$ FCH<sub>4</sub> estimates and investigate the possible effects of ice thaw and snowmelt on  $\Delta$ FCH<sub>4</sub>.

Another source of uncertainty in our study arose from the EC and chamber FCH<sub>4</sub> footprints. Since we used spatial medians of chamber FCH<sub>4</sub> measurements instead of upscaled chamber FCH<sub>4</sub> in the analyses to investigate cross-scale FCH<sub>4</sub> differences, the results should not be taken as indication of systematic methodological differences between EC and chamber FCH<sub>4</sub>. Thus, the next steps could include comparing EC and chamber methods by upscaling chamber FCH<sub>4</sub> to the EC footprint level, or downscaling EC FCH<sub>4</sub> to chamber level, using footprint models and indices of footprint spatial heterogeneity based on fine-scale land cover classification (Hartley et al., 2015; Metzger, 2018; Räsänen et al., 2021; Tuovinen et al., 2019; Xu et al., 2018). Future studies could apply high-resolution (e.g., 1-2 m) remotely-sensed data together with field surveys to determine chamber patch classes which could be used in upscaling chamber FCH<sub>4</sub> to the EC footprint level (Davidson et al., 2017; Forbrich et al., 2011; Morin et al., 2017; Rey-Sanchez et al., 2018; Schrier-Uijl et al., 2010; Stewart et al., 2024; Tuovinen et al., 2019), or downscaling EC FCH<sub>4</sub> to land cover classes (Forbrich et al., 2011; Rößger et al., 2019). By comparing footprint- and patch-weighted chamber FCH<sub>4</sub> to EC FCH<sub>4</sub>, we would expect  $\Delta$ FCH<sub>4</sub> to decrease or chamber FCH<sub>4</sub> exceed EC FCH<sub>4</sub> due to the incorporation of footprint FCH<sub>4</sub> heterogeneity (Budishchev et al., 2014; Schrier-Uijl et al., 2010). As our results may indicate FCH<sub>4</sub> hot spots and moments within the study sites as a possible  $\Delta$ FCH<sub>4</sub> driver, identifying FCH<sub>4</sub> hot spots within the EC footprint with the aid of footprint-weighted FCH<sub>4</sub> maps (Rey-Sanchez et al., 2022) could also assist in finding representative chamber FCH<sub>4</sub> locations to reconcile the ecosystem and plot-scale FCH<sub>4</sub> differences.

In addition, our cross-scale FCH<sub>4</sub> comparisons contain uncertainties due to differences in chamber FCH<sub>4</sub> outlier removal (Table C2), design and the gas analyzer used (Table C1) (Jentsch et al., 2025; Levy et al., 2011; Pihlatie et al., 2013; Pumpanen et al., 2004). To minimize these uncertainties in future comparison studies, it is therefore recommended to use chamber FCH<sub>4</sub> data that has been processed in as standardized a way as possible. Given that our results indicated ebullition removal from some of the chamber FCH<sub>4</sub> data as one potential driver of  $\Delta$ FCH<sub>4</sub>, future studies could also conduct cross-scale FCH<sub>4</sub> comparisons based on chamber FCH<sub>4</sub> data with ebullition events both included and excluded from a variety of wetland types. Similar comparisons could be done for the EC FCH<sub>4</sub> data where ebullition events are sometimes also removed following standard data quality protocols.

## 5 Conclusions

We explored the differences between ecosystem-scale (eddy covariance, EC) and plot-scale (chamber, spatially-aggregated median) instantaneous CH<sub>4</sub> flux (FCH<sub>4</sub>) across ten sites and in different temporal aggregations. Contrary to our expectations, we observed significantly higher median ecosystem-scale FCH<sub>4</sub> than plot-scale FCH<sub>4</sub> across all temporal scales. However, the median FCH<sub>4</sub> difference between ecosystem- and plot-scales ( $\Delta$ FCH<sub>4</sub>) remained relatively low. Ecosystem- and plot-scale FCH<sub>4</sub> correlated strongly from daily to annual scales, which indicates that ecosystem- and plot-scale FCH<sub>4</sub> observations could be combined in multi-site analyses at coarse temporal scales. However, care must be taken when combining cross-scale FCH<sub>4</sub> data, as variation in (based on instantaneous FCH<sub>4</sub>) and magnitude of  $\Delta$ FCH<sub>4</sub> (based on cumulative FCH<sub>4</sub>) was large at daily to annual scales, and the agreement was worst at the half-hourly to hourly scales. In addition,  $\Delta$ FCH<sub>4</sub> increased with FCH<sub>4</sub>

magnitude at all temporal scales, suggesting that combining ecosystem- and plot-scale FCH<sub>4</sub> in high CH<sub>4</sub>-emission ecosystems, such as wetlands, could lead to large FCH<sub>4</sub> uncertainties.

We attribute the higher ecosystem-scale FCH<sub>4</sub> than plot-scale FCH<sub>4</sub> mainly to the combination of selective chamber placement, ebullition removal from chamber FCH<sub>4</sub> data, and the spatiotemporal dynamics of the EC footprint which may have captured  
730 CH<sub>4</sub> emission events that were not detected by chambers. Our results highlight the importance of monthly and seasonal  
variation in variables related to plant activity, atmospheric pressure, wind direction, and friction velocity as drivers of  $\Delta$ FCH<sub>4</sub>  
at the ten sites. Between-chamber FCH<sub>4</sub> variation also led to higher  $\Delta$ FCH<sub>4</sub>, which highlights the mismatch of chamber and  
EC footprint coverage of the study sites as a  $\Delta$ FCH<sub>4</sub> driver. Nevertheless,  $\Delta$ FCH<sub>4</sub> varied strongly between sites and the models'  
735 ability to predict to other sites was limited by the low sample size, warranting further research on  $\Delta$ FCH<sub>4</sub> controls within and  
across ecosystem types. Based on our findings, we recommend the following:

- Cross-site efforts to upscale chamber FCH<sub>4</sub> to EC footprint level, or conversely, to downscale EC FCH<sub>4</sub> to chamber scale, using chamber measurements stratified by surface cover classes which take into account for vegetation and soil characteristics
- Further investigation of diel  $\Delta$ FCH<sub>4</sub> dynamics from a higher number of sites with automated chamber measurements,  
740 particularly related to the spatial representativeness of the chamber measurements in relation to the EC footprint and chamber artifacts on the observed FCH<sub>4</sub>
- Standardized protocols for chamber FCH<sub>4</sub> data quality control, especially related to ebullition removal (see Jentzsch et al., 2025 for recent recommendations for chamber FCH<sub>4</sub> data processing), and accounting for these differences when combining chamber and EC FCH<sub>4</sub> data
- 745 ● More widely adopted, standardized methods for examining heterogeneity of FCH<sub>4</sub> in EC footprints, which can inform representative chamber and EC tower placement within study sites (e.g., EC footprint modeling and targeted manual chamber sampling; Rey-Sanchez et al., 2022, Barba et al., 2018)
- Systematic bias and uncertainty of chamber and EC FCH<sub>4</sub> observations are recommended to be incorporated into model evaluation and parameterization studies

750 As syntheses and databases are increasingly utilizing both plot- and ecosystem-scale FCH<sub>4</sub> measurements, it is important to understand their differences across multiple sites. Taking these differences into account in future studies could improve ecosystem CH<sub>4</sub> budget estimates.

## Appendices

### Appendix A: Supplementary methods (Supplementary Methods A1-A2)

#### 755 Supplementary Methods A1.

Wind  $u$  and  $v$  component calculation.

Wind direction was separated into  $u$  (calculated with sine; equation 1) and  $v$  (calculated with cosine; equation 2) component vectors which combine both wind speed and direction for each half-hour measurement period.

760

$$u = -WS * \sin\left[\frac{2\pi * WD}{360}\right] \quad (1)$$

$$v = -WS * \cos\left[\frac{2\pi * WD}{360}\right], \quad (2)$$

765 where WS is wind speed ( $\text{m s}^{-1}$ ) and WD is wind direction in decimal degrees.

The  $u$  and  $v$  component averages were then calculated by taking the mean over the temporal unit in each aggregation (e.g., hour or day), resulting in temporally-aggregated  $u$  and  $v$  components in  $\text{m s}^{-1}$ .

## 770 **Supplementary Methods A2.**

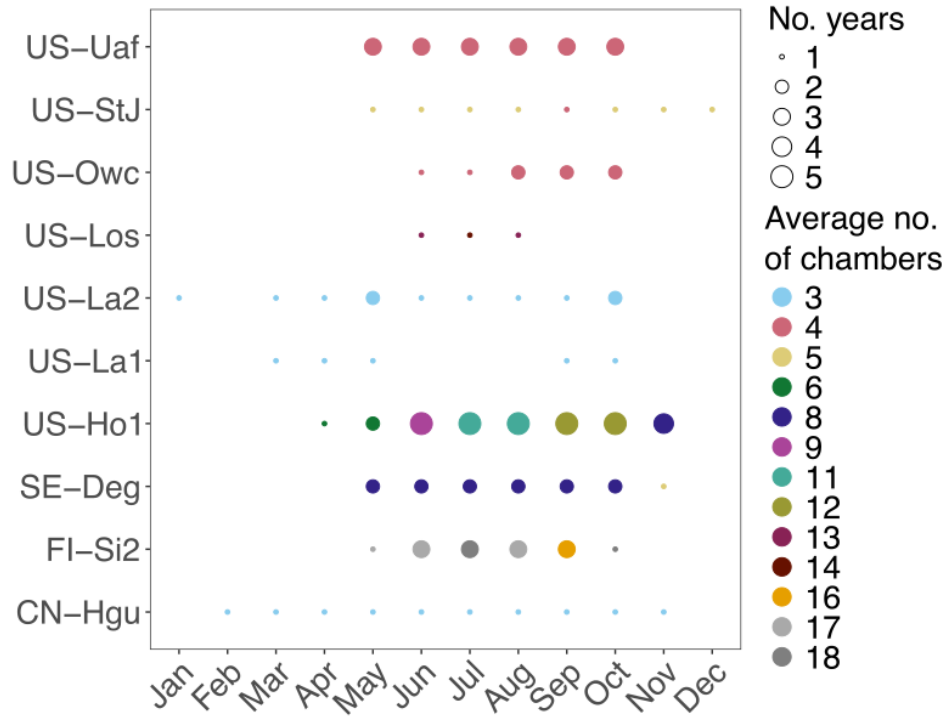
Details of linear mixed effects models.

Temporal autocorrelation and residual variance structures were examined and chosen based on Akaike Information Criteria (AIC) and residual diagnostics, with more emphasis on the latter. Temporal autocorrelation was modeled using an autoregressive structure of order 1 (AR1) in the daily, weekly, and monthly models. To meet the requirements of the corAR1 argument in R, random effects in these models were nested to account for site-specific sampling times (e.g., daily model:  $random = \sim 1 \mid Site/YearMonth$ ,  $correlation = corAR1(form = \sim Day \mid Site/YearMonth)$ ). The nesting allowed for the inclusion of temporal autocorrelation within each temporal scale, for example “YearMonth”, at the site level, reducing residual temporal autocorrelation compared to models with un-nested random effects. However, incorporating AR1 in the half-hourly model did not improve model fit or reduce residual variance and was therefore excluded. In addition, despite improvements in AIC in the hourly model, inclusion of AR1 led to model non-convergence and it had to be excluded from the model, leading to higher AIC but temporal autocorrelation and residual normality and variance heterogeneity were still acceptable when the random effect was nested ( $Site/Date$ ).

785 Heterogeneous residual variance caused by some of the predictors was modeled in some of the models using an exponential variance structure ( $varExp$ ; half-hourly and hourly: VPD,  $u^*$ , PA; daily: PA and TS; weekly: PA; monthly:  $uWD$ ,  $u^*$ ), as well as variance per stratum ( $varIdent$ ; weekly: Year). We also tested other variance structures but, according to AIC and residual diagnostics, exponential variance structure led to best model fit and some of the other structures led to model non-convergence.

790 Despite our efforts to account for the residual variance heterogeneity, some heterogeneity remained in the models while AIC and general model residual heterogeneity improved.

**Appendix B: Supplementary figures (Figures B1-B19)**



795 **Figure B1.** Number of individual chambers and years per month per site. The size of the point describes the number of years and color the average number of individual chambers used within each month across years.

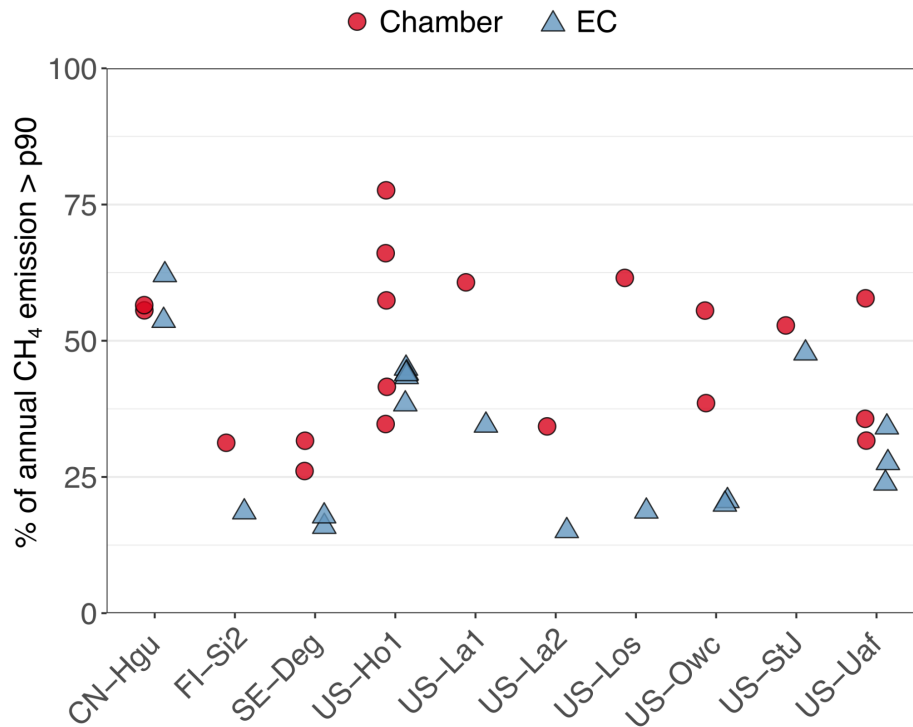


**Figure B2.** Contribution of high methane (CH<sub>4</sub>) emissions to annual CH<sub>4</sub> emissions per site in the unaggregated data set. For each site and year, high CH<sub>4</sub> emissions were estimated as CH<sub>4</sub> flux (FCH<sub>4</sub>) above the 90th percentile (p90) and their proportion (%) of the total annual CH<sub>4</sub> emission was calculated separately for chamber (red circle) and EC (blue triangle). In the unaggregated data set, all eddy covariance (EC) FCH<sub>4</sub> data is in the half-hourly scale, but the chamber data measurement frequency varies across sites (see Table S1).

805

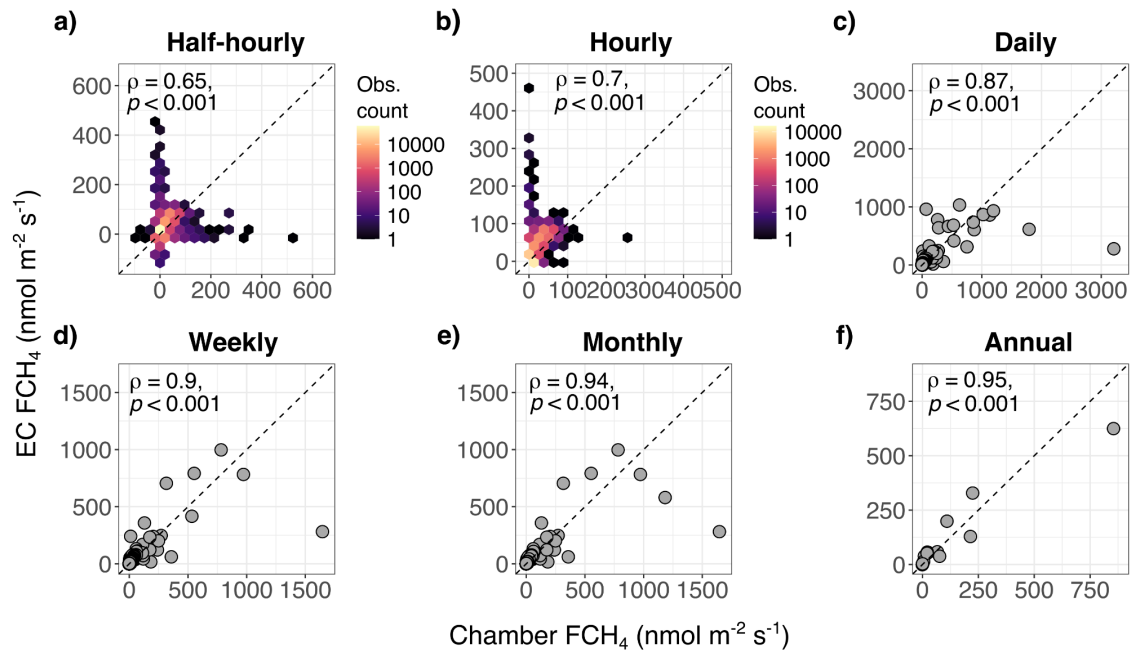


**Figure B3.** Relationship between eddy covariance (EC; ecosystem scale) methane (CH<sub>4</sub>) flux (FCH<sub>4</sub>) and chamber FCH<sub>4</sub> (plot  
 810 scale) with untransformed plot axes. Higher Spearman correlation coefficients (ρ) indicate stronger agreement between EC  
 FCH<sub>4</sub> and chamber FCH<sub>4</sub>. In a) and b) the points for half-hourly (n = 74482) and hourly (n = 40072) aggregations are shown  
 in hexagonal density clouds with a log-transformed color range to highlight trends in high point density areas (colors represent  
 number of observations per hexagon). For daily (c), weekly (d), monthly (e), and annual (f) aggregations, sample sizes were n  
 = 1879, 349, 121, and 22, respectively. The dashed line represents 1:1 line.

815

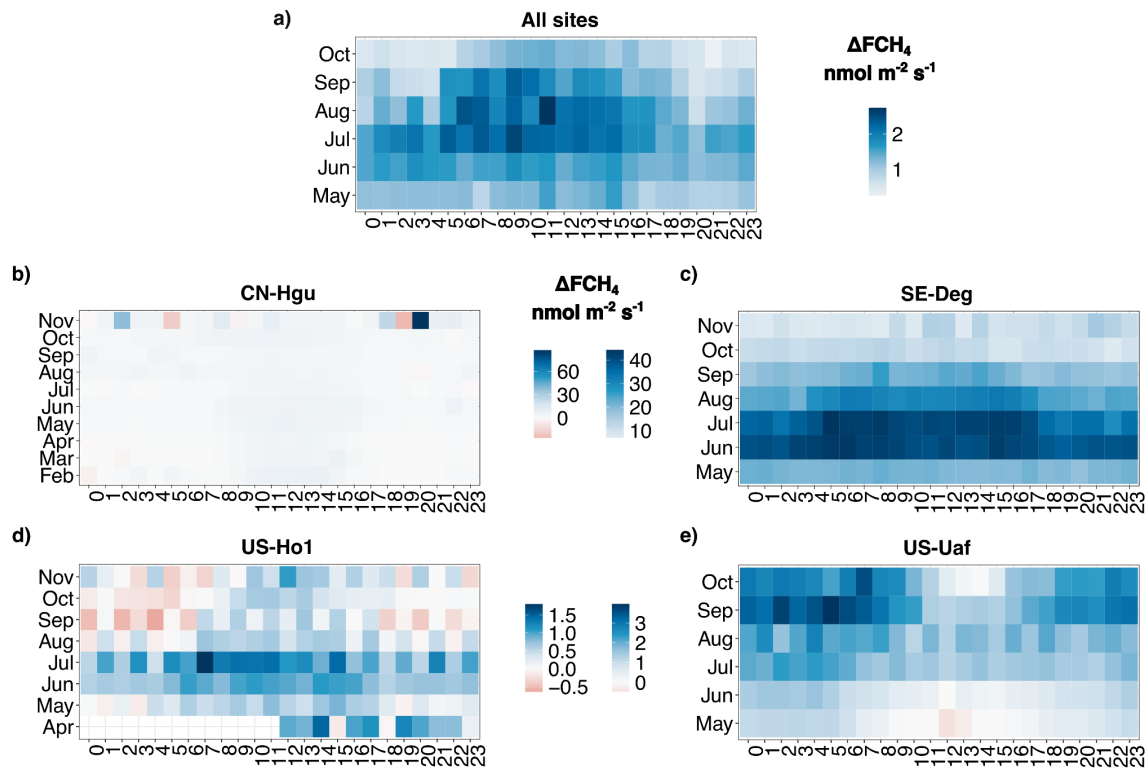
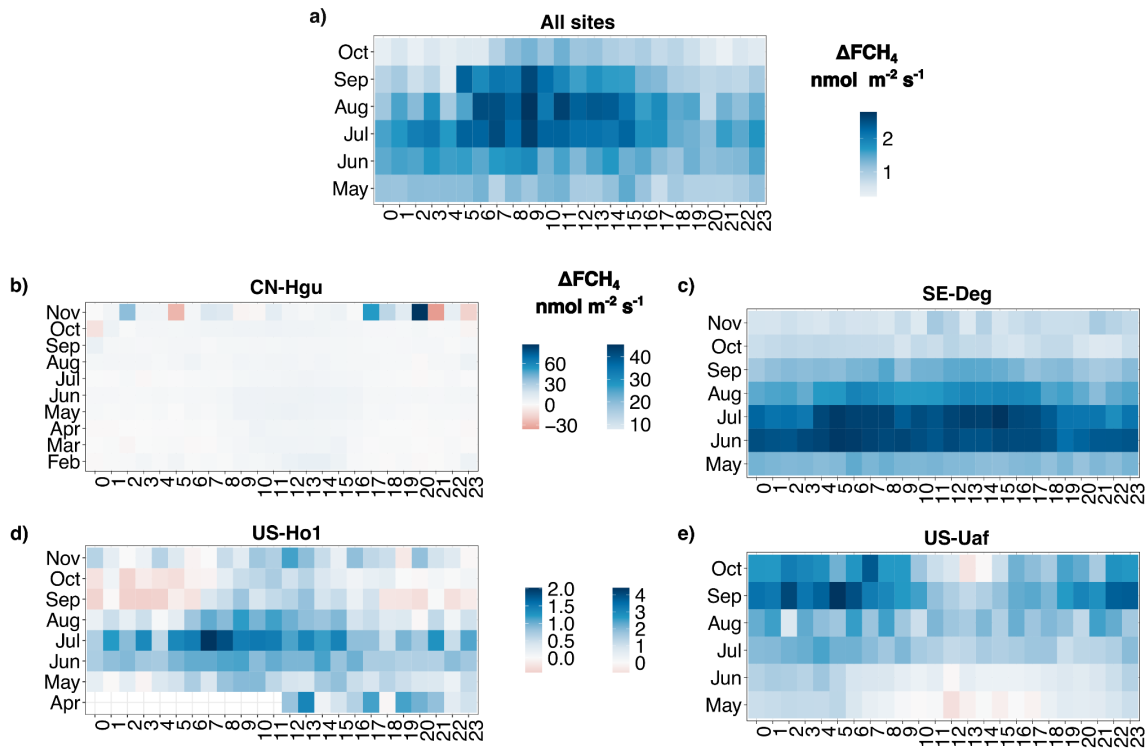


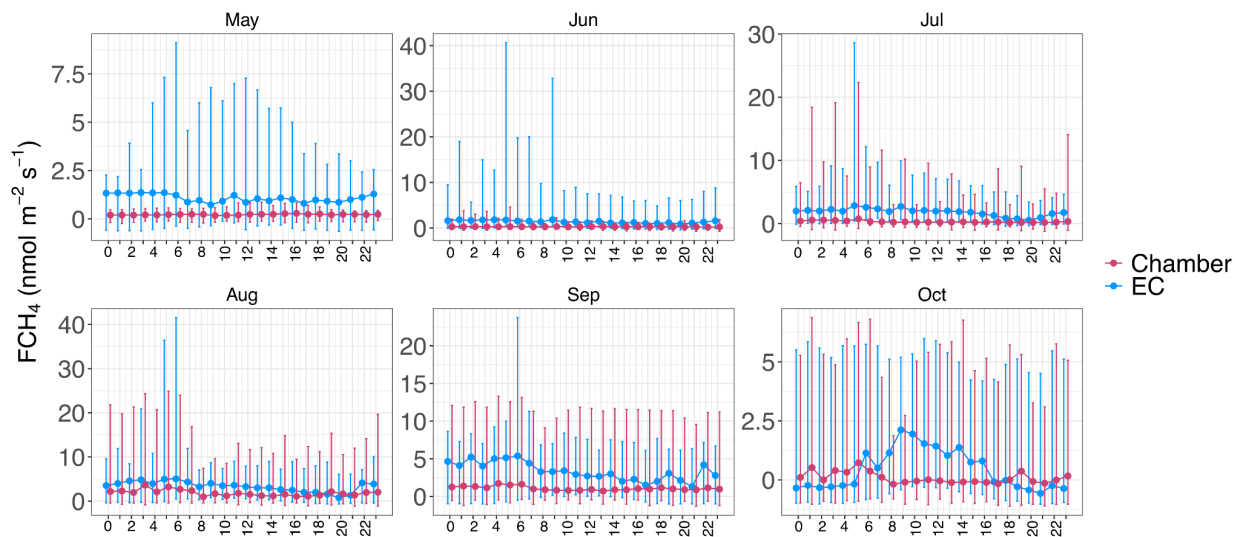
**Figure B4.** Heatmaps of hourly median methane ( $\text{CH}_4$ ) flux ( $\text{FCH}_4$ ) difference between ecosystem- and plot-scale  $\text{FCH}_4$  ( $\Delta\text{FCH}_4$ ) across months in the half-hourly aggregation. Positive  $\Delta\text{FCH}_4$  (blue) represents higher eddy covariance (EC)  $\text{FCH}_4$  than chamber  $\text{FCH}_4$ , and negative (red) higher chamber  $\text{FCH}_4$  than EC  $\text{FCH}_4$ . X axis represents hours of day (24 h) and y axis represents months. a) Data set containing all sites ( $n = 4$  sites). Only months which were included in all sites are shown (May-October). b) CN-Hgu (all months), c) SE-Deg (all months), d) US-Ho1 (all months), e) US-Uaf (all months).



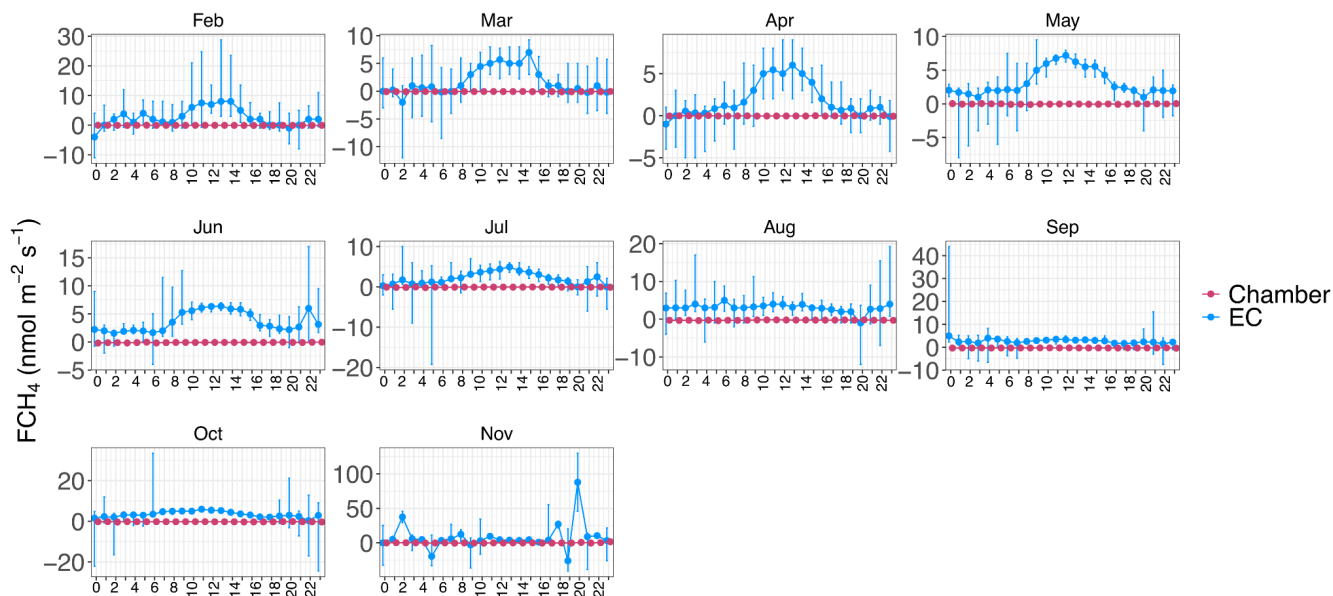
825 **Figure B5.** Heatmaps of hourly median methane ( $\text{CH}_4$ ) flux ( $\text{FCH}_4$ ) difference between ecosystem- and plot-scale  $\text{FCH}_4$  ( $\Delta\text{FCH}_4$ ) across months in the hourly aggregation. Positive  $\Delta\text{FCH}_4$  (blue) represents higher ecosystem-scale (eddy covariance; EC)  $\text{FCH}_4$  than plot-scale (chamber)  $\text{FCH}_4$ , and negative (red) higher plot-scale  $\text{FCH}_4$  than ecosystem-scale  $\text{FCH}_4$ . X axis represents hours of day (24 h) and y axis months. a) Data set containing all sites ( $n = 4$  sites). Only months which were included in all sites are shown (May-October). b) CN-Hgu (all months), c) SE-Deg (all months), d) US-Ho1 (all months), e) US-Uaf  
 830 (all months).





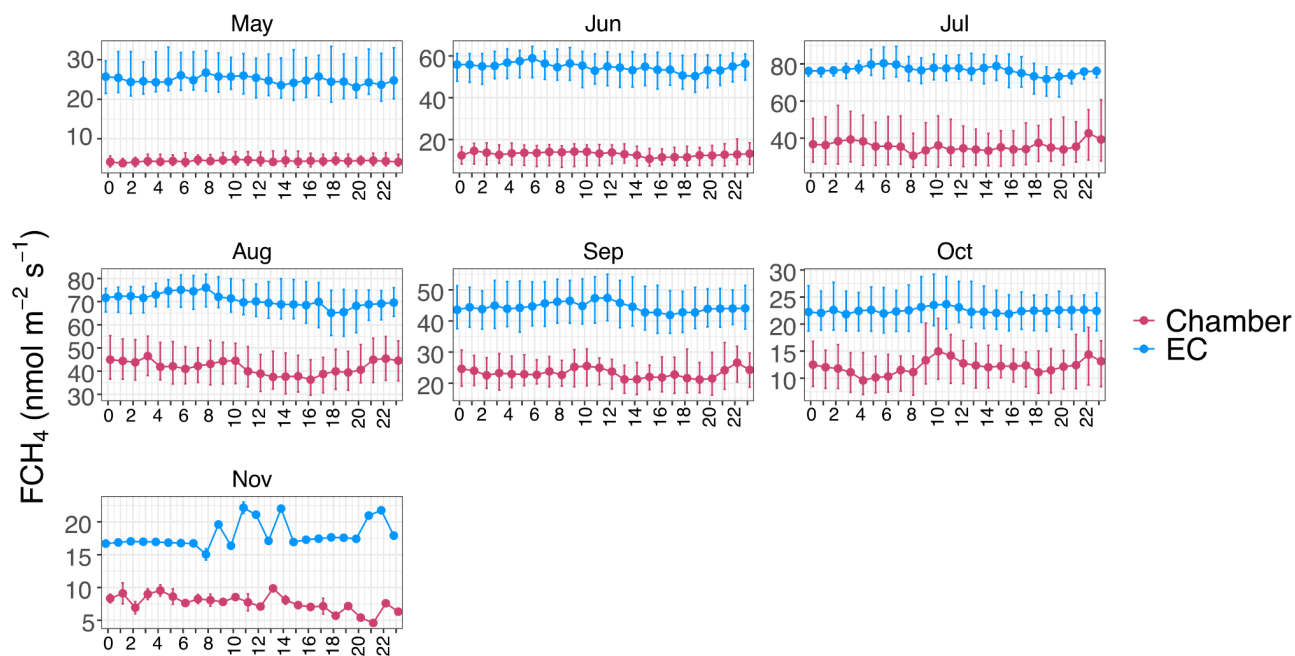


850 **Figure B8.** Hourly median chamber (red; plot scale) and eddy covariance (EC; ecosystem scale) methane ( $\text{CH}_4$ ) flux ( $FCH_4$ ; blue) per month in the half-hourly data set. Variation around the median is represented by the interquartile range (between 25% and 75%). Only months containing all sites ( $n = 4$ ) with automated chamber measurements are shown.



855 **Figure B9.** Hourly median chamber (red; plot scale) and eddy covariance (EC; ecosystem scale) methane ( $\text{CH}_4$ ) flux ( $FCH_4$ ; blue) per month in the half-hourly data set. Variation around the median is represented by the interquartile range (between 25% and 75%). Only months containing all sites ( $n = 4$ ) with automated chamber measurements are shown.

blue) per month at CN-Hgu in the half-hourly dataset. Variation around the median is represented by the interquartile range (between 25% and 75%).



860 **Figure B10.** Hourly median chamber (red; plot scale) and eddy covariance (EC; ecosystem scale) methane ( $\text{CH}_4$ ) flux ( $\text{FCH}_4$ ; blue) per month at SE-Deg in the half-hourly dataset. Variation around the median is represented by the interquartile range (between 25% and 75%).

865

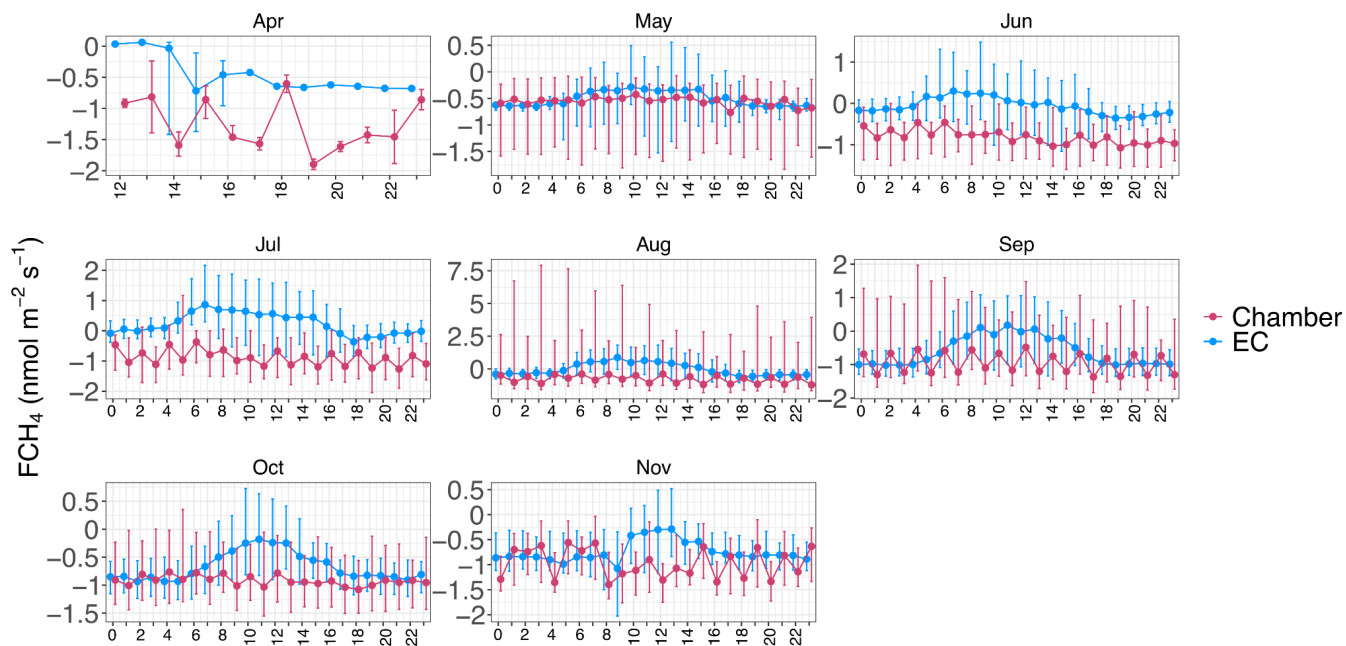
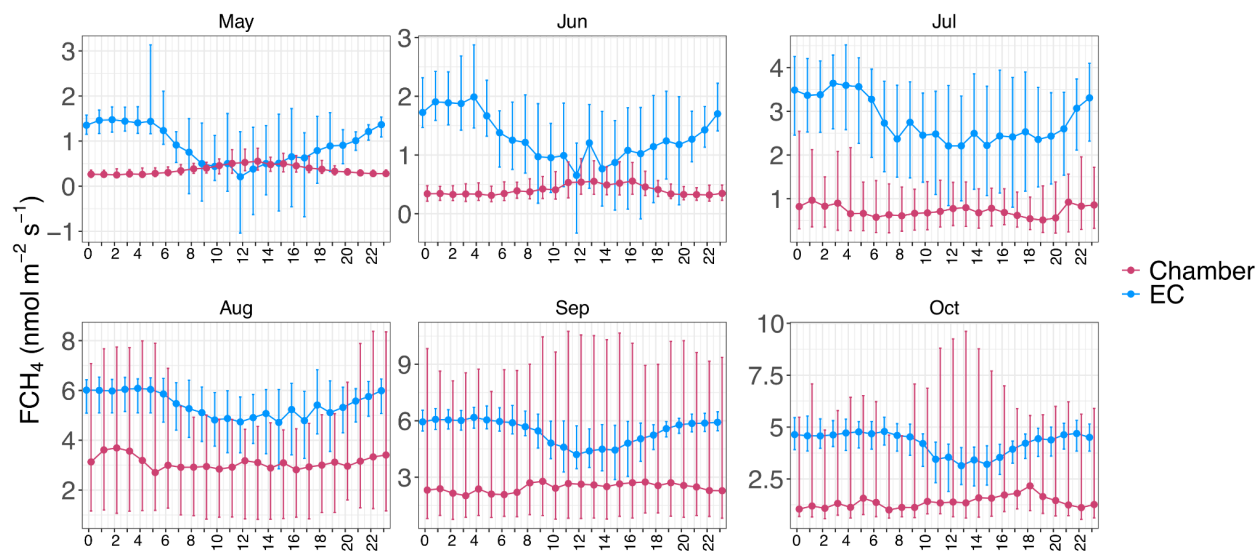


**Figure B11.** Hourly median chamber (red; plot scale) and eddy covariance (EC; ecosystem scale) methane (CH<sub>4</sub>) flux (FCH<sub>4</sub>; blue) per month at US-Ho1 in the half-hourly dataset. Variation around the median is represented by the interquartile range (between 25% and 75%).



875

**Figure B12.** Hourly median chamber (red; plot scale) and eddy covariance (EC; ecosystem scale) methane (CH<sub>4</sub>) flux (FCH<sub>4</sub>; blue) per month at US-Uaf in the half-hourly dataset. Variation around the median is represented by the interquartile range (between 25% and 75%).

880

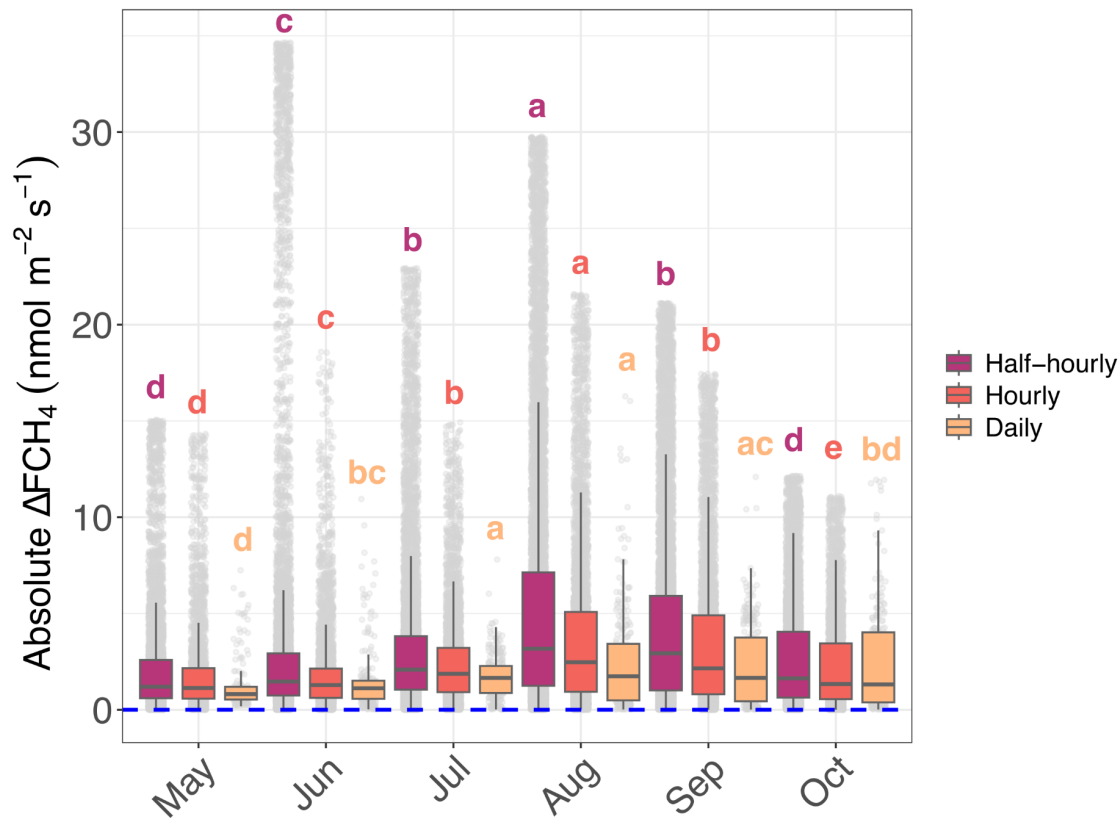


**Figure B13.** Absolute difference between ecosystem-scale (eddy covariance; EC) and plot-scale (chamber) methane (CH<sub>4</sub>) flux (FCH<sub>4</sub>) differences (ΔFCH<sub>4</sub>) between months in half-hourly, hourly and daily aggregations. Different colors represent different temporal aggregations and gray points show the underlying data. For visualization, we filtered out data points 1.5 x IQR below the first quartile and 1.5 x IQR above the third quartile but statistics were based on the original data. The letters indicate whether ΔFCH<sub>4</sub> differs significantly between months: months that share at least one shared letter are not significantly different ( $p > 0.05$ ) while months with different letters differ significantly ( $p \leq 0.05$ ). Pairwise comparisons were conducted with the Conover-Iman post hoc test. While there was data in other months, the May-October period was chosen for this figure due to these months including either all ( $n = 4$ ; half-hourly and hourly aggregations) or almost all sites ( $n = 7$  or 8 sites; daily aggregation). Weekly and monthly aggregations did not have significant ΔFCH<sub>4</sub> differences between months (Kruskal-Wallis  $p > 0.05$ ) and are not shown in this figure.

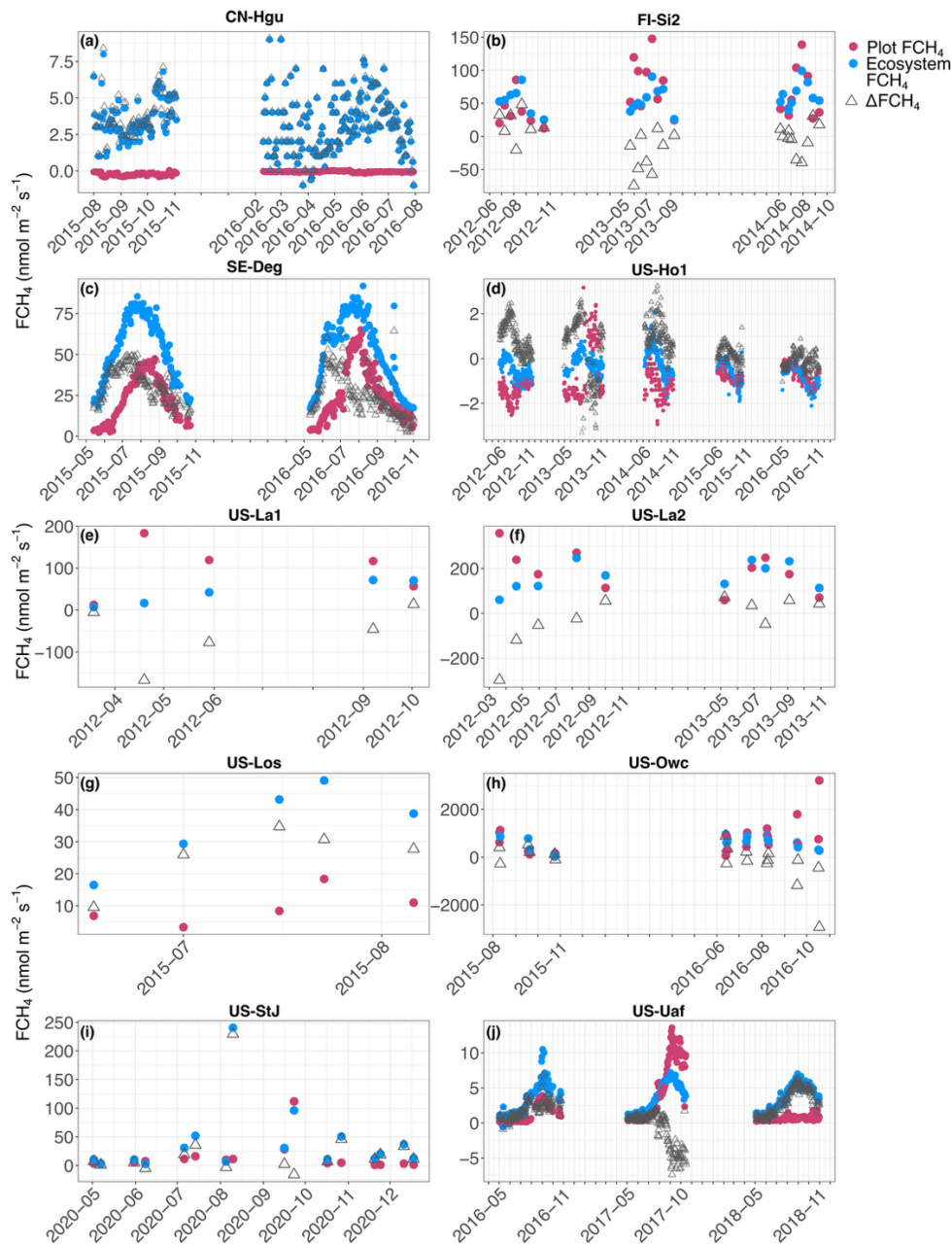
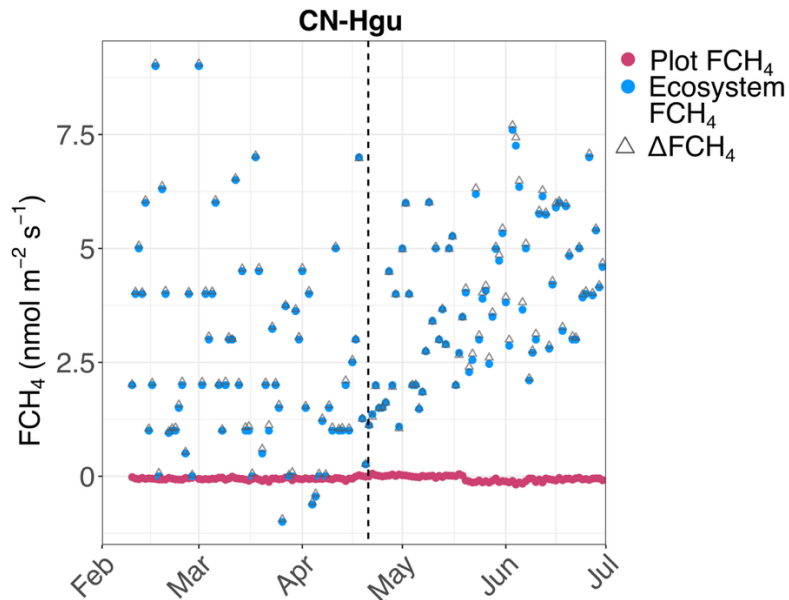


**Figure B14.** Site-specific trends in daily ecosystem- (eddy covariance; EC) and plot-scale (chamber) methane ( $\text{CH}_4$ ) flux ( $\text{FCH}_4$ ), and  $\text{FCH}_4$  difference between ecosystem and plot scales ( $\Delta\text{FCH}_4$ ) (a to j). Red circles represent plot- and blue ecosystem-scale  $\text{FCH}_4$  measurements. Hollow gray triangles are  $\Delta\text{FCH}_4$ . In d) 46 outlier points from 2013 were removed to

900 improve visualization. Negative  $\Delta FCH_4$  indicates higher plot-scale  $FCH_4$  than ecosystem-scale  $FCH_4$ , and positive higher ecosystem-scale  $FCH_4$  than plot-scale  $FCH_4$ .



905 **Figure B15.** Daily-aggregated methane ( $CH_4$ ) flux ( $FCH_4$ ) at CN-Hgu between February and July highlighting the higher ecosystem- than plot-scale  $FCH_4$  during the ice thawing period (February-end of April). Red circles represent plot- and blue ecosystem-scale  $FCH_4$  measurements. Hollow gray triangles are the difference between ecosystem- and plot-scale  $FCH_4$  ( $\Delta FCH_4$ ). Negative  $\Delta FCH_4$  indicates higher plot-scale  $FCH_4$  than ecosystem-scale  $FCH_4$ , and positive higher ecosystem-scale  $FCH_4$  than plot-scale  $FCH_4$ . The dashed vertical black line represents the mean end period of frozen-thawing period at a nearby  
910 peatland (between 2015 and 2016), calculated by Liu et al., (2021).

915

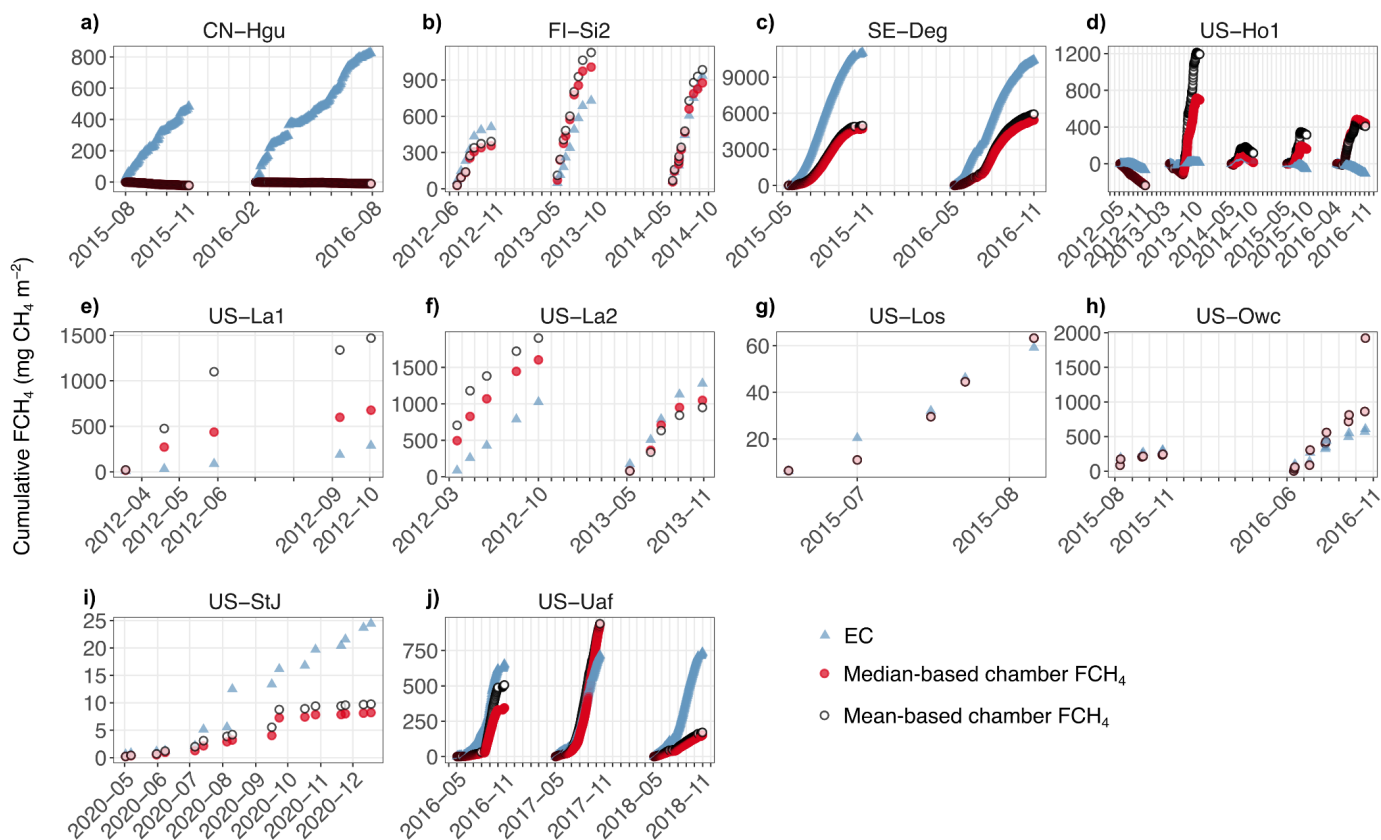


**Figure B16.** Cumulative sums of ecosystem-scale (eddy covariance; EC) and plot-scale (chamber) methane ( $\text{CH}_4$ ) flux ( $\text{FCH}_4$ ) at the daily scale across sites (a-j). Blue triangles represent EC, red points chamber  $\text{FCH}_4$  calculated from the median-based aggregation, and white points chamber  $\text{FCH}_4$  calculated from the mean-based aggregation. Note that since the chamber  $\text{FCH}_4$  data at FI-Si2, US-La1, and US-La2 lacked hourly timestamps, we roughly estimated daily cumulative  $\text{FCH}_4$  by using the daily chamber  $\text{FCH}_4$  median or mean for all 24 hours of the measurement date (EC cumulative  $\text{FCH}_4$  was calculated based on daily half-hourly  $\text{FCH}_4$  from FLUXNET- $\text{CH}_4$ ), and these estimates should thus be interpreted with caution.

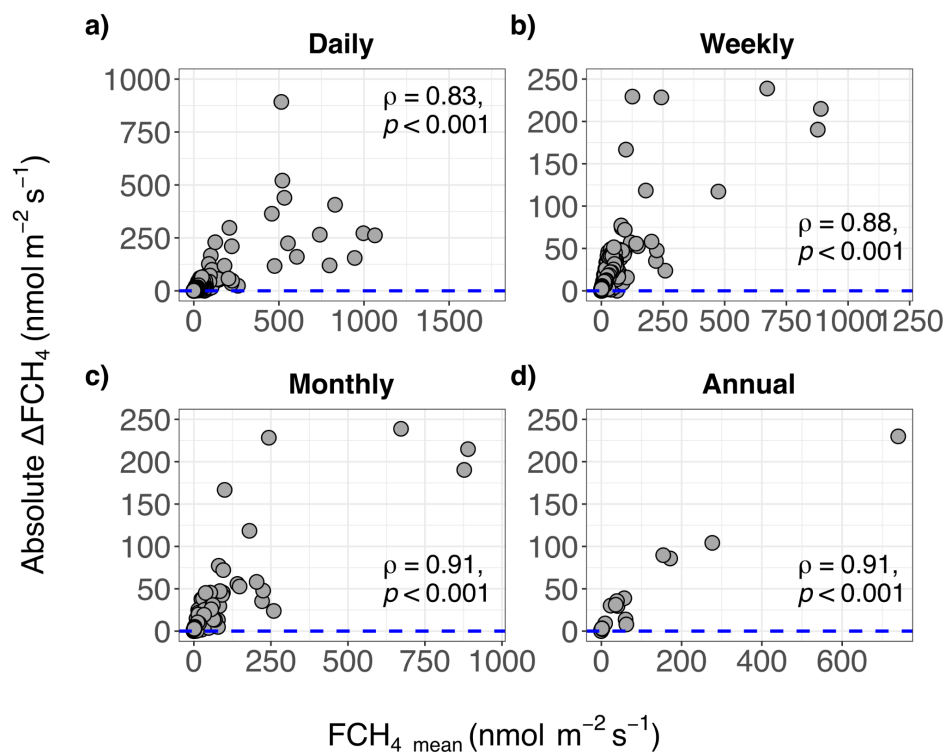


**Figure B17.** The relationship between methane ( $CH_4$ ) flux ( $FCH_4$ ) magnitude and absolute difference between ecosystem- and plot-scale  $FCH_4$  ( $\Delta FCH_4$ ) with outliers in daily (a), weekly (b), monthly (c) and annual (d) scales.  $FCH_{4\_mean}$  is the row-wise mean of eddy covariance (EC)  $FCH_4$  and chamber  $FCH_4$ , and EC-chamber  $FCH_4$  difference ( $\Delta FCH_4$ ) was calculated by subtracting chamber  $FCH_4$  from EC  $FCH_4$ . Positive  $\Delta FCH_4$  indicates higher EC  $FCH_4$  than chamber  $FCH_4$  and negative values higher chamber  $FCH_4$  than EC  $FCH_4$ . The blue dashed line represents the line of equality where EC  $FCH_4$  and chamber  $FCH_4$  are equal.  $\rho$  represents Spearman correlation coefficient, followed by its statistical significance ( $\alpha = 0.05$ ). Higher  $\rho$  represents stronger deviation from the line of equality, i.e.,  $\Delta FCH_4 = 0$  while perfect agreement between chamber and EC  $FCH_4$  would result in  $\rho = 0$ .

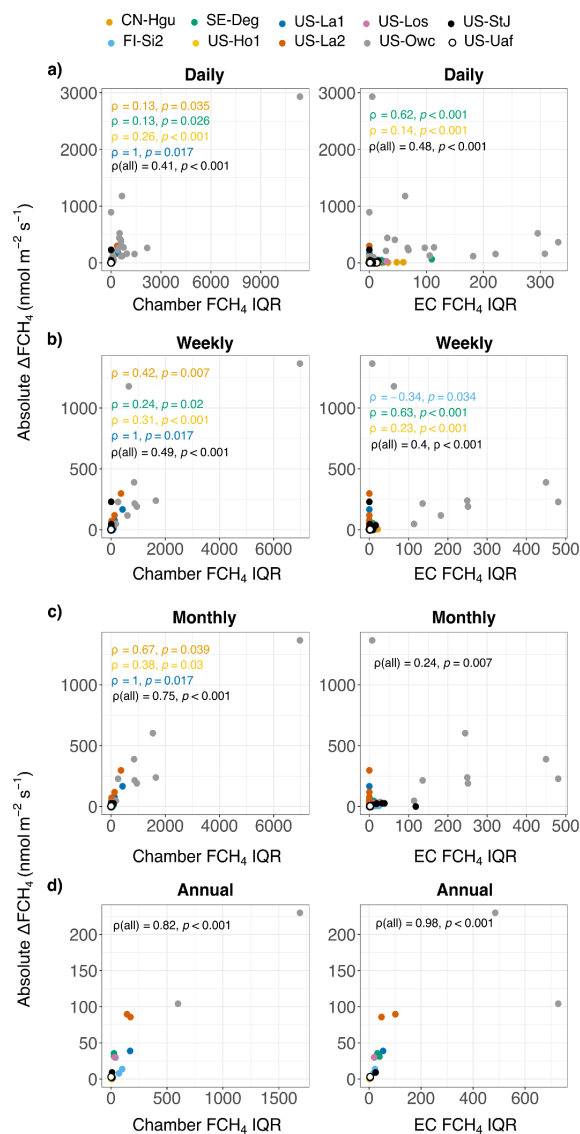
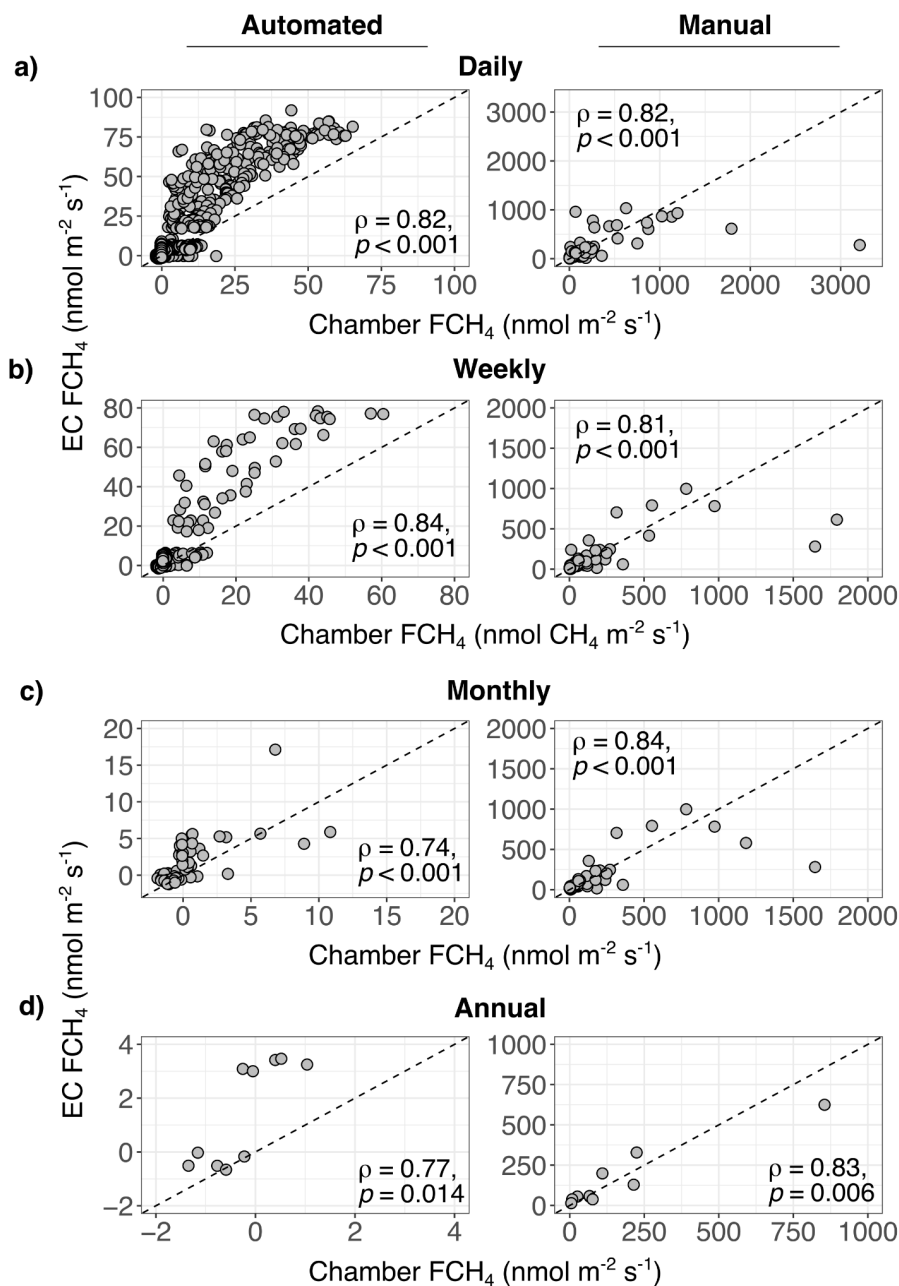


**Figure B18.** Untransformed absolute difference between ecosystem (eddy covariance; EC)- and plot-scale (chamber) methane (CH<sub>4</sub>) flux (FCH<sub>4</sub>) ( $\Delta FCH_4$ ), chamber and EC FCH<sub>4</sub> IQR in daily (a), weekly (b), monthly (c), and annual (d) aggregations. Different colors represent individual sites. Plots in the left panel show the relationship between daily variation in FCH<sub>4</sub> between individual chambers within each site and site-level absolute  $\Delta FCH_4$ . The right side panel shows the same but with daily

variation in EC FCH<sub>4</sub>. The strength and general direction of the relationship was measured with Spearman correlation coefficient ( $\rho$ ). “ $\rho$ (all)” refers to the Spearman correlation for the whole dataset.



955 **Figure B19.** Automated (left panel) and manual (right panel) chamber methane (CH<sub>4</sub>) flux (FCH<sub>4</sub>) had strong positive relationships with EC FCH<sub>4</sub> across sites and temporal scales (a to d). The dashed line represents the 1:1 line, and  $\rho$  Spearman

correlation coefficient of the relationship. Automated chambers were included in four sites (CN-Hgu, SE-Deg, US-Ho1, and US-Uaf) and manual chambers in six sites (FI-Si2, US-La1, US-La2, US-Los, US-Owc, and US-StJ). Half-hourly and hourly plots are in Fig. 3. Note different x and y axis scales.

## 960 Appendix C: Supplementary tables (Tables C1-C14)

**Table C1.** Methodological and data details of the site chamber (CH) and eddy covariance (EC) measurement systems. “CH method” refers to whether the chambers are manual or automated, and whether chambers were dark or transparent to sunlight. CH meas. frequency = chamber measurement frequency. CH-EC overlap is the total duration of overlap between chamber and EC measurements in days (note: the measurements are spread out over different seasons and years; see Fig. B1 and Table 1).  
 965 Gap-filled EC is the percentage of ANN-gap-filled EC methane (CH<sub>4</sub>) flux (FCH<sub>4</sub>) values of all EC FCH<sub>4</sub> values per site (in the unaggregated data set). Further details of the CH and EC measurement systems can be found in the corresponding references. Abbreviations in “CH analyzer”: LI-COR = LI-COR Biosciences, Nebraska, USA; Picarro = Picarro Inc., Santa Clara, CA, USA; Los Gatos = Los Gatos Research Inc., San Jose, CA, USA; Aerodyne = TILDAS CS, Aerodyne Research Inc., Billerica, MA, USA; Varian = Varian, Inc., Palo Alto, CA, USA; Shimadzu = Shimadzu Scientific Instruments, Kyoto,  
 970 Japan.

FLUX NET-CH <sub>4</sub> ID	Location (lat, lon)	CH method	CH analyzer	EC analyzer	EC tower height (m)	No. of CH	CH meas. frequency	EC-CH start, end year	EC-CH overlap days	Gap-filled EC (%)	CH data ref.	EC data ref.
CN-Hgu	32.845 278, 102.59	automated, dark	near-infrared laser gas analyzer (model 915-0011, Los Gatos)	open-path infrared gas analyzer (LI-7700; LI-COR)	3	3	56 min	2015, 2016	363	44	Wang et al. (2021)	Niu and Chen (2020)
FI-Si2	61.837 2, 24.196 7	manual, dark	gas chromatograph (Agilent Technologies 7890A) and liquid handler (Gilson GX-271)	open-path gas analyzer (LI-7700, LI-COR)	2.4	18	1-3 x month	2012, 2014	26	5	Korrensalo et al. (2018)	Alekseychik et al. (2021), Vesala et al. (2020)
SE-Deg	64.182 029, 19.556 539	automated, dark and transparent	cavity ring-down spectrometer (model GGA-24EP, Los Gatos)	Closed-path gas analyzer (Model 911-0011-0004,	3	4	1 hour	2015, 2016	338	31	Bond-Lamberty et al. (2020), Järveoja et al. (2018)	Nilsson and Peichl (2020)

Los Gatos)												
<b>US-Ho1</b>	45.204 1, - 68.740 2	automated, dark	cavity ring-down spectrometer (model G2121-i; Picarro) & Aerodyne Quantum Cascade Laser (Aerodyne)	Closed-path gas analyzer (model G2311-f, Picarro cavity ring-down spectrometer)	31	20	ca. 1 hour (varied between years and chambers)	2012, 2016	759	52	Richards on et al. (2019)	Richardson and Hollinger (2020)
<b>US-La1</b>	29.501 3, - 90.444 9	manual, dark	gas chromatograph (model CP-3800, Varian)	open-path gas analyzer (LI-7700, LI-COR)	3.4	3	1 x month	2012, 2012	5	0	Krauss et al. (2016)	Holm et al. (2020a)
<b>US-La2</b>	29.858 7, - 90.286 9	manual, dark	gas chromatograph (model CP-3800, Varian)	open-path gas analyzer (LI-7700, LI-COR)	3.6	3	1 x month	2012, 2013	10	10	Krauss et al. (2016)	Holm et al. (2020b)
<b>US-Los</b>	46.082 7, - 89.979 2	manual, dark	near-infrared laser gas analyzer (Los Gatos UGGA)	open-path gas analyzer (LI-7700, LI-COR)	10.2	14	1-3 x month	2015, 2015	5	31	Desai (2025b)	Desai (2025a), Desai and Thom (2020)
<b>US-Owc</b>	41.379 51667, - 82.512 4667	manual, dark	gas chromatograph (GC-2014, Shimadzu)	open-path gas analyzer (LI-7700, LI-COR)	2.7	4	1 x month	2015, 2016	18	50	Bohrer et al. (2019)	Bohrer et al. (2020)
<b>US-StJ</b>	39.088 21106, - 75.437 22534	manual, dark	near-infrared laser gas analyzer (Los Gatos)	open-path gas analyzer (LI-7700, LI-COR)	3.5	5	1-2 x month	2020	16	0	Hill and Vargas (2022)	Vargas (2018)
<b>US-Uaf</b>	64.866 27, - 147.85 553	automated, dark	near-infrared laser gas analyzer (Los Gatos)	closed-path gas analyzer (RMT200 Fast Methane Analyzer or Greenhouse Gas	6	5	30 min	2016, 2018	458	59	Ueyama et al. (2022)	Iwata et al. (2020)

**Table C2.** Details of chamber methane (CH<sub>4</sub>) flux (FCH<sub>4</sub>) data quality control and chamber placement rationale in the study sites. Data quality control was done by data providers prior to sharing chamber FCH<sub>4</sub> data, and a summary of the methods are listed here. For more details, please see the site-specific references. EC = eddy covariance.

Site	FCH <sub>4</sub> corrections	Low-quality FCH <sub>4</sub> data filtering	Ebullition removal	Chamber placement rationale	Reference
CN-Hgu	Air temperature and H <sub>2</sub> O dilution	$R^2 < 0.9$	No (ebullition assumed negligible)	To investigate the effect of experimental warming on CH <sub>4</sub> uptake. Both the warming treatment and the control each included three chambers. The chambers were located approx. 500 m from the EC tower and covered spatial variation in environmental conditions	Wang et al. (2021)
FI-Si2	Air temperature	Nonlinear changes in CH <sub>4</sub> concentrations removed (altogether 10.4% of measurements removed)	Yes	To cover spatial variation in vegetation and environmental conditions (three chambers per plant community/bog microtopography type: high hummock, hummock, high lawn, lawn, hollow, and bare peat). Chamber placement was based on a systematic survey of	Korrensalo et al. (2018)

SE-Deg	Air temperature and H <sub>2</sub> O dilution	$R^2 < 0.95$ and RMSE $> 0.02$	Yes	<p>surface cover within a 200 m radius the EC tower</p> <p>To understand how different microtopographic forms (water table level and vegetation composition) explain EC flux patterns. In addition, cross-checking the information from EC at the diel scale, especially during calm night-time conditions</p>	Bond-Lamberty et al. (2020), Järveoja et al. (2018)
US-Ho1	Air temperature, air pressure and H <sub>2</sub> O dilution	$R^2 < 0.9$	No	To sample representative land cover classes covered by the EC footprint for measuring CO <sub>2</sub> , CH <sub>4</sub> and N <sub>2</sub> O (3-5 chambers per upland control, upland trenched, transitional and wetland class)	Richardson et al. (2019)
US-La1	Air temperature	None (few data points discarded based on very low $R^2$ and standard deviation $> 3$ from the mean)	No	To sample representative areas (chambers installed around vegetation clusters to avoid cutting roots. Open water not included) within the EC footprint.	Krauss et al. (2016)
US-La2	Air temperature	None (few data points discarded based on very low $R^2$ and standard	No	To sample representative areas within the EC footprint (chambers	Krauss et al. (2016)

US-Los	Air temperature, air pressure and H <sub>2</sub> O dilution	deviation > 3 from the mean) None (but most mean R <sup>2</sup> > 0.9 across replicates; ca. 15% R <sup>2</sup> < 0.66)	No	installed around boardwalks) To sample representative landscapes (hummocks, hollows, shrubs, open water) within the EC footprint to evaluate drivers, spatial variation, and hotspots/moments of FCH <sub>4</sub> and ways to scale fluxes from chambers to EC to landscape	Desai (2025b)
US-Owc	Air temperature and air pressure	R <sup>2</sup> ≤ 0.85 (whole chamber measurement discarded if in n > 3 observations within measurement)	Yes	To sample random locations with equal sample size per patch type (open water, <i>Typha</i> sp., floating vegetation). Chambers were placed floating on the water, excluding plants	Bohrer et al. (2019)
US-StJ	Air temperature, air pressure and H <sub>2</sub> O dilution	R <sup>2</sup> < 0.9 (based on CO <sub>2</sub> flux measured simultaneously)	Yes	To sample representative (based on marsh vegetation) areas within the EC footprint that were safely accessible. The main goal was to investigate when to measure CH <sub>4</sub> fluxes with manual chambers in a spatiotemporally heterogeneous wetland and using this information, to see how	Hill and Vargas (2022a, 2022b)

and when to combine both EC and manual chamber measurements for analyses.

US-Uaf	Air temperature, air pressure and H <sub>2</sub> O dilution	RMSE > 0.3 ppb or R <sup>2</sup> < 0.1	No (ebullition assumed negligible)	To cover spatial variation in forest floor microtopography and vegetation in 2016-2018 (one chamber per wet <i>Sphagnum</i> , wet <i>Carex</i> spp., dry lichen, and dry <i>Carex</i> spp.)	Ueyama et al. (2022)
--------	---	--	------------------------------------	---	----------------------

---

980

985

990

**Table C3.** Details of the used environmental data. FLUXNET-CH<sub>4</sub> soil temperature data was from the topmost soil depths (2-10 cm below soil surface). Abbreviations: NEE = net ecosystem exchange, u\* = friction velocity, WD = wind direction, WS = wind speed, VPD = vapor pressure deficit, PA = air pressure, WTL = water table level, TS = soil temperature, ANN = artificial neural network, MDS = marginal distribution sampling.

Site	Environmental variable	Data	Data reference
<b>CN-Hgu</b>	NEE	Half-hourly FLUXNET-CH <sub>4</sub> : ANN-gap-filled	Delwiche et al. (2021); Knox et al. (2019)
	u*	Half-hourly FLUXNET-CH <sub>4</sub> : ANN-gap-filled	
	WD	Half-hourly FLUXNET-CH <sub>4</sub> : ANN-gap-filled	
	WS	Half-hourly FLUXNET-CH <sub>4</sub> : gap-filled	
	VPD	Half-hourly FLUXNET-CH <sub>4</sub> : gap-filled	
	PA	Half-hourly FLUXNET-CH <sub>4</sub> : gap-filled	
	WTL	-	
TS	Half-hourly FLUXNET-CH <sub>4</sub>	Delwiche et al. (2021); Knox et al. (2019)	
<b>FI-Si2</b>	NEE	Half-hourly FLUXNET-CH <sub>4</sub> : ANN-gap-filled	Delwiche et al. (2021); Knox et al. (2019)
	u*	Half-hourly FLUXNET-CH <sub>4</sub> : ANN-gap-filled	
	WD	Half-hourly FLUXNET-CH <sub>4</sub> : ANN-gap-filled	
	WS	Half-hourly FLUXNET-CH <sub>4</sub> : gap-filled	
	VPD	Half-hourly FLUXNET-CH <sub>4</sub> : gap-filled	
	PA	Half-hourly FLUXNET-CH <sub>4</sub> : gap-	

		filled	
	WTL	Mean of daily gap-filled FLUXNET-CH <sub>4</sub> WTL and chamber- associated WTL	Delwiche et al. (2021); Knox et al. (2019), Korrensalo et al. (2018)
	TS	Chamber-associated TS	Korrensalo et al. (2018)
<b>SE-Deg</b>	NEE	Half-hourly FLUXNET-CH <sub>4</sub> : ANN- gap-filled	
	u*	Half-hourly FLUXNET-CH <sub>4</sub> : ANN- gap-filled	
	WD	Half-hourly FLUXNET-CH <sub>4</sub> : ANN- gap-filled	Delwiche et al. (2021); Knox et al. (2019)
	WS	Half-hourly FLUXNET-CH <sub>4</sub> : gap- filled	
	VPD	Half-hourly FLUXNET-CH <sub>4</sub> : gap- filled	
	PA	Half-hourly FLUXNET-CH <sub>4</sub> : gap- filled	
	WTL	Mean of half-hourly gap-filled FLUXNET-CH <sub>4</sub> WTL and chamber- associated WTL	Delwiche et al. (2021); Knox et al. (2019); Järveoja et al. (2018); Bond- Lamberty et al. (2020)
	TS	Mean of half-hourly FLUXNET- CH <sub>4</sub> TS and chamber-associated TS	
<b>US-Ho1</b>	NEE	Half-hourly FLUXNET-CH <sub>4</sub> : ANN- gap-filled	
	u*	Half-hourly FLUXNET-CH <sub>4</sub> : ANN- gap-filled	
	WD	Half-hourly FLUXNET-CH <sub>4</sub> : ANN- gap-filled	Delwiche et al. (2021); Knox et al. (2019)
	WS	Half-hourly FLUXNET-CH <sub>4</sub> : gap- filled	
	VPD	Half-hourly FLUXNET-CH <sub>4</sub> : gap- filled	
	PA	Half-hourly FLUXNET-CH <sub>4</sub> : gap-	

		filled	
	WTL	Half-hourly FLUXNET-CH <sub>4</sub> : gap-filled	
	TS	Chamber-associated TS	Richardson et al. (2019)
<b>US-La1 &amp; US-La2</b>	NEE	Half-hourly FLUXNET-CH <sub>4</sub> : ANN-gap-filled	
	u*	Half-hourly FLUXNET-CH <sub>4</sub> : ANN-gap-filled	
	WD	Half-hourly FLUXNET-CH <sub>4</sub> : ANN-gap-filled	Delwiche et al. (2021);
	WS	Half-hourly FLUXNET-CH <sub>4</sub> : gap-filled	Knox et al. (2019)
	VPD	Half-hourly FLUXNET-CH <sub>4</sub> : gap-filled	
	PA	Half-hourly FLUXNET-CH <sub>4</sub> : gap-filled	
	WTL	Mean of daily FLUXNET-CH <sub>4</sub> WTL and chamber-associated WTL	Delwiche et al. (2021);
	TS	Mean of daily gap-filled FLUXNET-CH <sub>4</sub> TS and chamber-associated TS	Knox et al. (2019); Krauss et al. (2016)
<b>US-Los</b>	NEE	Half-hourly FLUXNET-CH <sub>4</sub> : ANN-gap-filled	
	u*	Half-hourly FLUXNET-CH <sub>4</sub> : ANN-gap-filled	
	WD	Half-hourly FLUXNET-CH <sub>4</sub> : ANN-gap-filled	Delwiche et al. (2021);
	WS	Half-hourly FLUXNET-CH <sub>4</sub> : gap-filled	Knox et al. (2019)
	VPD	Half-hourly FLUXNET-CH <sub>4</sub> : gap-filled	
	PA	Half-hourly FLUXNET-CH <sub>4</sub> : gap-filled	

	WTL	Mean of half-hourly gap-filled FLUXNET-CH <sub>4</sub> WTL and chamber- associated WTL	Delwiche et al. (2021); Knox et al. (2019); Pugh et al. (2018)
	TS	Mean of half-hourly FLUXNET- CH <sub>4</sub> TS and chamber-associated TS	
<b>US-Owc</b>	NEE	Half-hourly FLUXNET-CH <sub>4</sub> : ANN- gap-filled	
	u*	Half-hourly FLUXNET-CH <sub>4</sub> : ANN- gap-filled	
	WD	Half-hourly FLUXNET-CH <sub>4</sub> : ANN- gap-filled	Delwiche et al. (2021); Knox et al. (2019)
	WS	Half-hourly FLUXNET-CH <sub>4</sub> : gap- filled	
	VPD	Half-hourly FLUXNET-CH <sub>4</sub> : gap- filled	
	PA	Half-hourly FLUXNET-CH <sub>4</sub> : gap- filled	
	WTL	Mean of half-hourly gap-filled FLUXNET-CH <sub>4</sub> WTL and chamber- associated WTL	Delwiche et al. (2021); Knox et al. (2019); Bohrer et al. (2019)
	TS	Half-hourly FLUXNET-CH <sub>4</sub> TS	Delwiche et al. (2021); Knox et al. (2019)
<b>US-StJ</b>	NEE	Half-hourly: MDS-gap-filled	
	u*	Half-hourly: not gap-filled	
	WD	Half-hourly: not gap-filled	Hill and Vargas (2022); Vargas (2018)
	WS	Half-hourly: not gap-filled	
	VPD	Half-hourly: not gap-filled	

	PA	Half-hourly: not gap-filled	
	WTL	Half-hourly: gap-filled with a linear relationship with NOAA water table level	
	TS	Half-hourly: gap-filled with a linear relationship with water temperature	
<b>US-Uaf</b>	NEE	Half-hourly FLUXNET-CH <sub>4</sub> : ANN-gap-filled	
	u*	Half-hourly FLUXNET-CH <sub>4</sub> : ANN-gap-filled	
	WD	Half-hourly FLUXNET-CH <sub>4</sub> : ANN-gap-filled	Delwiche et al. (2021);
	WS	Half-hourly FLUXNET-CH <sub>4</sub> : gap-filled	Knox et al. (2019)
	VPD	Half-hourly FLUXNET-CH <sub>4</sub> : gap-filled	
	PA	Half-hourly FLUXNET-CH <sub>4</sub> : gap-filled	
	WTL	Mean of half-hourly gap-filled FLUXNET-CH <sub>4</sub> WTL and chamber-associated WTL	Delwiche et al. (2021);
	TS	Mean of half-hourly FLUXNET-CH <sub>4</sub> TS and chamber-associated TS	Knox et al. (2019); Ueyama et al. (2023)

**Table C4.** Descriptive statistics and Wilcoxon-Mann-Whitney test results based on temporal aggregations from chamber and eddy covariance (EC) methane (CH<sub>4</sub>) flux (FCH<sub>4</sub>) means instead of medians. Proportions of annual chamber and EC CH<sub>4</sub> emission (i.e., FCH<sub>4</sub> ≤ 0 excluded) above the 90<sup>th</sup> percentile (p90) are reported to highlight the contribution of high CH<sub>4</sub> emission values to FCH<sub>4</sub>. Abbreviations: IQR = interquartile range, SD = standard deviation, CV = coefficient of variation (%), EC = eddy covariance.

<b>Data set</b>	<b>ΔFCH<sub>4</sub> median (IQR), nmol m<sup>-2</sup> s<sup>-1</sup></b>	<b>ΔFCH<sub>4</sub> mean (SD), nmol m<sup>-2</sup> s<sup>-1</sup></b>	<b>ΔFCH<sub>4</sub> CV (%)</b>	<b>Wilcoxon- Mann- Whitney test</b>	<b>Chamber FCH<sub>4</sub> p90 (% of total FCH<sub>4</sub>)</b>	<b>EC FCH<sub>4</sub> p90 (% of total FCH<sub>4</sub>)</b>
<b>Half-hourly</b>	1.23 (5.74)	4.84 (18.56)	206	$p < 0.001$ (n <sub>EC</sub> = 74482, n <sub>CH</sub> = 74482)	36.42 (46)	64.31 (44)
<b>Hourly</b>	1.19 (5.42)	4.76 (16.28)	198	$p < 0.001$ (n <sub>EC</sub> = 40072, n <sub>CH</sub> = 40072)	36.62 (46)	75.81 (24)
<b>Daily</b>	1.11 (4.77)	-1.16 (170.67)	1106	$p < 0.001$ (n <sub>EC</sub> = 1879, n <sub>CH</sub> = 1879)	43.47 (78)	66.67 (60)
<b>Weekly</b>	1.03 (6.73)	-19.55 (284.31)	770	$p = 0.015$ (n <sub>EC</sub> = 349, n <sub>CH</sub> = 349)	98.12 (82)	77.82 (64)
<b>Monthly</b>	1.05 (13.15)	-58.55 (472.15)	566	$p = 0.511$ (n <sub>EC</sub> = 121, n <sub>CH</sub> = 121)	315.38 (78)	218.47 (63)
<b>Annual</b>	0.28 (16.93)	-70.94 (311.86)	333	$p = 0.972$ (n <sub>EC</sub> = 22, n <sub>CH</sub> = 22)	307.19 (72)	251.67 (60)

1005

**Table C5.** Descriptive statistics and Wilcoxon-Mann-Whitney test results for the difference between ecosystem- and plot-scale methane (CH<sub>4</sub>) flux (FCH<sub>4</sub>) ( $\Delta$ FCH<sub>4</sub>) based on cumulative eddy covariance (EC) and chamber FCH<sub>4</sub> (mg CH<sub>4</sub> m<sup>-2</sup>) at daily to annual aggregations (note: cumulative FCH<sub>4</sub> were calculated only for exact EC-chamber FCH<sub>4</sub> timestamps and do not represent cumulative sums for ecosystem CH<sub>4</sub> budget calculations). Due to a lack of hourly timestamps in the chamber FCH<sub>4</sub> data at FI-Si2, US-La1 and US-La2, these three sites were excluded from this table, resulting in n = 7 sites. Results are given separately for data sets based on median (left) and mean (right) aggregations of chamber and EC FCH<sub>4</sub> at each temporal scale. The EC and chamber data sample sizes in Wilcoxon-Mann-Whitney tests are reported as n<sub>EC</sub> and n<sub>CH</sub>, respectively. Abbreviations: IQR = interquartile range, SD = standard deviation, CV = coefficient of variation (%).

	Median-based aggregation				Mean-based aggregation			
Data set	$\Delta$ FCH <sub>4</sub> median (IQR), mg CH <sub>4</sub> m <sup>-2</sup>	$\Delta$ FCH <sub>4</sub> mean (SD), mg CH <sub>4</sub> m <sup>-2</sup>	$\Delta$ FCH <sub>4</sub> CV (%)	Wilcoxon-Mann-Whitney test	$\Delta$ FCH <sub>4</sub> median (IQR), mg CH <sub>4</sub> m <sup>-2</sup>	$\Delta$ FCH <sub>4</sub> mean (SD), mg CH <sub>4</sub> m <sup>-2</sup>	$\Delta$ FCH <sub>4</sub> CV (%)	Wilcoxon-Mann-Whitney test
<b>Daily</b>	1.29 (5.5)	5.88 (29.22)	303	$p < 0.001$ (n <sub>EC</sub> = 1838, n <sub>CH</sub> = 1838)	1.15 (5.47)	4.99 (29.1)	305	$p < 0.001$ (n <sub>EC</sub> = 1838, n <sub>CH</sub> = 1838)
<b>Weekly</b>	6.39 (32.68)	34.65 (117.8)	212	$p = 0.006$ (n <sub>EC</sub> = 312, n <sub>CH</sub> = 312)	5.53 (32.52)	29.37 (116.05)	211	$p = 0.028$ (n <sub>EC</sub> = 312, n <sub>CH</sub> = 312)
<b>Monthly</b>	13.4 (93.83)	117.5 (385.22)	213	$p = 0.314$ (n <sub>EC</sub> = 92, n <sub>CH</sub> = 92)	8.85 (88.37)	99.62 (385.22)	209	$p = 0.485$ (n <sub>EC</sub> = 92, n <sub>CH</sub> = 92)
<b>Annual</b>	37.1 (742.78)	675.63 (2024.37)	193	$p = 0.897$ (n <sub>EC</sub> = 16, n <sub>CH</sub> = 16)	35.23 (781.38)	572.81 (1945.22)	188	$p = 0.897$ (n <sub>EC</sub> = 16, n <sub>CH</sub> = 16)

1020

**Table C6.** Linear mixed effects model results for assessing the slopes between ecosystem-scale (eddy covariance; EC) methane (CH<sub>4</sub>) flux (FCH<sub>4</sub>) and plot-scale (chamber) FCH<sub>4</sub>. To meet residual normality assumptions of linear mixed models, EC FCH<sub>4</sub> was transformed with inverse hyperbolic sine (IHS) and the fixed effect estimates, *p*-values and standard errors (SE) are in transformed scale. Average marginal effects (AME) and their 95% confidence intervals (CI) are reported in the back-transformed units (nmol m<sup>-2</sup> s<sup>-1</sup>) and represent the average change in EC FCH<sub>4</sub> with a 1 nmol m<sup>-2</sup> s<sup>-1</sup> increase in chamber FCH<sub>4</sub> across all chamber FCH<sub>4</sub> observations. AME CIs were obtained with parametric simulation from the fixed effect estimate and covariance. Half-hourly and hourly models are not included due to non-convergence and residual non-normality.

<b>Model</b>	<b>Fixed effect</b>	<b>Estimate <math>\beta</math> (IHS scale)</b>	<b><i>p</i>-value</b>	<b>SE</b>	<b>AME (95% CI)</b>
<b>Daily</b>	Intercept	3.647	< 0.001	0.657	0.007 (0.0006-
	Chamber FCH <sub>4</sub>	0.0004	0.031	0.0002	0.032)
<b>Weekly</b>	Intercept	3.612	< 0.001	0.645	0.011 (-0.0007-
	Chamber FCH <sub>4</sub>	0.0006	0.066	0.0003	0.049)
<b>Monthly</b>	Intercept	3.591	< 0.001	0.646	0.009 (-0.005-
	Chamber FCH <sub>4</sub>	0.0005	0.183	0.0004	0.049)
<b>Annual</b>	Intercept	3.653	< 0.001	0.636	0.02 (0.002-0.088)
	Chamber FCH <sub>4</sub>	0.001	0.044	0.0004	

1030

1035

**Table C7.** Wilcoxon-Mann-Whitney test results for half-hourly aggregation. The eddy covariance (EC) and chamber data sample sizes in Wilcoxon Mann-Whitney tests are reported as  $n_{EC}$  and  $n_{CH}$ , respectively. Proportions of annual chamber and EC methane ( $CH_4$ ) emission (i.e.,  $CH_4$  flux ( $FCH_4$ )  $\leq 0$  excluded) above the 90<sup>th</sup> percentile (p90) are reported as the mean of year-specific 90<sup>th</sup> percentiles (not in parentheses) and percentages (in parentheses). This data set contains chamber measurements only from automated chambers (n=4 sites). Abbreviations: IQR = interquartile range, CV = coefficient of variation (%).

Site	Mean EC FCH <sub>4</sub> (SD), <i>nmol m<sup>-2</sup>s<sup>-1</sup></i>	Mean chamber FCH <sub>4</sub> (SD), <i>nmol m<sup>-2</sup>s<sup>-1</sup></i>	Median EC FCH <sub>4</sub> (IQR, CV), <i>nmol m<sup>-2</sup>s<sup>-1</sup></i>	Median chamber FCH <sub>4</sub> (IQR, CV), <i>nmol m<sup>-2</sup>s<sup>-1</sup></i>	Median $\Delta FCH_4$ (IQR, CV), <i>nmol m<sup>-2</sup>s<sup>-1</sup></i>	Chamber FCH <sub>4</sub> p90 (% of total FCH <sub>4</sub> )	EC FCH <sub>4</sub> p90 (% of total FCH <sub>4</sub> )	Wilcoxon-Mann- Whitney test
CN-Hgu	4.73 (25.36)	-0.12 (0.35)	3.0 (6.0, 241)	-0.1 (0.24, 165)	3.12 (6.04, 239)	0.63 (55)	20 (58)	$p < 0.001$ ( $n_{EC} = 9571$ , $n_{CH} = 9571$ )
SE-Deg	53.18 (22.31)	25.19 (18.24)	54.1 (36.28, 42)	21.61 (24.24, 72)	26.94 (23.98, 62)	50.5 (25)	79.85 (17)	$p < 0.001$ ( $n_{EC} = 13987$ , $n_{CH} = 13987$ )
US-Ho1	-0.21 (1.84)	1.21 (10.47)	-0.4 (1.32, 158)	-0.89 (1.44, 334)	0.38 (2.36, 311)	18.06 (49)	3.24 (43)	$p < 0.001$ ( $n_{EC} = 30716$ , $n_{CH} = 30716$ )
US-Uaf	3.61 (4.35)	2.45 (3.58)	3.39 (4.17, 107)	0.78 (2.32, 146)	1.22 (3.76, 146)	5.73 (36)	6.99 (29)	$p < 0.001$ ( $n_{EC} = 20208$ , $n_{CH} = 20208$ )

1045

**Table C8.** Wilcoxon-Mann-Whitney test results for hourly aggregation. The eddy covariance (EC) and chamber data sample sizes in Wilcoxon Mann-Whitney tests are reported as  $n_{EC}$  and  $n_{CH}$ , respectively. Proportions of annual chamber and EC methane ( $CH_4$ ) emission (i.e.,  $CH_4$  flux ( $FCH_4$ )  $\leq 0$  excluded) above the 90<sup>th</sup> percentile (p90) are reported as the mean of year-specific 90<sup>th</sup> percentiles (not in parentheses) and percentages (in parentheses). This data set contains chamber measurements only from automated chambers ( $n = 4$  sites). Abbreviations: IQR = interquartile range, CV = coefficient of variation (%).

Site	Mean EC FCH <sub>4</sub> (SD), <i>nmol CH<sub>4</sub> m<sup>-2</sup>s<sup>-1</sup></i>	Mean chamber FCH <sub>4</sub> (SD), <i>nmol CH<sub>4</sub> m<sup>-2</sup>s<sup>-1</sup></i>	Median EC FCH <sub>4</sub> (IQR, CV), <i>nmol CH<sub>4</sub> m<sup>-2</sup>s<sup>-1</sup></i>	Median chamber FCH <sub>4</sub> (IQR, CV), <i>nmol CH<sub>4</sub> m<sup>-2</sup>s<sup>-1</sup></i>	Median $\Delta FCH_4$ (IQR, CV), <i>nmol CH<sub>4</sub> m<sup>-2</sup>s<sup>-1</sup></i>	Chamber FCH <sub>4</sub> p90 (% of total FCH <sub>4</sub> )	EC FCH <sub>4</sub> p90 (% of total FCH <sub>4</sub> )	Wilcoxon-Mann- Whitney test
<b>CN-Hgu</b>	4.56 (22.87)	-0.11 (0.26)	3.0 (6.11, 229)	-0.09 (0.2, 145)	3.08 (5.99, 227)	0.6 (54)	19.75 (56)	$p < 0.001$ ( $n_{EC} = 5305$ , $n_{CH} = 5305$ )
<b>SE-Deg</b>	53.17 (22.05)	25.11 (17.42)	54.41 (36.28, 41)	21.6 (25.34, 69)	26.9 (23.04, 51)	49.59 (23)	79.67 (17)	$p < 0.001$ ( $n_{EC} = 7243$ , $n_{CH} = 7243$ )
<b>US-Ho1</b>	-0.21 (1.53)	-0.37 (3.05)	-0.36 (1.23, 149)	-0.95 (1.27, 192)	0.47 (1.95, 188)	7.43 (53)	2.82 (41)	$p < 0.001$ ( $n_{EC} = 17215$ , $n_{CH} = 17215$ )
<b>US-Uaf</b>	3.61 (3.71)	2.37 (3.53)	3.32 (4.04, 96)	0.73 (2.17, 149)	1.28 (3.55, 137)	5.47 (35)	7.02 (27)	$p < 0.001$ ( $n_{EC} = 10309$ , $n_{CH} = 10309$ )

1055

1060 **Table C9.** Wilcoxon-Mann-Whitney test results for daily aggregation. The eddy covariance (EC) and chamber data sample sizes in Wilcoxon-Mann-Whitney tests are reported as  $n_{EC}$  and  $n_{CH}$ , respectively. Proportions of annual chamber and EC  $CH_4$  emission (i.e.,  $CH_4$  flux ( $FCH_4$ )  $\leq 0$  excluded) above the 90<sup>th</sup> percentile (p90) are reported as the mean of year-specific 90<sup>th</sup> percentiles (not in parentheses) and percentages (in parentheses). This dataset contains all sites ( $n=10$ ). Note: due to small sample sizes ( $n=5$ ) in US-La1 and US-Los, the Wilcoxon-Mann-Whitney test results should be interpreted with caution.

1065 Abbreviations: IQR = interquartile range, CV = coefficient of variation (%).

Site	Mean EC FCH <sub>4</sub> (SD), nmol CH <sub>4</sub> m <sup>-2</sup> s <sup>-1</sup>	Mean chamber FCH <sub>4</sub> (SD), nmol CH <sub>4</sub> m <sup>-2</sup> s <sup>-1</sup>	Median EC FCH <sub>4</sub> (IQR, CV), nmol CH <sub>4</sub> m <sup>-2</sup> s <sup>-1</sup>	Median chamber FCH <sub>4</sub> (IQR, CV), nmol CH <sub>4</sub> m <sup>-2</sup> s <sup>-1</sup>	Median $\Delta FCH_4$ (IQR, CV), nmol CH <sub>4</sub> m <sup>-2</sup> s <sup>-1</sup>	Chamber FCH <sub>4</sub> p90 (% of total FCH <sub>4</sub> )	EC FCH <sub>4</sub> p90 (% of total FCH <sub>4</sub> )	Wilcoxon-Mann- Whitney test
<b>CN-Hgu</b>	3.22 (1.79)	-0.12 (0.11)	3.0 (2.14, 55)	-0.07 (0.12, 93)	3.2 (2.21, 54)	0.04 (17)	5.69 (20)	$p < 0.001$ ( $n_{EC} = 265$ , $n_{CH} = 265$ )
<b>FI-Si2</b>	57.13 (18.74)	62.14 (37.85)	54.37 (21.48, 33)	49.46 (57.04, 61)	0.81 (30.53, 132)	98.37 (25)	77.5 (19)	$p = 0.737$ ( $n_{EC} = 26$ , $n_{CH} = 26$ )
<b>SE-Deg</b>	52.44 (20.75)	24.24 (15.76)	55.88 (39.7, 40)	21.39 (24.96, 65)	0.81 (30.53, 132)	48.56 (21)	78.16 (15)	$p < 0.001$ ( $n_{EC} = 317$ , $n_{CH} = 317$ )
<b>US-Ho1</b>	-0.43 (0.54)	-0.68 (1.67)	-0.45 (0.73, 96)	-1.01 (0.9, 130)	0.39 (1.22, 165)	2.04 (52)	0.4 (39)	$p < 0.001$ ( $n_{EC} = 759$ , $n_{CH} = 759$ )
<b>US-La1</b>	41.49 (29.79)	97.72 (65.37)	42.12 (53.85, 72)	116.91 (62.59, 67)	-45.43 (71.64, 115)	157.64 (37)	71.03 (34)	$p = 0.222$ ( $n_{EC} = 5$ , $n_{CH} = 5$ )
<b>US-La2</b>	163.74 (63.81)	191.35 (93.46)	150.22 (103.39, 39)	189.16 (117.65, 49)	5.75 (103.92, 141)	276.98 (32)	226.3 (30)	$p = 0.436$ ( $n_{EC} = 10$ , $n_{CH} = 10$ )
<b>US-Los</b>	35.37 (12.78)	9.61 (5.62)	38.75 (13.82, 36)	8.43 (4.09, 58)	27.75 (4.74, 37)	15.42 (38)	46.72 (28)	$p = 0.016$ ( $n_{EC} = 5$ , $n_{CH} = 5$ )

<b>US-Owc</b>	607.26 (289.11)	770.24 (766.66)	652.8 (490.18, 48)	579.95 (721.2, 100)	-108.22 (485.14, 169)	1306.07 (46)	936.62 (28)	$p = 0.988$ ( $n_{EC} = 18,$ $n_{CH} = 18)$
<b>US-StJ</b>	39.2 (58.96)	13.98 (27.01)	16.4 (29.69, 150)	5.26 (8.31, 193)	9.15 (20.85, 202)	22.15 (63)	73.94 (54)	$p = 0.007$ ( $n_{EC} = 16,$ $n_{CH} = 16)$
<b>US-Uaf</b>	3.5 (2.09)	2.15 (3.12)	3.49 (3.96, 60)	0.66 (2.0, 145)	1.27 (2.29, 111)	4.97 (25)	6.09 (20)	$p < 0.001$ ( $n_{EC} = 458,$ $n_{CH} = 458)$

1070

1075

1080 **Table C10.** Wilcoxon-Mann-Whitney test results for weekly aggregation. The eddy covariance (EC) and chamber data sample  
 sizes in Wilcoxon-Mann-Whitney tests are reported as  $n_{EC}$  and  $n_{CH}$ , respectively. Proportions of annual chamber and EC  
 methane ( $CH_4$ ) emission (i.e.,  $CH_4$  flux ( $FCH_4$ )  $\leq 0$  excluded) above the 90<sup>th</sup> percentile (p90) are reported as the mean of year-  
 specific 90<sup>th</sup> percentiles (not in parentheses) and percentages (in parentheses). This dataset contains all sites ( $n = 10$ ). Note:  
 1085 due to small sample sizes ( $n = 5$ ) in US-La1 and US-Los, the Wilcoxon-Mann-Whitney test results should be interpreted with  
 caution. Abbreviations: IQR = interquartile range, CV = coefficient of variation (%).

Site	Mean EC FCH <sub>4</sub> (SD), nmol CH <sub>4</sub> m <sup>-2</sup> s <sup>-1</sup>	Mean chamber FCH <sub>4</sub> (SD), nmol CH <sub>4</sub> m <sup>-2</sup> s <sup>-1</sup>	Median EC FCH <sub>4</sub> (IQR, CV), nmol CH <sub>4</sub> m <sup>-2</sup> s <sup>-1</sup>	Median chamber FCH <sub>4</sub> (IQR, CV), nmol CH <sub>4</sub> m <sup>-2</sup> s <sup>-1</sup>	Median $\Delta FCH_4$ (IQR, CV), nmol CH <sub>4</sub> m <sup>-2</sup> s <sup>-1</sup>	Chamber FCH <sub>4</sub> p90 (% of total FCH <sub>4</sub> )	EC FCH <sub>4</sub> p90 (% of total FCH <sub>4</sub> )	Wilcoxon-Mann- Whitney test
<b>CN-Hgu</b>	3.02 (1.18)	-0.12 (0.11)	3.0 (1.98, 39)	-0.07 (0.13, 90)	3.08 (1.98, 39)	0.02 (59)	4.26 (20)	$p < 0.001$ ( $n_{EC} = 40$ , $n_{CH} = 40$ )
<b>FI-Si2</b>	55.43 (17.61)	59.55 (35.23)	53.36 (18.93, 32)	49.46 (48.82, 59)	1.45 (24.92, 139)	88.39 (27)	73.87 (22)	$p = 0.789$ ( $n_{EC} = 22$ , $n_{CH} = 22$ )
<b>SE-Deg</b>	50.17 (21.18)	22.73 (15.64)	50.94 (38.12, 42)	18.74 (22.04, 69)	24.83 (19.9, 43)	46.5 (27)	76.31 (19)	$p < 0.001$ ( $n_{EC} = 50$ , $n_{CH} = 50$ )
<b>US-Ho1</b>	-0.42 (0.48)	-0.69 (1.34)	-0.42 (0.72, 90)	-0.99 (0.91, 112)	0.32 (1.28, 146)	6.02 (43)	0.41 (27)	$p < 0.001$ ( $n_{EC} = 119$ , $n_{CH} = 119$ )
<b>US-La1</b>	41.49 (29.79)	97.72 (65.37)	42.12 (53.85, 72)	116.91 (62.59, 67)	-45.43 (71.64, 115)	157.64 (37)	71.03 (34)	$p = 0.222$ ( $n_{EC} = 5$ , $n_{CH} = 5$ )
<b>US-La2</b>	163.74 (63.81)	191.35 (93.46)	150.22 (103.39, 39)	189.16 (117.65, 49)	5.75 (103.92, 141)	276.98 (32)	226.3 (30)	$p = 0.436$ ( $n_{EC} = 10$ , $n_{CH} = 10$ )
<b>US-Los</b>	35.37 (12.78)	9.61 (5.62)	38.75 (13.82, 36)	8.43 (4.09, 58)	27.75 (4.74, 37)	15.42 (38)	46.72 (28)	$p = 0.016$ ( $n_{EC} = 5$ , $n_{CH} = 5$ )

<b>US-Owc</b>	561.44 (287.63)	753.88 (619.97)	642.45 (446.31, 51)	552.85 (657.0, 82)	47.22 (728.26, 145)	1185.44 (56)	828.1 (45)	$p = 0.796$ (n <sub>EC</sub> = 9, n <sub>CH</sub> = 9)
<b>US-StJ</b>	39.2 (58.96)	13.98 (27.01)	16.4 (29.69, 150)	5.26 (8.31, 193)	9.15 (20.85, 202)	22.12 (63)	73.94 (54)	$p = 0.007$ (n <sub>EC</sub> = 16, n <sub>CH</sub> = 16)
<b>US-Uaf</b>	3.4 (1.97)	2.01 (3.04)	3.46 (3.82, 58)	0.64 (1.87, 151)	1.18 (2.13, 107)	4.76 (29)	5.85 (23)	$p < 0.001$ (n <sub>EC</sub> = 73, n <sub>CH</sub> = 73)

1090

1095

1100

**Table C11.** Wilcoxon-Mann-Whitney test results for monthly aggregation. The eddy covariance (EC) and chamber data sample sizes in Wilcoxon-Mann-Whitney tests are reported as  $n_{EC}$  and  $n_{CH}$ , respectively. Proportions of annual chamber and EC methane ( $CH_4$ ) emission (i.e.,  $CH_4$  flux ( $FCH_4$ )  $\leq 0$  excluded) above the 90<sup>th</sup> percentile ( $p_{90}$ ) are reported as the mean of year-specific 90<sup>th</sup> percentiles (not in parentheses) and percentages (in parentheses). This dataset contains all sites ( $n = 10$ ). Note: due to small sample sizes ( $n = 5$ ) in US-La1 and US-Los, the Wilcoxon-Mann-Whitney test results should be interpreted with caution. Abbreviations: IQR = interquartile range, CV = coefficient of variation (%). \* CN-Hgu had only negative chamber  $FCH_4$  values and chamber  $p_{90}$  was not calculated for this site.

Site	Mean EC $FCH_4$ (SD), $nmol CH_4 m^{-2}s^{-1}$	Mean chamber $FCH_4$ (SD), $nmol CH_4 m^{-2}s^{-1}$	Median EC $FCH_4$ (IQR, CV), $nmol CH_4 m^{-2}s^{-1}$	Median chamber $FCH_4$ (IQR, CV), $nmol CH_4 m^{-2}s^{-1}$	Median $\Delta FCH_4$ (IQR, CV), $nmol CH_4 m^{-2}s^{-1}$	Chamber $FCH_4$ $p_{90}$ (% of total $FCH_4$ )	EC $FCH_4$ $p_{90}$ (% of total $FCH_4$ )	Wilcoxon- Mann- Whitney test
CN-Hgu	3.1 (1.06)	-0.12 (0.1)	3.0 (1.08, 34)	-0.07 (0.14, 84)	3.05 (1.2, 34)	-*	4.14 (30)	$p < 0.001$ ( $n_{EC} = 10$ , $n_{CH} = 10$ )
FI-Si2	52.49 (16.25)	51.0 (26.4)	53.36 (23.22, 31)	47.79 (44.33, 52)	2.68 (26.17, 120)	73.18 (32)	68.51 (29)	$p = 0.635$ ( $n_{EC} = 14$ , $n_{CH} = 14$ )
SE-Deg	46.58 (22.45)	20.66 (15.23)	46.85 (44.64, 48)	15.7 (22.22, 74)	25.1 (11.52, 46)	40.22 (33)	73.06 (25)	$p = 0.002$ ( $n_{EC} = 13$ , $n_{CH} = 13$ )
US-Ho1	-0.44 (0.45)	-0.8 (0.97)	-0.46 (0.6, 86)	-1.05 (0.8, 88)	0.35 (1.12, 124)	2.86 (67)	0.28 (41)	$p < 0.001$ ( $n_{EC} = 32$ , $n_{CH} = 32$ )
US-La1	41.49 (29.79)	97.72 (65.37)	42.12 (53.85, 72)	116.91 (62.59, 67)	-45.43 (71.64, 115)	157.64 (37)	71.03 (34)	$p = 0.222$ ( $n_{EC} = 5$ , $n_{CH} = 5$ )
US-La2	163.74 (63.81)	191.35 (93.46)	150.22 (103.39, 39)	189.16 (117.65, 49)	5.75 (103.92, 141)	276.98 (32)	226.3 (30)	$p = 0.436$ ( $n_{EC} = 10$ , $n_{CH} = 10$ )
US-Los	32.8 (14.3)	7.78 (2.88)	38.75 (13.34, 44)	6.91 (2.78, 37)	27.75 (14.07, 57)	10.18 (47)	42.28 (44)	$p = 0.1$ ( $n_{EC} = 3$ , $n_{CH} = 3$ )
US-Owc	575.34 (301.58)	705.33 (549.45)	642.45 (446.31, 52)	667.58 (756.29, 78)	131.03 (524.49, 144)	1056.3 (58)	828.57 (47)	$p = 0.798$ ( $n_{EC} = 8$ , $n_{CH} = 8$ )
US-StJ	24.14 (19.65)	9.92 (11.72)	21.19 (22.71, 81)	6.0 (7.45, 118)	18.45 (22.01, 82)	20.73 (47)	44.15 (33)	$p = 0.105$ ( $n_{EC} = 8$ , $n_{CH} = 8$ )
US-Uaf	3.39 (1.87)	2.17 (3.15)	3.42 (3.87, 55)	0.65 (1.97, 145)	1.24 (1.84, 114)	4.5 (34)	5.52 (28)	$p = 0.006$ ( $n_{EC} = 18$ , $n_{CH} = 18$ )

**Table C12.** Wilcoxon-Mann-Whitney test results for annual aggregation. The eddy covariance (EC) and chamber data sample sizes in Wilcoxon-Mann-Whitney tests are reported as  $n_{EC}$  and  $n_{CH}$ , respectively. Annual chamber and EC methane ( $CH_4$ ) flux ( $FCH_4$ ) 90<sup>th</sup> percentiles were not calculated for this aggregation. This dataset contains all sites ( $n = 10$ ). Note: due to small sample sizes ( $n = 5$ ) in US-La1 and US-Los, the Wilcoxon-Mann-Whitney test results should be interpreted with caution. 115 Abbreviations: IQR = interquartile range, CV = coefficient of variation (%).

Site	Mean EC $FCH_4$ (SD), $nmol CH_4 m^{-2}s^{-1}$	Mean chamber $FCH_4$ (SD), $nmol CH_4 m^{-2}s^{-1}$	Median EC $FCH_4$ (IQR, CV), $nmol CH_4 m^{-2}s^{-1}$	Median chamber $FCH_4$ (IQR, CV), $nmol CH_4 m^{-2}s^{-1}$	Median $\Delta FCH_4$ (IQR, CV), $nmol CH_4 m^{-2}s^{-1}$	Wilcoxon-Mann-Whitney test
CN-Hgu	3.04 (0.06)	-0.15 (0.14)	3.04 (0.04, 2)	-0.15 (0.1, 94)	3.2 (0.14, 6)	-
FI-Si2	55.7 (2.45)	53.01 (23.84)	55.19 (2.41, 4)	66.22 (20.91, 45)	-7.85 (21.73, 138)	$p = 0.7$ ( $n_{EC} = 3$ , $n_{CH} = 3$ )
SE-Deg	54.08 (3.69)	20.78 (0.59)	54.08 (2.61, 7)	20.78 (0.42, 3)	33.3 (2.19, 9)	-
US-Ho1	-0.38 (0.27)	-0.82 (0.45)	-0.51 (0.34, 70)	-0.77 (0.57, 55)	0.25 (0.78, 111)	$p = 0.095$ ( $n_{EC} = 5$ , $n_{CH} = 5$ )
US-La1	37.77 (-)	76.56 (-)	37.77 (-,-)	76.56 (-,-)	-38.79 (-,-)	-
US-La2	163.81 (49.76)	161.89 (74.25)	163.81 (35.19, 30)	161.89 (52.5, 46)	1.93 (87.69, 141)	-
US-Los	38.18 (-)	8.12 (-)	38.18 (-,-)	8.12 (-,-)	30.05 (-,-)	-
US-Owc	476.61 (209.52)	539.49 (445.72)	476.61 (148.15, 44)	539.49 (315.17, 83)	-62.88 (167.02, 141)	-
US-StJ	14.06 (-)	4.97 (-)	14.06 (-,-)	4.97 (-,-)	9.09 (-,-)	-
US-Uaf	3.38 (0.11)	0.65 (0.34)	3.42 (0.11, 3)	0.52 (0.32, 52)	2.95 (0.41, 16)	$p = 0.1$ ( $n_{EC} = 3$ , $n_{CH} = 3$ )

1120 **Table C13.** Final linear mixed effects model results of significant predictors of the difference between ecosystem- and plot-  
scale methane (CH<sub>4</sub>) flux (FCH<sub>4</sub>) ( $\Delta$ FCH<sub>4</sub>) for the half-hourly model (site n = 3) with soil temperature (TS) instead of Month  
as one of the predictors. Absolute  $\Delta$ FCH<sub>4</sub> was Yeo-Johnson-transformed, centered and scaled, while all continuous predictors  
were only centered and scaled. The predictors are listed in decreasing order based on  $\beta$ -coefficients. The reference level in  
Hour was 0 and May in Month. Abbreviations: SE = standard error, Df = degrees of freedom of denominator, LOOCV = leave-  
1125 one-out cross validation, MAE = mean absolute error, RMSE = root mean square error, PA = air pressure (kPa), u\* = friction  
velocity (m s<sup>-1</sup>), WTL = water table level (cm), TS = soil temperature (°C), NEE = net ecosystem exchange ( $\mu$ mol CO<sub>2</sub> m<sup>-2</sup> s<sup>-1</sup>),  
VPD = vapor pressure deficit (hPa), vWD = v wind component (m s<sup>-1</sup>), uWD = u wind component (m s<sup>-1</sup>).

Predictors	$\beta$ - coefficient	SE	<i>p</i> -value ( <i>t</i> -test)	Marginal R <sup>2</sup>	Conditional R <sup>2</sup>	Df	Random effect variation explained, %	LOOCV		
								R <sup>2</sup>	MAE	RMSE
Intercept	0.0581	0.5465	0.9153	0.0109	0.805	43522	-0.94	1.36	1.5	
<b><u>Fixed effects</u></b>										
Hour										
- 5 AM	0.0838	0.0166	<b>0</b>			43522				
u*	0.0836	0.004	<b>0</b>			43522				
Hour	-0.0565	0.01	<b>0</b>			43522				
- 6 AM	0.0727	0.0163	<b>0</b>			43522				
PA	-0.0684	0.0105	<b>0</b>			43522				
Hour										
- 4 AM	0.0567	0.0163	<b>0.0005</b>			43522				
- 7 AM	0.0489	0.0165	<b>0.003</b>			43522				
- 10 AM	-0.0406	0.0169	<b>0.0161</b>			43522				
- 8 AM	0.0392	0.0166	<b>0.0181</b>			43522				
- 3 AM	0.0375	0.0166	<b>0.0238</b>			43522				
- 10 PM	-0.0311	0.0163	0.0559			43522				
- 5 PM	-0.0294	0.0166	0.0776			43522				
NEE	-0.0289	0.004	<b>0</b>			43522				
TS	-0.027	0.0068	<b>0.0001</b>			43522				
VPD	-0.0268	0.0054	<b>0</b>			43522				
Hour										
- 3 PM	-0.0248	0.0172	0.1498			43522				
- 9 PM	-0.0246	0.0168	0.1412			43522				
- 6 PM	-0.0221	0.0163	0.1741			43522				
- 8 PM	-0.0201	0.0165	0.2224			43522				
- 7 PM	-0.018	0.0165	0.2745			43522				
vWD	-0.018	0.0036	<b>0</b>			43522				

Hour				
- 2 AM	0.0175	0.0163	0.2827	43522
- 1 PM	-0.0148	0.0173	0.394	43522
- 12 PM	-0.0094	0.0172	0.5833	43522
- 1 AM	0.0072	0.0166	0.6597	43522
- 11 PM	-0.0054	0.0165	0.7413	43522
- 2 PM	-0.0042	0.0171	0.8068	43522
- 11 AM	-0.0028	0.0172	0.8698	43522
- 9 AM	-0.0024	0.0171	0.8847	43522
- 4 PM	-0.0013	0.0167	0.9376	43522

**Random effects**

Site	72.29
Date	8

---

|130

|135

|140

**Table C14.** Half-hourly and hourly linear mixed effects model results after backward variable selection. In the models, absolute the difference between ecosystem- and plot-scale methane (CH<sub>4</sub>) flux (FCH<sub>4</sub>) ( $\Delta$ FCH<sub>4</sub>) was Yeo-Johnson-transformed, centered and scaled, while all continuous predictors were only centered and scaled. Note that in both models temporal variables were included in nested random effects (see Supplementary Methods A2). In both models, the reference level in dominant vegetation type was *Sphagnum* moss, 0 in Hour and May in Month. Note that we excluded TS from the half-hourly model due to high multicollinearity with Month (VIF > 3; see models with TS instead of Month in S17). The predictors are listed in a decreasing order according to their  $\beta$ -coefficients. SE = standard error, Df = degrees of freedom of denominator, LOOCV = leave-one-out cross validation, MAE = mean absolute error, RMSE = root mean square error, PA = air pressure (kPa), u\* = friction velocity (m s<sup>-1</sup>), WTL = water table level (cm), TS = soil temperature (°C), NEE = net ecosystem exchange (145  $\mu$ mol CO<sub>2</sub> m<sup>-2</sup>s<sup>-1</sup>), VPD = vapor pressure deficit (hPa), vWD = v wind component (m s<sup>-1</sup>), uWD = u wind component (m s<sup>-1</sup>).

Data set	Predictors	$\beta$ -coefficient	SE	<i>p</i> -value ( <i>t</i> -test)	Marginal R <sup>2</sup>	Conditional R <sup>2</sup>	Df	Random effect variation explained, %		
								R <sup>2</sup>	MAE	RMSE
Half-hourly (n=3 sites)	Intercept	-0.236	0.5259	0.6537	0.0329	0.7933	43522	-0.62	1.37	1.22
	<b><u>Fixed effects</u></b>									
	Month									
	- Aug	0.4626	0.0291	<b>0</b>			1408			
	- Jul	0.4169	0.029	<b>0</b>			1408			
	- Sep	0.3972	0.0294	<b>0</b>			1408			
	- Jun	0.2157	0.0293	<b>0</b>			1408			
	- Apr	0.1615	0.0164	0.6751			1408			
	- Oct	0.1105	0.0316	<b>0.0005</b>			1408			
	u*	0.0876	0.0039	<b>0</b>			43522			
	Hour									
	- 5 AM	0.0873	0.0166	<b>0</b>			43522			
	- 6 AM	0.0742	0.0163	<b>0</b>			43522			
	WTL	0.0617	0.0121	<b>0</b>			43522			
Hour										
- 4 AM	0.0593	0.0163	<b>0.0003</b>			43522				
PA	-0.056	0.0097	<b>0</b>			43522				

Hour				
- 7 AM	0.0486	0.0165	<b>0.0032</b>	43522
- 10 AM	-0.0449	0.0168	<b>0.0075</b>	43522
- 3 AM	0.0409	0.0166	<b>0.0137</b>	43522

<b>VPD</b>	-0.0394	0.0049	<b>0</b>	43522
------------	---------	--------	----------	-------

Hour				
- 8 AM	0.0376	0.0166	<b>0.0235</b>	43522

Month				
- Nov	0.0372	0.0535	0.4865	1408

Hour				
- 10 PM	-0.0323	0.0163	0.0476	43522
- 5 PM	-0.0323	0.0166	0.0515	43522
- 3 PM	-0.0297	0.0171	0.0825	43522

<b>NEE</b>	-0.0295	0.0039	<b>0</b>	43522
------------	---------	--------	----------	-------

Hour				
- 9 PM	-0.0259	0.0168	0.1221	43522
- 6 PM	-0.0245	0.0163	0.1319	43522
- 8 PM	-0.0207	0.0164	0.2072	43522
- 1 PM	-0.0206	0.0172	0.2309	43522
- 7 PM	-0.0198	0.0165	0.2293	43522
- 2 AM	0.0194	0.0163	0.2336	43522

<b>vWD</b>	-0.0179	0.0035	<b>0</b>	43522
------------	---------	--------	----------	-------

Hour				
- 12 PM	-0.0155	0.0171	0.363	43522
- 2 PM	-0.0095	0.017	0.5736	43522
- 1 AM	0.0089	0.0166	0.5925	43522
- 11 AM	-0.008	0.0171	0.6385	43522
- 11 PM	-0.0052	0.0165	0.7522	43522

	- 4 PM	-0.0049	0.0166	0.7696			43522				
	- 9 AM	-0.0045	0.0171	0.7928			43522				
	<b>Random effects</b>										
	Site							72.44			
	Date							6.22			
<b>Hourly</b> (n=3 sites)	Intercept	-0.2978	0.5368	0.5791	0.0439	0.816	25231		-0.46	1.22	1.37
	<b>Fixed effects</b>										
	Month										
	- Aug	0.6418	0.0359	<b>0</b>			1405				
	- Jul	0.5815	0.0365	<b>0</b>			1405				
	- Sep	0.5118	0.035	<b>0</b>			1405				
	- Apr	-0.3979	0.4686	0.3959			1405				
	- Jun	0.27	0.0354	<b>0</b>			1405				
	- Oct	0.1829	0.0373	<b>0</b>			1405				
	Hour										
	- 5 AM	0.1371	0.0208	<b>0</b>			25231				
	WTL	0.0936	0.0142	<b>0</b>			25231				
	Hour										
	- 7 AM	0.0926	0.0207	<b>0</b>			25231				
	- 3 AM	0.0841	0.0206	<b>0</b>			25231				
	TS	-0.0838	0.0092	<b>0</b>			25231				
	Hour										
	- 6 AM	0.0831	0.0204	<b>0</b>			25231				
	u*	0.0687	0.0051	<b>0</b>			25231				
	Hour										
	- 9 AM	0.0657	0.0216	<b>0.0024</b>			25231				
	- 8 AM	0.0656	0.0207	<b>0.0016</b>			25231				
	- 1 AM	0.0594	0.0206	<b>0.0039</b>			25231				
	- 11 PM	0.0578	0.0204	<b>0.0046</b>			25231				
	- 1 PM	0.0488	0.0222	<b>0.028</b>			25231				
	- 7 PM	0.0479	0.0206	<b>0.0197</b>			25231				
	- 11 AM	0.0476	0.022	<b>0.0302</b>			25231				
	PA	-0.0458	0.0117	<b>0.0001</b>			25231				
	Hour										
	- 4 AM	0.0417	0.0201	<b>0.0383</b>			25231				

- 3 PM	0.0417	0.0218	0.056	25231
- 2 AM	0.0377	0.0201	0.0612	25231
- 12 PM	0.0336	0.0219	0.1259	25231
- 2 PM	0.0272	0.0218	0.2113	25231
- 5 PM	0.0267	0.021	0.2039	25231
<b>NEE</b>	-0.0243	0.0052	<b>0</b>	25231
Hour				
- 10 AM	-0.0183	0.0215	0.3942	25231
<b>VPD</b>	-0.0181	0.0066	<b>0.0063</b>	25231
Month				
- Nov	0.0176	0.0628	0.7792	1405
Hour				
- 6 PM	-0.0167	0.0204	0.4144	25231
- 9 PM	0.0149	0.0207	0.4738	25231
- 4 PM	0.0148	0.0212	0.4851	25231
- 8 PM	-0.0129	0.0202	0.523	25231
- 10 PM	-0.0121	0.0202	0.5514	25231
vWD	-0.0081	0.0045	0.0705	25231

**Random effects**

Site	72.46
Date	8.29

---

1160 **Table C15.** Full linear mixed effects model results. In the models, absolute the difference between ecosystem- and plot-scale methane (CH<sub>4</sub>) flux (FCH<sub>4</sub>) ( $\Delta$ FCH<sub>4</sub>) was Yeo-Johnson-transformed, centered and scaled, while all continuous predictors were only centered and scaled. This table presents the full models with both nonsignificant and significant predictors before backward variable selection. The final daily and monthly models were the full models which are shown in Table 3 of the main text. Note that in all models temporal variables were included in nested random effects (see methods and Supplementary  
 1165 Methods A2). In all models, the reference level in site dominant vegetation (VEG) was *Sphagnum* moss, 0 in Hour and May in Month. Annual models were not included due to an inadequate number of observations. Due to lack of complete case observations, US-Owc was not included in the weekly and monthly models (n = 7 sites). We excluded TS from the half-hourly model due to high multicollinearity with Month (VIF > 3). Due to multicollinearity in the weekly model, we built one model without NEE and one without VPD. Fixed effects are listed in decreasing order based on their  $\beta$ -coefficients. SE = standard  
 1170 error, Df = degrees of freedom of denominator, LOOCV = leave-one-out cross validation, MAE = mean absolute error, RMSE = root mean square error, PA = air pressure (kPa), u\* = friction velocity (m s<sup>-1</sup>), WTL = water table level (cm), TS = soil temperature (°C), NEE = net ecosystem exchange ( $\mu$ mol CO<sub>2</sub> m<sup>-2</sup> s<sup>-1</sup>), VPD = vapor pressure deficit (hPa), vWD = v wind component (m s<sup>-1</sup>), uWD = u wind component (m s<sup>-1</sup>).

Data set	Predictors	$\beta$ - coefficient	SE	<i>p</i> -value ( <i>t</i> -test)	Marginal R <sup>2</sup>	Conditional R <sup>2</sup>	Df	Random effect variation explained, %	LOOCV			
									R <sup>2</sup>	MAE	RMSE	
Half- hourly (n=3 sites)	Intercept	0.0962	0.7069	0.8917	0.2041	0.8518	43521		-2.27	1.46	1.55	
	<b><u>Fixed effects</u></b>											
	VEG											
	- Tree	-0.9969	1.2237	0.5648			1					
	Month											
	- Aug	0.4629	0.029	<b>0</b>			1408					
	- Jul	0.4172	0.029	<b>0</b>			1408					
	- Sep	0.3974	0.0294	<b>0</b>			1408					
	- Jun	0.2161	0.0294	<b>0</b>			1408					
	- Apr	0.1613	0.3852	0.6753			1408					
	- Oct	0.1109	0.0316	<b>0.0005</b>			1408					
	u*	0.088	0.004	<b>0</b>			43521					
Hour												
- 5 AM	0.0873	0.0166	<b>0</b>			43521						

- 6 AM	0.0741	0.0163	<b>0</b>	43521
<b>WTL</b>	0.0615	0.0121	<b>0</b>	43521
Hour				
- 4 AM	0.0592	0.0163	<b>0.0003</b>	43521
<b>PA</b>	-0.056	0.0097	<b>0</b>	43521
Hour				
- 7 AM	0.0484	0.0165	<b>0.0033</b>	43521
- 10 AM	-0.0451	0.0168	<b>0.0073</b>	43521
- 3 AM	0.0409	0.0166	<b>0.0138</b>	43521
<b>VPD</b>	-0.0393	0.0049	<b>0</b>	43521
Month				
- Nov	0.0376	0.0535	0.4822	1408
Hour				
- 8 AM	0.0373	0.0166	<b>0.0244</b>	43521
- 5 PM	-0.0325	0.0166	0.0502	43521
- 10 PM	-0.0323	0.0163	0.0476	43521
- 3 PM	-0.0299	0.0171	0.0808	43521
<b>NEE</b>	-0.0294	0.0039	<b>0</b>	43521
Hour				
- 9 PM	-0.0259	0.0168	0.1219	43521
- 6 PM	-0.0247	0.0163	0.1296	43521
- 8 PM	-0.0208	0.0164	0.2056	43521
- 1 PM	-0.0207	0.0172	0.2282	43521
- 7 PM	-0.0199	0.0165	0.2267	43521
- 2 AM	0.0194	0.0163	0.234	43521
<b>vWD</b>	-0.0182	0.0036	<b>0</b>	43521
Hour				
- 12 PM	-0.0156	0.0171	0.3593	43521
- 2 PM	-0.0097	0.017	0.5678	43521

- 1 AM	0.0089	0.0166	0.5925	43521
- 11 AM	-0.0082	0.0171	0.6317	43521
- 11 PM	-0.0052	0.0165	0.7538	43521
- 4 PM	-0.0051	0.0166	0.7589	43521
- 9 AM	-0.0047	0.0171	0.7818	43521
uWD	-0.0015	0.0035	0.6716	43521

**Random effects**

Site	75.96
Date	5.43

<b>Hourly</b> (n=3 sites)	Intercept	0.0199	0.7487	0.9788	0.2116	0.8752	25230	-2.45	1.53	1.62
---------------------------------	-----------	--------	--------	--------	--------	--------	-------	-------	------	------

**Fixed effects**

VEG

- Tree	-0.9517	1.2957	0.5967	1
--------	---------	--------	--------	---

**Month**

- Aug	0.6413	0.036	0	1405
-------	--------	-------	---	------

- Jul	0.5811	0.0366	0	1405
-------	--------	--------	---	------

- Sep	0.5114	0.035	0	1405
-------	--------	-------	---	------

- Apr	-0.3974	0.4686	0.3966	1405
-------	---------	--------	--------	------

- Jun	0.2697	0.0355	0	1405
-------	--------	--------	---	------

- Oct	0.1826	0.0373	0	1405
-------	--------	--------	---	------

Hour

- 5 AM	0.1371	0.0208	0	25230
--------	--------	--------	---	-------

<b>WTL</b>	0.0933	0.0142	0	25230
------------	--------	--------	---	-------

Hour

- 7 AM	0.0927	0.0207	0	25230
--------	--------	--------	---	-------

- 3 AM	0.0841	0.0206	0	25230
--------	--------	--------	---	-------

<b>TS</b>	-0.0837	0.0093	0	25230
-----------	---------	--------	---	-------

Hour

- 6 AM	0.0831	0.0204	<b>0</b>	25230
<b>u*</b>	0.0685	0.0052	<b>0</b>	25230
Hour				
- 9 AM	0.0658	0.0217	<b>0.0024</b>	25230
- 8 AM	0.0656	0.0207	<b>0.0015</b>	25230
- 1 AM	0.0594	0.0206	<b>0.0039</b>	25230
- 11 PM	0.0578	0.0204	<b>0.0046</b>	25230
- 1 PM	0.0488	0.0222	<b>0.028</b>	25230
- 7 PM	0.048	0.0206	<b>0.0196</b>	25230
- 11 AM	0.0476	0.022	<b>0.0302</b>	25230
<b>PA</b>	-0.0455	0.0117	<b>0.0001</b>	25230
Hour				
- 3 PM	0.0417	0.0218	0.0558	25230
- 4 AM	0.0417	0.0201	<b>0.0384</b>	25230
- 2 AM	0.0377	0.0201	0.0611	25230
- 12 PM	0.0336	0.0219	0.126	25230
- 2 PM	0.0272	0.0218	0.2111	25230
- 5 PM	0.0268	0.021	0.2028	25230
<b>NEE</b>	-0.0244	0.0052	<b>0</b>	25230
Hour				
- 10 AM	-0.0183	0.0215	0.3958	25230
<b>VPD</b>	-0.0182	0.0066	<b>0.0061</b>	25230
Month				
- Nov	0.0177	0.0628	0.7786	1405
Hour				
- 6 PM	-0.0166	0.0204	0.4159	25230
- 4 PM	0.0149	0.0212	0.4826	25230
- 9 PM	0.0149	0.0207	0.4738	25230
- 8 PM	-0.0129	0.0202	0.5236	25230

- 10 PM	-0.0121	0.0202	0.5505	25230
vWD	-0.0079	0.0045	0.0833	25230
uWD	0.0009	0.0044	0.8346	25230

### Random effects

Site	77.37
Date	6.81

<b>Weekly</b> (no NEE, n=9 sites)	Intercept	0.3046	0.3665	0.407	0.5468	0.8357	180	-1.15	1.34	1.58
---	-----------	--------	--------	-------	--------	--------	-----	-------	------	------

### Fixed effects

VEG

- Tree	-1.4712	0.702	0.0903	5
- Aerenchymatous	0.9949	0.5112	0.1092	5
- Ericaceous shrub	0.5253	0.7163	0.4962	5

Month

- Apr	0.3907	0.416	0.3502	86
- Nov	0.3193	0.2602	0.2232	86
- Dec	0.316	0.6993	0.6524	86
- <b>Jul</b>	0.3104	0.142	<b>0.0315</b>	86
- <b>Aug</b>	0.3012	0.1442	<b>0.0396</b>	86
- <b>Sep</b>	0.2964	0.14	<b>0.0371</b>	86
- Jun	0.2082	0.1388	0.1373	86
- Oct	0.169	0.1457	0.2492	86

WTL -0.0727 0.0551 0.1887 180

PA -0.0604 0.0407 0.14 180

VPD -0.0352 0.0318 0.2701 180

u\* 0.0317 0.0272 0.244 180

Month

- Mar -0.0234 0.5319 0.9649 86

vWD -0.0167 0.0175 0.3418 180

TS	-0.0104	0.06	0.862				180			
uWD	-0.0081	0.0198	0.6819				180			
<b><u>Random effects</u></b>										
Site									63.74	
Year-month									6.38e <sup>-07</sup>	
<b>Weekly</b> (no VPD, n=9 sites)	Intercept	0.3008	0.3724	0.4202	0.5423	0.8365	180			-1.03 1.3 1.54
<b><u>Fixed effects</u></b>										
	VEG									
	- Tree	-1.4642	0.713	0.0952			5			
	-Aerenchymatous	0.9763	0.5228	0.1208			5			
	-Ericaceous shrub	0.4435	0.7268	0.5684			5			
	Month									
	- Apr	0.3611	0.4145	0.386			86			
	- Dec	0.3525	0.7059	0.6188			86			
	- Nov	0.3375	0.263	0.2029			86			
	- <b>Aug</b>	0.317	0.1484	<b>0.0355</b>			86			
	- <b>Jul</b>	0.3144	0.1438	<b>0.0315</b>			86			
	- <b>Sep</b>	0.3086	0.1408	<b>0.0311</b>			86			
	- Jun	0.2001	0.141	0.1596			86			
	- Oct	0.1847	0.1473	0.2134			86			
	- Mar	-0.0786	0.5287	0.8822			86			
	PA	-0.0737	0.039	0.0603			180			
	WTL	-0.07	0.0546	0.2046			180			
	u*	0.032	0.0276	0.2464			180			
	TS	-0.019	0.0637	0.7663			180			
	vWD	-0.0184	0.0175	0.2962			180			
	uWD	-0.0137	0.0201	0.4953			180			
	NEE	0.01	0.0266	0.7117			180			
<b><u>Random effects</u></b>										

## 1175 **Code and data availability**

The timestamp-aligned data sets containing ecosystem and plot-scale CH<sub>4</sub> flux and environmental data at half-hourly, hourly, daily, weekly, monthly, and annual scales can be accessed via Zenodo (Määttä et al., 2025; doi: 10.5281/zenodo.17312404). The R code used for processing the EC and chamber CH<sub>4</sub> flux data, statistical analyses and producing the figures can be accessed at [https://github.com/tiia-maa/Cross-site-comparison-of-ecosystem-and-plot-scale-methane-fluxes-across-multiple-](https://github.com/tiia-maa/Cross-site-comparison-of-ecosystem-and-plot-scale-methane-fluxes-across-multiple-sites.git)  
1180 sites.git.

## **Author contribution**

TM, AM, SB, KD, AD, SF, EFC, RJ, SK, GM, LM, ZO, OS, MU, RV, EW, ZZ, AT, and MH conceptualized the study. Data was provided by AD, GB, JJ, AK, KK, LM, MN, SN, MP, KS, ET, MU, RV, JW, EW, and ZZ, and data curation was conducted by TM, AM, AD, GB, KD, EFC, JJ, SK, AK, KK, GM, MN, SN, MP, KS, ET, MU, RV, JW, EW, and ZZ. Formal analysis  
1185 (data processing and statistical analyses) and visualization were done by TM. Investigation was conducted by TM and AM. AM supervised the study. Project administration was done by TM, AM and RJ. Funding acquisition for the study was done by AM and RJ. TM and AM prepared the original manuscript draft and TM, AM, AD, GB, SB, KD, SF, EFC, RJ, JJ, SK, LM, MN, ZO, MP, OS, ET, MU, RV, JW, EW, ZZ, AT, and MH contributed to the review and editing.

## **Competing interests**

1190 The authors declare that they have no conflict of interest.

## **Acknowledgements**

We thank Kendalynn Morris for feedback on the manuscript. We acknowledge funding from the University of Zurich Stiftung für Wissenschaftliche Forschung (STWF-22-028) and the Swiss National Science Foundation (SNSF) (project 200021\_215214) awarded to AM. This work was also supported by COMPASS-FME, a multi-institutional project supported  
1195 by the U.S. Department of Energy, Office of Science, Biological and Environmental Research as part of the Environmental System Science Program. The Pacific Northwest National Laboratory is operated for DOE by Battelle Memorial Institute under contract DE-AC05-76RL01830. RBJ acknowledges support from the Gordon and Betty Moore Foundation through Grants GBMF5439 ‘Advancing Understanding of the Global Methane Cycle’ and GBMF11519 ‘Advancing the understanding of methane emissions from tropical wetlands’ to Stanford University and from the USGS Powell Synthesis Center (Scaling

1200 tropical wetland methane fluxes regionally and globally). SB was funded by the USGS Ecosystems Land Change Science Program and U.S. Department of Energy, Office of Science, Office of Biological and Environmental Research (Grant DE-SC0023084). Any use of trade, firm, or product names is for descriptive purposes only and does not imply endorsement by the U.S. Government. MU was supported by the Arctic Challenge for Sustainability II and III (JPMXD1420318865; JPMXD1720251001). ZO was supported by the US Department of the Treasury (grant no. DISL-MESC-ALCOE-06). JJ, 1205 MBN and MP acknowledge financial support from the Swedish Research Council (VR) and SLU to ICOS-Sweden and SITES, and additional funding from VR (#2019-04676 & #2018-03966) and the Kempe Foundation (#JCK-1108 and #JCSMK23-0221). ARD acknowledges support for the US Dept of Energy Ameriflux Management Project support to ChEAS core site cluster. OS acknowledges financial support through the Canada Research Chair program (CRC-2018-00259) and the NSERC Discovery Grants program (DGPIN-2018-05743). EJW acknowledges support from the US Greenhouse Gas Center and the 1210 NASA Terrestrial Ecology Program. We thank Yang Qi for assistance in preliminary PlanetScope data processing.

## References

- Alduchov, O. A. and Eskridge, R.: Improved Magnus form approximation of saturation vapor pressure, *Journal of Applied Meteorology*, 35, 601–609, [https://doi.org/10.1175/1520-0450\(1996\)035<0601:IMFAOS>2.0.CO;2](https://doi.org/10.1175/1520-0450(1996)035<0601:IMFAOS>2.0.CO;2), 1996.
- 1215 Alekseychik, P., Korrensalo, A., Mammarella, I., Launiainen, S., Tuittila, E.-S., Korpela, I., and Vesala, T.: Carbon balance of a Finnish bog: temporal variability and limiting factors based on 6 years of eddy-covariance data, *Biogeosciences*, 18, 4681–4704, <https://doi.org/10.5194/bg-18-4681-2021>, 2021.
- Anthony, T. L. and Silver, W. L.: Hot moments drive extreme nitrous oxide and methane emissions from agricultural peatlands, *Glob. Chang. Biol.*, 27, 5141–5153, <https://doi.org/10.1111/gcb.15802>, 2021.
- 1220 Anthony, T. L. and Silver, W. L.: Hot spots and hot moments of greenhouse gas emissions in agricultural peatlands, *Biogeochemistry*, 167, 461–477, <https://doi.org/10.1007/s10533-023-01095-y>, 2023.
- Aubinet, M.: Eddy covariance CO<sub>2</sub> flux measurements in nocturnal conditions: an analysis of the problem, *Ecol. Appl.*, 18, 1368–1378, <https://doi.org/10.1890/06-1336.1>, 2008.
- Aubinet, M., Vesala, T., and Papale, D.: *Eddy Covariance: A Practical Guide to Measurement and Data Analysis*, Springer Science & Business Media, 438 pp., <https://doi.org/10.1007/978-94-007-2351-1>, 2012.
- 1225 Baldocchi, D.: Assessing the eddy covariance technique for evaluating carbon dioxide exchange rates of ecosystems: past, present and future: carbon balance and eddy covariance, *Glob. Chang. Biol.*, 9, 479–492, <https://doi.org/10.1046/j.1365-2486.2003.00629.x>, 2003.
- Baldocchi, D., Detto, M., Sonnentag, O., Verfaillie, J., Teh, Y. A., Silver, W., and Kelly, N. M.: The challenges of measuring methane fluxes and concentrations over a peatland pasture, *Agric. For. Meteorol.*, 153, 177–187, 1230 <https://doi.org/10.1016/j.agrformet.2011.04.013>, 2012.
- Bansal, S., Post van der Burg, M., Fern, R. R., Jones, J. W., Lo, R., McKenna, O. P., Tangen, B. A., Zhang, Z., and Gleason, R. A.: Large increases in methane emissions expected from North America’s largest wetland complex, *Sci. Adv.*, 9,

- 235 Bansal, S., Creed, I. F., Tangen, B. A., Bridgham, S. D., Desai, A. R., Krauss, K. W., Neubauer, S. C., Noe, G. B., Rosenberry, D. O., Trettin, C., Wickland, K. P., Allen, S. T., Arias-Ortiz, A., Armitage, A. R., Baldocchi, D., Banerjee, K., Bastviken, D., Berg, P., Bogard, M. J., Chow, A. T., Conner, W. H., Craft, C., Creamer, C., DelSontro, T., Duberstein, J. A., Eagle, M., Fennessy, M. S., Finkelstein, S. A., Göckede, M., Grunwald, S., Halabisky, M., Herbert, E., Jahangir, M. M. R., Johnson, O. F., Jones, M. C., Kelleway, J. J., Knox, S., Kroeger, K. D., Kuehn, K. A., Lobb, D., Loder, A. L., Ma, S., Maher, D. T., McNicol, G., Meier, J., Middleton, B. A., Mills, C., Mistry, P., Mitra, A., Mobilian, C., 240 Nahlik, A. M., Newman, S., O'Connell, J. L., Oikawa, P., van der Burg, M. P., Schutte, C. A., Song, C., Stagg, C. L., Turner, J., Vargas, R., Waldrop, M. P., Wallin, M. B., Wang, Z. A., Ward, E. J., Willard, D. A., Yarwood, S., and Zhu, X.: Practical guide to measuring wetland carbon pools and fluxes, *Wetlands (Wilmington)*, 43, 105, <https://doi.org/10.1007/s13157-023-01722-2>, 2023b.
- 245 Barba, J., Cueva, A., Bahn, M., Barron-Gafford, G. A., Bond-Lamberty, B., Hanson, P. J., Jaimes, A., Kulmala, L., Pumpanen, J., Scott, R. L., Wohlfahrt, G., and Vargas, R.: Comparing ecosystem and soil respiration: Review and key challenges of tower-based and soil measurements, *Agric. For. Meteorol.*, 249, 434–443, <https://doi.org/10.1016/j.agrformet.2017.10.028>, 2018.
- Bartoń, K.: MuMIn: Multi-Model Inference, <https://doi.org/10.32614/CRAN.package.MuMIn>, 2024
- 250 Becker, R. A., Allan R. Wilks, A. R., Brownrigg Ray Minka Thomas, and Deckmyn, A.: maps: Draw Geographical Maps, 2023.
- van den Berg, M., van den Elzen, E., Ingwersen, J., Kosten, S., Lamers, L. P. M., and Streck, T.: Contribution of plant-induced pressurized flow to CH<sub>4</sub> emission from a Phragmites fen, *Sci. Rep.*, 10, 12304, <https://doi.org/10.1038/s41598-020-69034-7>, 2020.
- 255 Bohrer, G., Ju, Y., Arend, K., Morin, T., Rey-Sanchez, C., Wrighton, K., and Villa, J.: Methane and CO<sub>2</sub> chamber fluxes and porewater concentrations US-OWC Ameriflux wetland site, 2015–2018, <https://doi.org/10.15485/1568865>, 2019.
- Bohrer, G., Kerns, J., Morin, T., Rey-Sanchez, A., Villa, J., and Ju, Y.: FLUXNET-CH<sub>4</sub> US-OWC Old Woman Creek, <https://doi.org/10.18140/FLX/1669690>, 2020.
- 260 Bond-Lamberty, B., Christianson, D. S., Malhotra, A., Pennington, S. C., Sihi, D., AghaKouchak, A., Anjileli, H., Altaf Arain, M., Armesto, J. J., Ashraf, S., Ataka, M., Baldocchi, D., Andrew Black, T., Buchmann, N., Carbone, M. S., Chang, S.-C., Crill, P., Curtis, P. S., Davidson, E. A., Desai, A. R., Drake, J. E., El-Madany, T. S., Gavazzi, M., Görres, C.-M., Gough, C. M., Goulden, M., Gregg, J., Gutiérrez Del Arroyo, O., He, J.-S., Hirano, T., Hopple, A., Hughes, H., Järveoja, J., Jassal, R., Jian, J., Kan, H., Kaye, J., Kominami, Y., Liang, N., Lipson, D., Macdonald, C. A., Maseyk, K., Mathes, K., Mauritz, M., Mayes, M. A., McNulty, S., Miao, G., Migliavacca, M., Miller, S., Miniati, C. F., Nietz, J. G., Nilsson, M. B., Noormets, A., Norouzi, H., O'Connell, C. S., Osborne, B., Oyonarte, C., Pang, Z., Peichl, M., 265 Pendall, E., Perez-Quezada, J. F., Phillips, C. L., Phillips, R. P., Raich, J. W., Renchon, A. A., Ruehr, N. K., Sánchez-Cañete, E. P., Saunders, M., Savage, K. E., Schrumph, M., Scott, R. L., Seibt, U., Silver, W. L., Sun, W., Szutu, D., Takagi, K., Takagi, M., Teramoto, M., Tjoelker, M. G., Trumbore, S., Ueyama, M., Vargas, R., Varner, R. K., Verfaillie, J., Vogel, C., Wang, J., Winston, G., Wood, T. E., Wu, J., Wutzler, T., Zeng, J., Zha, T., Zhang, Q., and Zou, J.: COSORE: A community database for continuous soil respiration and other soil-atmosphere greenhouse gas 270 flux data, *Glob. Chang. Biol.*, 26, 7268–7283, <https://doi.org/10.1111/gcb.15353>, 2020.
- Bubier, J., Costello, A., Moore, T. R., Roulet, N. T., and Savage, K.: Microtopography and methane flux in boreal peatlands, northern Ontario, Canada, *Can. J. Bot.*, 71, 1056–1063, <https://doi.org/10.1139/b93-122>, 1993.

- Bubier, J. L.: The relationship of vegetation to methane emission and hydrochemical gradients in northern peatlands, *J. Ecol.*, 83, 403–420, <https://doi.org/10.2307/2261594>, 1995.
- 1275 Budishchev, A., Mi, Y., van Huissteden, J., Belelli-Marchesini, L., Schaepman-Strub, G., Parmentier, F. J. W., Fratini, G., Gallagher, A., Maximov, T. C., and Dolman, A. J.: Evaluation of a plot-scale methane emission model using eddy covariance observations and footprint modelling, *Biogeosciences*, 11, 4651–4664, <https://doi.org/10.5194/bg-11-4651-2014>, 2014.
- 1280 Cernusak, L. A., Ubierna, N., Jenkins, M. W., Garrity, S. R., Rahn, T., Powers, H. H., Hanson, D. T., Sevanto, S., Wong, S. C., McDowell, N. G., and Farquhar, G. D.: Saturation of vapour pressure inside leaves of two conifer species, *Sci. Rep.*, 8, 7667, <https://doi.org/10.1038/s41598-018-25838-2>, 2018.
- Chaichana, N., Bellingrath-Kimura, S. D., Komiya, S., Fujii, Y., Noborio, K., Dietrich, O., and Pakoktom, T.: Comparison of Closed Chamber and Eddy Covariance Methods to Improve the Understanding of Methane Fluxes from Rice Paddy Fields in Japan, *Atmosphere*, 9, 356, <https://doi.org/10.3390/atmos9090356>, 2018.
- 1285 Chamberlain, S. D., Verfaillie, J., Eichelmann, E., Hemes, K. S., and Baldocchi, D. D.: Evaluation of density corrections to methane fluxes measured by open-path eddy covariance over contrasting landscapes, *Boundary Layer Meteorol.*, 165, 197–210, <https://doi.org/10.1007/s10546-017-0275-9>, 2017.
- Chen, W., Zhang, F., Wang, B., Wang, J., Tian, D., Han, G., Wen, X., Yu, G., and Niu, S.: Diel and seasonal dynamics of ecosystem-scale methane flux and their determinants in an alpine meadow, *J. Geophys. Res. Biogeosci.*, 124, 1731–1745, <https://doi.org/10.1029/2019jg005011>, 2019.
- 1290 Chen, W., Wang, B., Zhang, F., Li, Z., Wang, J., Yu, G., Wen, X., and Niu, S.: Hysteretic relationship between plant productivity and methane uptake in an alpine meadow, *Agric. For. Meteorol.*, 288–289, 107982, <https://doi.org/10.1016/j.agrformet.2020.107982>, 2020.
- 1295 Cho, R., Schroth, M. H., and Zeyer, J.: Circadian methane oxidation in the root zone of rice plants, *Biogeochemistry*, 111, 317–330, <https://doi.org/10.1007/s10533-011-9651-6>, 2012.
- Christiansen, J. R., Outhwaite, J., and Smukler, S. M.: Comparison of CO<sub>2</sub>, CH<sub>4</sub> and N<sub>2</sub>O soil-atmosphere exchange measured in static chambers with cavity ring-down spectroscopy and gas chromatography, *Agric. For. Meteorol.*, 211–212, 48–57, <https://doi.org/10.1016/j.agrformet.2015.06.004>, 2015.
- 1300 Chu, H., Luo, X., Ouyang, Z., Chan, W. S., Dengel, S., Biraud, S. C., Torn, M. S., Metzger, S., Kumar, J., Arain, M. A., Arkebauer, T. J., Baldocchi, D., Bernacchi, C., Billesbach, D., Black, T. A., Blanken, P. D., Bohrer, G., Bracho, R., Brown, S., Brunsell, N. A., Chen, J., Chen, X., Clark, K., Desai, A. R., Duman, T., Durden, D., Fares, S., Forbrich, I., Gamon, J. A., Gough, C. M., Griffis, T., Helbig, M., Hollinger, D., Humphreys, E., Ikawa, H., Iwata, H., Ju, Y., Knowles, J. F., Knox, S. H., Kobayashi, H., Kolb, T., Law, B., Lee, X., Litvak, M., Liu, H., Munger, J. W., Noormets, A., Novick, K., Oberbauer, S. F., Oechel, W., Oikawa, P., Papuga, S. A., Pendall, E., Prajapati, P., Prueger, J., 1305 Quinton, W. L., Richardson, A. D., Russell, E. S., Scott, R. L., Starr, G., Staebler, R., Stoy, P. C., Stuart-Haëntjens, E., Sonntag, O., Sullivan, R. C., Suyker, A., Ueyama, M., Vargas, R., Wood, J. D., and Zona, D.: Representativeness of Eddy-Covariance flux footprints for areas surrounding AmeriFlux sites, *Agric. For. Meteorol.*, 301–302, 108350, <https://doi.org/10.1016/j.agrformet.2021.108350>, 2021.
- 1310 Chu, H., Christianson, D. S., Cheah, Y.-W., Pastorello, G., O'Brien, F., Geden, J., Ngo, S.-T., Hollowgrass, R., Leibowitz, K., Beekwilder, N. F., Sandesh, M., Dengel, S., Chan, S. W., Santos, A., Delwiche, K., Yi, K., Buechner, C., Baldocchi, D., Papale, D., Keenan, T. F., Biraud, S. C., Agarwal, D. A., and Torn, M. S.: AmeriFlux BASE data pipeline to support network growth and data sharing, *Sci. Data*, 10, 614, <https://doi.org/10.1038/s41597-023-02531-2>, 2023.

- Clark, W. A. and Avery, K. L.: The effects of data aggregation in statistical analysis, *Geogr. Anal.*, 8, 428–438, <https://doi.org/10.1111/j.1538-4632.1976.tb00549.x>, 1976.
- 1315 Clement, R. J., Verma, S. B., and Verry, E. S.: Relating chamber measurements to eddy correlation measurements of methane flux, *J. Geophys. Res. D: Atmos.*, 100, 21047–21056, <https://doi.org/10.1029/95JD02196>, 1995.
- Davidson, E. A., Savage, K., Verchot, L. V., and Navarro, R.: Minimizing artifacts and biases in chamber-based measurements of soil respiration, *Agric. For. Meteorol.*, 113, 21–37, [https://doi.org/10.1016/s0168-1923\(02\)00100-4](https://doi.org/10.1016/s0168-1923(02)00100-4), 2002.
- 1320 Davidson, S. J., Santos, M. J., Sloan, V. L., Reuss-Schmidt, K., Phoenix, G. K., Oechel, W. C., and Zona, D.: Upscaling CH<sub>4</sub> Fluxes Using High-Resolution Imagery in Arctic Tundra Ecosystems, *Remote Sensing*, 9, 1227, <https://doi.org/10.3390/rs9121227>, 2017.
- Delwiche, K. B., Knox, S. H., Malhotra, A., Fluet-Chouinard, E., McNicol, G., Feron, S., Ouyang, Z., Papale, D., Trotta, C., Canfora, E., and Others: FLUXNET-CH<sub>4</sub>: A global, multi-ecosystem dataset and analysis of methane seasonality from freshwater wetlands, *Earth System Science Data Discussions*, 2021, 1–111, 2021.
- 1325 Desai, A. R.: AmeriFlux BASE US-Los Lost Creek, Ver. 33-5, AmeriFlux AMP, [https://doi.org/10.17190/AMF/1246071\\_2025a](https://doi.org/10.17190/AMF/1246071_2025a).
- Desai, A. R.: In Situ Carbon Dioxide and Methane Flux Measurements Using Opaque Chambers in a Sedge Fen Wetland (US-Los Lost Creek AmeriFlux Site, Wisconsin, Summer 2015) ver 1. Environmental Data Initiative (1), <https://doi.org/10.6073/pasta/fc48a416ab7c580f2fd0d5450668a23a>, 2025b.
- 1330 Desai, A. R. and Thom, J.: FLUXNET-CH<sub>4</sub> US-Los Lost Creek, <https://doi.org/10.18140/FLX/1669682>, 2020.
- Desai, A. R., Xu, K., Tian, H., Weishampel, P., Thom, J., Baumann, D., Andrews, A. E., Cook, B. D., King, J. Y., and Kolka, R.: Landscape-level terrestrial methane flux observed from a very tall tower, *Agric. For. Meteorol.*, 201, 61–75, <https://doi.org/10.1016/j.agrformet.2014.10.017>, 2015.
- 1335 Detto, M., Verfaillie, J., Anderson, F., Xu, L., and Baldocchi, D.: Comparing laser-based open- and closed-path gas analyzers to measure methane fluxes using the eddy covariance method, *Agric. For. Meteorol.*, 151, 1312–1324, <https://doi.org/10.1016/j.agrformet.2011.05.014>, 2011.
- Deventer, M. J., Griffis, T. J., Roman, D. T., Kolka, R. K., Wood, J. D., Erickson, M., Baker, J. M., and Millet, D. B.: Error characterization of methane fluxes and budgets derived from a long-term comparison of open- and closed-path eddy covariance systems, *Agric. For. Meteorol.*, 278, 107638, <https://doi.org/10.1016/j.agrformet.2019.107638>, 2019.
- 1340 Dinno, A.: `conover.test`: Conover-Iman Test of Multiple Comparisons Using Rank Sums, <https://doi.org/10.32614/CRAN.package.conover.test>, 2024.
- Erkkilä, K.-M., Ojala, A., Bastviken, D., Biermann, T., Heiskanen, J. J., Lindroth, A., Peltola, O., Rantakari, M., Vesala, T., and Mammarella, I.: Methane and carbon dioxide fluxes over a lake: comparison between eddy covariance, floating chambers and boundary layer method, *Biogeosciences*, 15, 429–445, <https://doi.org/10.5194/bg-15-429-2018>, 2018.
- 1345 Forbrich, I., Kutzbach, L., Hormann, A., and Wilmking, M.: A comparison of linear and exponential regression for estimating diffusive CH<sub>4</sub> fluxes by closed-chambers in peatlands, *Soil Biol. Biochem.*, 42, 507–515, <https://doi.org/10.1016/j.soilbio.2009.12.004>, 2010.
- Forbrich, I., Kutzbach, L., Wille, C., Becker, T., Wu, J., and Wilmking, M.: Cross-evaluation of measurements of peatland

- methane emissions on microform and ecosystem scales using high-resolution landcover classification and source weight modelling, *Agric. For. Meteorol.*, 151, 864–874, <https://doi.org/10.1016/j.agrformet.2011.02.006>, 2011.
- 1350 Fox, J. and Weisberg, S.: An R companion to applied regression, 3rd ed., SAGE Publications, Thousand Oaks, CA, 608 pp., <https://www.john-fox.ca/Companion/>, 2018.
- Griebel, A., Bennett, L. T., Metzen, D., Cleverly, J., Burba, G., and Arndt, S. K.: Effects of inhomogeneities within the flux footprint on the interpretation of seasonal, annual, and interannual ecosystem carbon exchange, *Agric. For. Meteorol.*, 221, 50–60, <https://doi.org/10.1016/j.agrformet.2016.02.002>, 2016.
- 1355 Grossiord, C., Buckley, T. N., Cernusak, L. A., Novick, K. A., Poulter, B., Siegwolf, R. T. W., Sperry, J. S., and McDowell, N. G.: Plant responses to rising vapor pressure deficit, *New Phytol.*, 226, 1550–1566, <https://doi.org/10.1111/nph.16485>, 2020.
- Hargreaves, K. J., Fowler, D., Pitcairn, C. E. R., and Aurela, M.: Annual methane emission from Finnish mires estimated from eddy covariance campaign measurements, *Theor. Appl. Climatol.*, 70, 203–213, <https://doi.org/10.1007/s007040170015>, 2001.
- 1360 Hartley, I. P., Hill, T. C., Wade, T. J., Clement, R. J., Moncrieff, J. B., Prieto-Blanco, A., Disney, M. I., Huntley, B., Williams, M., Howden, N. J. K., Wookey, P. A., and Baxter, R.: Quantifying landscape-level methane fluxes in subarctic Finland using a multiscale approach, *Glob. Chang. Biol.*, 21, 3712–3725, <https://doi.org/10.1111/gcb.12975>, 2015.
- 1365 Heusinkveld, B. G., Jacobs, A. F. G., and Holtslag, A. A. M.: Effect of open-path gas analyzer wetness on eddy covariance flux measurements: A proposed solution, *Agric. For. Meteorol.*, 148, 1563–1573, <https://doi.org/10.1016/j.agrformet.2008.05.010>, 2008.
- Hill, A. C. and Vargas, R.: Carbon dioxide and methane chamber flux data from temperate *S. alterniflora* salt-marsh, <https://doi.org/10.6084/M9.FIGSHARE.20099321.V1>, 2022a.
- 1370 Hill, A. C. and Vargas, R.: Methane and carbon dioxide fluxes in a temperate tidal salt marsh: Comparisons between plot and ecosystem measurements, *J. Geophys. Res. Biogeosci.*, 127, <https://doi.org/10.1029/2022jg006943>, 2022b.
- Hollinger, D. Y. and Richardson, A. D.: Uncertainty in eddy covariance measurements and its application to physiological models, *Tree Physiol.*, 25, 873–885, <https://doi.org/10.1093/treephys/25.7.873>, 2005.
- 1375 Holm, G., Perez, B., McWhorter, D., Krauss, K., Raynie, R., and Killebrew, C.: FLUXNET-CH4 US-LA1 Pointe-aux-Chenes Brackish Marsh, <https://doi.org/10.18140/FLX/1669680>, 2020a.
- Holm, G., Perez, B., McWhorter, D., Krauss, K., Raynie, R., and Killebrew, C.: FLUXNET-CH4 US-LA2 Salvador WMA Freshwater Marsh, <https://doi.org/10.18140/FLX/1669681>, 2020b.
- Intergovernmental Panel on Climate Change (IPCC): Climate Change 2021 – the physical science basis, Cambridge University Press, <https://doi.org/10.1017/9781009157896>, 2023.
- 1380 Irvin, J., Zhou, S., McNicol, G., Lu, F., Liu, V., Fluet-Chouinard, E., Ouyang, Z., Knox, S. H., Lucas-Moffat, A., Trotta, C., Papale, D., Vitale, D., Mammarella, I., Alekseychik, P., Aurela, M., Avati, A., Baldocchi, D., Bansal, S., Bohrer, G., Campbell, D. I., Chen, J., Chu, H., Dalmagro, H. J., Delwiche, K. B., Desai, A. R., Euskirchen, E., Feron, S., Goeckede, M., Heimann, M., Helbig, M., Helfter, C., Hemes, K. S., Hirano, T., Iwata, H., Jurasinski, G., Kalhori, A., Kondrich, A., Lai, D. Y. F., Lohila, A., Malhotra, A., Merbold, L., Mitra, B., Ng, A., Nilsson, M. B., Noormets, A., 1385 Peichl, M., Rey-Sanchez, A. C., Richardson, A. D., Runkle, B. R. K., Schäfer, K. V. R., Sonntag, O., Stuart-

- 1390 Haëntjens, E., Sturtevant, C., Ueyama, M., Valach, A. C., Vargas, R., Vourlitis, G. L., Ward, E. J., Wong, G. X., Zona, D., Alberto, M. C. R., Billesbach, D. P., Celis, G., Dolman, H., Friborg, T., Fuchs, K., Gogo, S., Gondwe, M. J., Goodrich, J. P., Gottschalk, P., Hörtnagl, L., Jacotot, A., Koebsch, F., Kasak, K., Maier, R., Morin, T. H., Nemitz, E., Oechel, W. C., Oikawa, P. Y., Ono, K., Sachs, T., Sakabe, A., Schuur, E. A., Shortt, R., Sullivan, R. C., Szutu, D. J., Tuittila, E.-S., Varlagin, A., Verfaillie, J. G., Wille, C., Windham-Myers, L., Poulter, B., and Jackson, R. B.: Gap-filling eddy covariance methane fluxes: Comparison of machine learning model predictions and uncertainties at FLUXNET-CH4 wetlands, *Agric. For. Meteorol.*, 308-309, 108528, <https://doi.org/10.1016/j.agrformet.2021.108528>, 2021.
- 1395 Iwata, H., Kosugi, Y., Ono, K., Mano, M., Sakabe, A., Miyata, A., and Takahashi, K.: Cross-validation of open-path and closed-path eddy-covariance techniques for observing methane fluxes, *Boundary Layer Meteorol.*, 151, 95–118, <https://doi.org/10.1007/s10546-013-9890-2>, 2014.
- Iwata, H., Ueyama, M., and Harazono, Y.: FLUXNET-CH4 US-Uaf University of Alaska, Fairbanks, <https://doi.org/10.18140/FLX/1669701>, 2020.
- 1400 Järveoja, J., Nilsson, M. B., Gažovič, M., Crill, P. M., and Peichl, M.: Partitioning of the net CO<sub>2</sub> exchange using an automated chamber system reveals plant phenology as key control of production and respiration fluxes in a boreal peatland, *Glob. Chang. Biol.*, 24, 3436–3451, <https://doi.org/10.1111/gcb.14292>, 2018.
- Jentzsch, K., van Delden, L., Fuchs, M., and Treat, C. C.: An expert survey on chamber measurement techniques and data handling procedures for methane fluxes, *Earth System Science Data*, 17, 2331–2372, <https://doi.org/10.5194/essd-17-2331-2025>, 2025.
- 1405 Juselius-Rajamäki, T., Piilo, S., Salminen-Paatero, S., Tuomaala, E., Virtanen, T., Korhola, A., Autio, A., Marttila, H., Ala-Aho, P., Lohila, A., and Väliiranta, M.: External and internal drivers behind the formation, vegetation succession, and carbon balance of a subarctic fen margin, *Biogeosciences*, 22, 3047–3071, <https://doi.org/10.5194/bg-22-3047-2025>, 2025.
- 1410 Knapp, A. K. and Yavitt, J. B.: Evaluation of a closed-chamber method for estimating methane emissions from aquatic plants, *Tellus B Chem. Phys. Meteorol.*, 44, 63–71, <https://doi.org/10.1034/j.1600-0889.1992.00006.x>, 1992.
- Knox, S. H., Matthes, J. H., Sturtevant, C., Oikawa, P. Y., Verfaillie, J., and Baldocchi, D.: Biophysical controls on interannual variability in ecosystem-scale CO<sub>2</sub> and CH<sub>4</sub> exchange in a California rice paddy: Interannual variability rice CH<sub>4</sub> fluxes, *J. Geophys. Res. Biogeosci.*, 121, 978–1001, <https://doi.org/10.1002/2015jg003247>, 2016.
- 1415 Knox, S. H., Jackson, R. B., Poulter, B., McNicol, G., Fluet-Chouinard, E., Zhang, Z., Hugelius, G., Bousquet, P., Canadell, J. G., Saunio, M., Papale, D., Chu, H., Keenan, T. F., Baldocchi, D., Torn, M. S., Mammarella, I., Trotta, C., Aurela, M., Bohrer, G., Campbell, D. I., Cescatti, A., Chamberlain, S., Chen, J., Chen, W., Dengel, S., Desai, A. R., Euskirchen, E., Friborg, T., Gasbarra, D., Goded, I., Goeckede, M., Heimann, M., Helbig, M., Hirano, T., Hollinger, D. Y., Iwata, H., Kang, M., Klatt, J., Krauss, K. W., Kutzbach, L., Lohila, A., Mitra, B., Morin, T. H., Nilsson, M. B., Niu, S., Noormets, A., Oechel, W. C., Peichl, M., Peltola, O., Reba, M. L., Richardson, A. D., Runkle, B. R. K., 1420 Ryu, Y., Sachs, T., Schäfer, K. V. R., Schmid, H. P., Shurpali, N., Sonnentag, O., Tang, A. C. I., Ueyama, M., Vargas, R., Vesala, T., Ward, E. J., Windham-Myers, L., Wohlfahrt, G., and Zona, D.: FLUXNET-CH<sub>4</sub> Synthesis Activity: Objectives, Observations, and Future Directions, *Bull. Am. Meteorol. Soc.*, 100, 2607–2632, <https://doi.org/10.1175/BAMS-D-18-0268.1>, 2019.
- 1425 Knox, S. H., Bansal, S., McNicol, G., Schafer, K., Sturtevant, C., Ueyama, M., Valach, A. C., Baldocchi, D., Delwiche, K., Desai, A. R., Euskirchen, E., Liu, J., Lohila, A., Malhotra, A., Melling, L., Riley, W., Runkle, B. R. K., Turner, J., Vargas, R., Zhu, Q., Alto, T., Fluet-Chouinard, E., Goeckede, M., Melton, J. R., Sonnentag, O., Vesala, T., Ward, E.,

- 1430 Zhang, Z., Feron, S., Ouyang, Z., Alekseychik, P., Aurela, M., Bohrer, G., Campbell, D. I., Chen, J., Chu, H., Dalmagro, H. J., Goodrich, J. P., Gottschalk, P., Hirano, T., Iwata, H., Jurasinski, G., Kang, M., Koebisch, F., Mammarella, I., Nilsson, M. B., Ono, K., Peichl, M., Peltola, O., Ryu, Y., Sachs, T., Sakabe, A., Sparks, J. P., Tuittila, E.-S., Vourlitis, G. L., Wong, G. X., Windham-Myers, L., Poulter, B., and Jackson, R. B.: Identifying dominant environmental predictors of freshwater wetland methane fluxes across diurnal to seasonal time scales, *Glob. Chang. Biol.*, 27, 3582–3604, <https://doi.org/10.1111/gcb.15661>, 2021.
- 1435 Koebisch, F., Jurasinski, G., Koch, M., Hofmann, J., and Glatzel, S.: Controls for multi-scale temporal variation in ecosystem methane exchange during the growing season of a permanently inundated fen, *Agric. For. Meteorol.*, 204, 94–105, <https://doi.org/10.1016/j.agrformet.2015.02.002>, 2015.
- Korkiakoski, M., Tuovinen, J.-P., Aurela, M., Koskinen, M., Minkkinen, K., Ojanen, P., Penttilä, T., Rainne, J., Laurila, T., and Lohila, A.: Methane exchange at the peatland forest floor – automatic chamber system exposes the dynamics of small fluxes, *Biogeosciences*, 14, 1947–1967, <https://doi.org/10.5194/bg-14-1947-2017>, 2017.
- 1440 Korrensalo, A., Männistö, E., Alekseychik, P., Mammarella, I., Rinne, J., Vesala, T., and Tuittila, E.-S.: Small spatial variability in methane emission measured from a wet patterned boreal bog, *Biogeosciences*, 15, 1749–1761, <https://doi.org/10.5194/bg-15-1749-2018>, 2018.
- 1445 Krauss, K. W., Holm, G. O., Perez, B. C., McWhorter, D. E., Cormier, N., Moss, R. F., Johnson, D. J., Neubauer, S. C., and Raynie, R. C.: Component greenhouse gas fluxes and radiative balance from two deltaic marshes in Louisiana: Pairing chamber techniques and eddy covariance, *Journal of Geophysical Research: Biogeosciences*, 121, 1503–1521, <https://doi.org/10.1002/2015JG003224>, 2016.
- Kroon, P. S., Hensen, A., Jonker, H. J. J., Zahniser, M. S., van 't Veen, W. H., and Vermeulen, A. T.: Suitability of quantum cascade laser spectroscopy for CH<sub>4</sub> and N<sub>2</sub>O eddy covariance flux measurements, *Biogeosciences*, 4, 715–728, <https://doi.org/10.5194/bg-4-715-2007>, 2007.
- 1450 Kroon, P. S., Hensen, A., Jonker, H. J. J., Ouwersloot, H. G., Vermeulen, A. T., and Bosveld, F. C.: Uncertainties in eddy covariance flux measurements assessed from CH<sub>4</sub> and N<sub>2</sub>O observations, *Agric. For. Meteorol.*, 150, 806–816, <https://doi.org/10.1016/j.agrformet.2009.08.008>, 2010.
- Kuhn, M. A., Varner, R. K., Bastviken, D., Crill, P., MacIntyre, S., Turetsky, M., Walter Anthony, K., McGuire, A. D., and Olefeldt, D.: BAWLD-CH<sub>4</sub>: a comprehensive dataset of methane fluxes from boreal and arctic ecosystems, *Earth System Science Data*, 13, 5151–5189, <https://doi.org/10.5194/essd-13-5151-2021>, 2021.
- 1455 Kutzbach, L., Wagner, D., and Pfeiffer, E.-M.: Effect of microrelief and vegetation on methane emission from wet polygonal tundra, Lena Delta, Northern Siberia, *Biogeochemistry*, 69, 341–362, <https://doi.org/10.1023/B:BIOG.0000031053.81520.db>, 2004.
- 1460 Lai, D. Y. F., Roulet, N. T., Humphreys, E. R., Moore, T. R., and Dalva, M.: The effect of atmospheric turbulence and chamber deployment period on autochamber CO<sub>2</sub> and CH<sub>4</sub> flux measurements in an ombrotrophic peatland, *Biogeosciences*, 9, 3305–3322, <https://doi.org/10.5194/bg-9-3305-2012>, 2012.
- Langensiepen, M., Kupisch, M., van Wijk, M. T., and Ewert, F.: Analyzing transient closed chamber effects on canopy gas exchange for optimizing flux calculation timing, *Agric. For. Meteorol.*, 164, 61–70, <https://doi.org/10.1016/j.agrformet.2012.05.006>, 2012.
- 1465 Lawrence, M. G.: The relationship between relative humidity and the dewpoint temperature in moist air: A simple conversion and applications, *Bull. Am. Meteorol. Soc.*, 86, 225–234, <https://doi.org/10.1175/bams-86-2-225>, 2005.

- Levy, P. E., Gray, A., Leeson, S. R., Gaiawyn, J., Kelly, M. P. C., Cooper, M. D. A., Dinsmore, K. J., Jones, S. K., and Sheppard, L. J.: Quantification of uncertainty in trace gas fluxes measured by the static chamber method, *Eur. J. Soil Sci.*, 62, 811–821, <https://doi.org/10.1111/j.1365-2389.2011.01403.x>, 2011.
- 1470 Livingston, G. P. and Hutchinson, G. L.: Enclosure-based measurement of trace gas exchange: applications and sources of error, in: *Methods in ecology: biogenic trace gas emissions from soil and water*, Blackwell Scientific Publications Inc., 14–51, 1995.
- Liu, X., Zhu, D., Zhan, W., Chen, H., Zhu, Q., Zhang, J., Wu, N., and He, Y.: Dominant influence of non-thawing periods on annual CO<sub>2</sub> emissions from Zoige peatlands: Five-year eddy covariance analysis, *Ecol. Indic.*, **129**, 107913, <https://doi.org/10.1016/j.ecolind.2021.107913>, 2021.
- 1475 Long, K. D., Flanagan, L. B., and Cai, T.: Diurnal and seasonal variation in methane emissions in a northern Canadian peatland measured by eddy covariance, *Glob. Chang. Biol.*, 16, 2420–2435, <https://doi.org/10.1111/j.1365-2486.2009.02083.x>, 2010.
- 1480 Marushchak, M. E., Friberg, T., Biasi, C., Herbst, M., Johansson, T., Kiepe, I., Liimatainen, M., Lind, S. E., Martikainen, P. J., Virtanen, T., Soegaard, H., and Shurpali, N. J.: Methane dynamics in the subarctic tundra: combining stable isotope analyses, plot- and ecosystem-scale flux measurements, *Biogeosciences*, 13, 597–608, <https://doi.org/10.5194/bg-13-597-2016>, 2016.
- 1485 McGuire, A. D., Christensen, T. R., Hayes, D., Heroult, A., Euskirchen, E., Kimball, J. S., Koven, C., Lafleur, P., Miller, P. A., Oechel, W., Peylin, P., Williams, M., and Yi, Y.: An assessment of the carbon balance of Arctic tundra: comparisons among observations, process models, and atmospheric inversions, *Biogeosciences*, 9, 3185–3204, <https://doi.org/10.5194/bg-9-3185-2012>, 2012.
- 1490 McNicol, G., Fluet-Chouinard, E., Ouyang, Z., Knox, S., Zhang, Z., Aalto, T., Bansal, S., Chang, K.-Y., Chen, M., Delwiche, K., Feron, S., Goeckede, M., Liu, J., Malhotra, A., Melton, J. R., Riley, W., Vargas, R., Yuan, K., Ying, Q., Zhu, Q., Alekseychik, P., Aurela, M., Billesbach, D. P., Campbell, D. I., Chen, J., Chu, H., Desai, A. R., Euskirchen, E., Goodrich, J., Griffis, T., Helbig, M., Hirano, T., Iwata, H., Jurasinski, G., King, J., Koebsch, F., Kolka, R., Krauss, K., Lohila, A., Mammarella, I., Nilson, M., Noormets, A., Oechel, W., Peichl, M., Sachs, T., Sakabe, A., Schulze, C., Sonnentag, O., Sullivan, R. C., Tuittila, E.-S., Ueyama, M., Vesala, T., Ward, E., Wille, C., Wong, G. X., Zona, D., Windham-Myers, L., Poulter, B., and Jackson, R. B.: Upscaling wetland methane emissions from the FLUXNET-CH<sub>4</sub> eddy covariance network (UpCH<sub>4</sub> v1.0): Model development, network assessment, and budget comparison, *AGU Adv.*, 4, <https://doi.org/10.1029/2023av000956>, 2023.
- 1495 Meijide, A., Manca, G., Goded, I., Magliulo, V., di Tommasi, P., Seufert, G., and Cescatti, A.: Seasonal trends and environmental controls of methane emissions in a rice paddy field in Northern Italy, *Biogeosci. Discuss.*, 8, 8999–9032, <https://doi.org/10.5194/bgd-8-8999-2011>, 2011.
- Metzger, S.: Surface-atmosphere exchange in a box: Making the control volume a suitable representation for in-situ observations, *Agric. For. Meteorol.*, 255, 68–80, <https://doi.org/10.1016/j.agrformet.2017.08.037>, 2018.
- 1500 Montaldo, N. and Oren, R.: The way the wind blows matters to ecosystem water use efficiency, *Agric. For. Meteorol.*, 217, 1–9, <https://doi.org/10.1016/j.agrformet.2015.11.002>, 2016.
- Morin, T. H.: Advances in the eddy covariance approach to CH<sub>4</sub> monitoring over two and a half decades, *J. Geophys. Res. Biogeosci.*, 124, 453–460, <https://doi.org/10.1029/2018jg004796>, 2019.
- Morin, T. H., Bohrer, G., Frasson, R. P. d., Naor-Azreli, L., Mesi, S., Stefanik, K. C., and Schäfer, K. V. R.: Environmental

- 1505 drivers of methane fluxes from an urban temperate wetland park, *Journal of Geophysical Research: Biogeosciences*, 119, 2188–2208, <https://doi.org/10.1002/2014JG002750>, 2014.
- Morin, T. H., Bohrer, G., Stefanik, K. C., Rey-Sanchez, A. C., Matheny, A. M., and Mitsch, W. J.: Combining eddy-covariance and chamber measurements to determine the methane budget from a small, heterogeneous urban floodplain wetland park, *Agric. For. Meteorol.*, 237–238, 160–170, <https://doi.org/10.1016/j.agrformet.2017.01.022>, 2017.
- 1510 Männistö, E., Korrensalo, A., Alekseychik, P., Mammarella, I., Peltola, O., Vesala, T., and Tuittila, E. S.: Multi-year methane ebullition measurements from water and bare peat surfaces of a patterned boreal bog, *Biogeosciences*, 16, 2409–2421, <https://doi.org/10.5194/bg-16-2409-2019>, 2019.
- Määttä, T., Desai, A., Ueyama, M., Vargas, R., Ward, E. J., Zhang, Z., Bohrer, G., Delwiche, K., Fluet-Chouinard, E., Järveoja, J., Knox, S., Melling, L., Nilsson, M. B., Peichl, M., Tang, A. C. I., Tuittila, E.-S., Wang, J., Bansal, S., Feron, S., Helbig, M., Korrensalo, A., Krauss, K. W., McNicol, G., Niu, S., Ouyang, Z., Savage, K., Sonnentag, O., Jackson, R., and Malhotra, A.: Cross-site comparison of ecosystem- and plot-scale methane fluxes from wetlands and uplands (Version v1), Zenodo [data set], <https://doi.org/10.5281/zenodo.17312404>, 2025.
- 1515 Nadeau, D. F., Rousseau, A. N., Coursolle, C., Margolis, H. A., and Parlange, M. B.: Summer methane fluxes from a boreal bog in northern Quebec, Canada, using eddy covariance measurements, *Atmos. Environ.* (1994), 81, 464–474, <https://doi.org/10.1016/j.atmosenv.2013.09.044>, 2013.
- 1520 Nakano, T.: A comparison of regression methods for estimating soil–atmosphere diffusion gas fluxes by a closed-chamber technique, *Soil Biol. Biochem.*, 36, 107–113, <https://doi.org/10.1016/j.soilbio.2003.07.005>, 2004.
- van der Nat, F.-F. W. A., Middelburg\*, J. J., Van Meteren, D., and Wielemakers, A.: Diel methane emission patterns from *Scirpus lacustris* and *Phragmites australis*, *Biogeochemistry*, 41, 1–22, <https://doi.org/10.1023/a:1005933100905>, 1998.
- 1525 Nilsson, M. and Peichl, M.: FLUXNET-CH4 SE-Deg Degero, <https://doi.org/10.18140/FLX/1669659>, 2020.
- Niu, S. and Chen, W.: FLUXNET-CH4 CN-Hgu Hongyuan, <https://doi.org/10.18140/FLX/1669632>, 2020.
- Niu, S., Luo, Y., Fei, S., Montagnani, L., Bohrer, G., Janssens, I. A., Gielen, B., Rambal, S., Moors, E., and Matteucci, G.: Seasonal hysteresis of net ecosystem exchange in response to temperature change: patterns and causes: SEASONAL HYSTERESIS OF NET ECOSYSTEM EXCHANGE, *Glob. Chang. Biol.*, 17, 3102–3114, <https://doi.org/10.1111/j.1365-2486.2011.02459.x>, 2011.
- 1530 Oikawa, P. Y., Sihi, D., Forbrich, I., Fluet-Chouinard, E., Najarro, M., Thomas, O., Shahan, J., Arias-Ortiz, A., Russell, S., Knox, S. H., McNicol, G., Wolfe, J., Windham-Myers, L., Stuart-Haentjens, E., Bridgham, S. D., Needelman, B., Vargas, R., Schäfer, K., Ward, E. J., Megonigal, P., and Holmquist, J.: A new coupled biogeochemical modeling approach provides accurate predictions of methane and carbon dioxide fluxes across diverse tidal wetlands, *J. Geophys. Res. Biogeosci.*, 129, <https://doi.org/10.1029/2023jg007943>, 2024.
- 1535 Parmentier, F. J. W., van Huissteden, J., van der Molen, M. K., Schaepman-Strub, G., Karsanaev, S. A., Maximov, T. C., and Dolman, A. J.: Spatial and temporal dynamics in eddy covariance observations of methane fluxes at a tundra site in northeastern Siberia, *J. Geophys. Res.*, 116, <https://doi.org/10.1029/2010jg001637>, 2011.
- 1540 Peltola, O., Hensen, A., Helfter, C., Belevi Marchesini, L., Bosveld, F. C., van den Bulk, W. C. M., Elbers, J. A., Haapanala, S., Holst, J., Laurila, T., Lindroth, A., Nemitz, E., Röckmann, T., Vermeulen, A. T., and Mammarella, I.: Evaluating the performance of commonly used gas analysers for methane eddy covariance flux measurements: the InGOS inter-

comparison field experiment, *Biogeosciences*, 11, 3163–3186, <https://doi.org/10.5194/bg-11-3163-2014>, 2014.

- 1545 Peltola, O., Vesala, T., Gao, Y., Rätty, O., Alekseychik, P., Aurela, M., Chojnicki, B., Desai, A. R., Dolman, A. J., Euskirchen, E. S., Friborg, T., Göckede, M., Helbig, M., Humphreys, E., Jackson, R. B., Jocher, G., Joos, F., Klatt, J., Knox, S. H., Kowalska, N., Kutzbach, L., Lienert, S., Lohila, A., Mammarella, I., Nadeau, D. F., Nilsson, M. B., Oechel, W. C., Peichl, M., Pypker, T., Quinton, W., Rinne, J., Sachs, T., Samson, M., Schmid, H. P., Sonnentag, O., Wille, C., Zona, D., and Aalto, T.: Monthly gridded data product of northern wetland methane emissions based on upscaling eddy covariance observations, *Earth Syst. Sci. Data*, 11, 1263–1289, <https://doi.org/10.5194/essd-11-1263-2019>, 2019.
- Peterson, R.: Finding optimal normalizing transformations via bestNormalize, *R J.*, 13, 310, <https://doi.org/10.32614/rj-2021-041>, 2021.
- 1555 Phillips, C. L., Bond-Lamberty, B., Desai, A. R., Lavoie, M., Risk, D., Tang, J., Todd-Brown, K., and Vargas, R.: The value of soil respiration measurements for interpreting and modeling terrestrial carbon cycling, *Plant Soil*, 413, 1–25, <https://doi.org/10.1007/s11104-016-3084-x>, 2017.
- Pihlatie, M. K., Christiansen, J. R., Aaltonen, H., Korhonen, J. F. J., Nordbo, A., Rasilo, T., Benanti, G., Giebels, M., Helmy, M., Sheehy, J., Jones, S., Juszczak, R., Klefoth, R., Lobo-do-Vale, R., Rosa, A. P., Schreiber, P., Serça, D., Vicca, S., Wolf, B., and Pumpanen, J.: Comparison of static chambers to measure CH<sub>4</sub> emissions from soils, *Agric. For. Meteorol.*, 171–172, 124–136, <https://doi.org/10.1016/j.agrformet.2012.11.008>, 2013.
- 1560 Pinheiro J, Bates D, R Core Team: nlme: Linear and Nonlinear Mixed Effects Models, <https://doi.org/10.32614/CRAN.package.nlme>, 2023.
- Pinheiro, J. C. and Bates, D. M.: *Mixed-Effects Models in S and S-PLUS*, Springer, New York, <https://doi.org/10.1007/b98882>, 2000.
- 1565 Pollet, T. V., Stulp, G., Henzi, S. P., and Barrett, L.: Taking the aggravation out of data aggregation: A conceptual guide to dealing with statistical issues related to the pooling of individual-level observational data, *Am. J. Primatol.*, 77, 727–740, <https://doi.org/10.1002/ajp.22405>, 2015.
- Pumpanen, J., Kolari, P., Ilvesniemi, H., Minkkinen, K., Vesala, T., Niinistö, S., Lohila, A., Larmola, T., Morero, M., Pihlatie, M., and Janssens, I.: Comparison of different chamber techniques for measuring soil CO<sub>2</sub> efflux, *Agric. For. Meteorol.*, 123, 159–176, <https://doi.org/10.1016/j.agrformet.2003.12.001>, 2004.
- 1570 Räsänen, A., Manninen, T., Korkiakoski, M., Lohila, A., and Virtanen, T.: Predicting catchment-scale methane fluxes with multi-source remote sensing, *Landsc. Ecol.*, 36, 1177–1195, <https://doi.org/10.1007/s10980-021-01194-x>, 2021.
- R Core Team: *R: A Language and Environment for Statistical Computing*. R Foundation for Statistical Computing, Vienna, Austria, <https://www.R-project.org>, 2024.
- 1575 Rebmann, C., Göckede, M., Foken, T., Aubinet, M., Aurela, M., Berbigier, P., Bernhofer, C., Buchmann, N., Carrara, A., Cescatti, A., Ceulemans, R., Clement, R., Elbers, J. A., Granier, A., Grünwald, T., Guyon, D., Havránková, K., Heinesch, B., Knohl, A., Laurila, T., Longdoz, B., Marcolla, B., Markkanen, T., Miglietta, F., Moncrieff, J., Montagnani, L., Moors, E., Nardino, M., Ourcival, J.-M., Rambal, S., Rannik, Ü., Rotenberg, E., Sedlak, P., Unterhuber, G., Vesala, T., and Yakir, D.: Quality analysis applied on eddy covariance measurements at complex forest sites using footprint modelling, *Theor. Appl. Climatol.*, 80, 121–141, <https://doi.org/10.1007/s00704-004-0095-y>, 2005.
- 1580

- Rey-Sanchez, C., Morin, T. H., Stefanik, K. C., Wrighton, K., and Bohrer, G.: Determining total emissions and environmental drivers of methane flux in a Lake Erie estuarine marsh, *Ecol. Eng.*, 114, 7–15, <https://doi.org/10.1016/j.ecoleng.2017.06.042>, 2018.
- 1585 Rey-Sanchez, C., Arias-Ortiz, A., Kasak, K., Chu, H., Szutu, D., Verfaillie, J., and Baldocchi, D.: Detecting hot spots of methane flux using footprint-weighted flux maps, *J. Geophys. Res. Biogeosci.*, 127, e2022JG006977, <https://doi.org/10.1029/2022JG006977>, 2022.
- 1590 Rey-Sanchez, C., Arias-Ortiz, A., Kasak, K., Shortt, R., Szutu, D., Verfaillie, J., Lorenson, T., Liira, M., Somelar, P., Espenberg, M., and Baldocchi, D.: Explaining hot spots of methane flux in a restored wetland: the role of water level, soil disturbance, and methanotrophy, *Environ. Res. Lett.*, 20, 074064, <https://doi.org/10.1088/1748-9326/ade45b>, 2025.
- Richardson, A. D. and Hollinger, D.: FLUXNET-CH4 US-Ho1 Howland Forest (main tower), <https://doi.org/10.18140/FLX/1669675>, 2020.
- 1595 Richardson, A. D., Hollinger, D. Y., Burba, G. G., Davis, K. J., Flanagan, L. B., Katul, G. G., William Munger, J., Ricciuto, D. M., Stoy, P. C., Suyker, A. E., Verma, S. B., and Wofsy, S. C.: A multi-site analysis of random error in tower-based measurements of carbon and energy fluxes, *Agric. For. Meteorol.*, 136, 1–18, <https://doi.org/10.1016/j.agrformet.2006.01.007>, 2006.
- 1600 Richardson, A. D., Mahecha, M. D., Falge, E., Kattge, J., Moffat, A. M., Papale, D., Reichstein, M., Stauch, V. J., Braswell, B. H., Churkina, G., Kruijt, B., and Hollinger, D. Y.: Statistical properties of random CO2 flux measurement uncertainty inferred from model residuals, *Agric. For. Meteorol.*, 148, 38–50, <https://doi.org/10.1016/j.agrformet.2007.09.001>, 2008.
- Richardson, A. D., Hollinger, D. Y., Shoemaker, J. K., Hughes, H., Savage, K., and Davidson, E. A.: Six years of ecosystem-atmosphere greenhouse gas fluxes measured in a sub-boreal forest, *Sci. Data*, 6, 117, <https://doi.org/10.1038/s41597-019-0119-1>, 2019.
- 1605 Rinne, J., Riutta, T., Pihlatie, M., Aurela, M., Haapanala, S., Tuovinen, J.-P., Tuittila, E.-S., and Vesala, T.: Annual cycle of methane emission from a boreal fen measured by the eddy covariance technique, *Tellus B Chem. Phys. Meteorol.*, 59, <https://doi.org/10.3402/tellusb.v59i3.17009>, 2007.
- Riutta, T., Laine, J., Aurela, M., Rinne, J., Vesala, T., Laurila, T., Haapanala, S., Pihlatie, M., and Tuittila, E.-S.: Spatial variation in plant community functions regulates carbon gas dynamics in a boreal fen ecosystem, *Tellus B Chem. Phys. Meteorol.*, 59, 838, <https://doi.org/10.1111/j.1600-0889.2007.00302.x>, 2007.
- 1610 Rößger, N., Wille, C., Holl, D., Göckede, M., and Kutzbach, L.: Scaling and balancing carbon dioxide fluxes in a heterogeneous tundra ecosystem of the Lena River Delta, *Biogeosciences*, 16, 2591–2615, <https://doi.org/10.5194/bg-16-2591-2019>, 2019.
- Sachs, T., Wille, C., Boike, J., and Kutzbach, L.: Environmental controls on ecosystem-scale CH4 emission from polygonal tundra in the Lena River Delta, Siberia, *J. Geophys. Res.*, 113, <https://doi.org/10.1029/2007jg000505>, 2008.
- 1615 Saunois, M., Martinez, A., Poulter, B., Zhang, Z., Raymond, P., Regnier, P., Canadell, J. G., Jackson, R. B., Patra, P. K., Bousquet, P., Ciais, P., Dlugokencky, E. J., Lan, X., Allen, G. H., Bastviken, D., Beerling, D. J., Belikov, D. A., Blake, D. R., Castaldi, S., Crippa, M., Deemer, B. R., Dennison, F., Etiope, G., Gedney, N., Höglund-Isaksson, L., Holgerson, M. A., Hopcroft, P. O., Hugelius, G., Ito, A., Jain, A. K., Janardanan, R., Johnson, M. S., Kleinen, T., Krummel, P., Lauerwald, R., Li, T., Liu, X., McDonald, K. C., Melton, J. R., Mühle, J., Müller, J., Murguia-Flores,

- 1620 F., Niwa, Y., Noce, S., Pan, S., Parker, R. J., Peng, C., Ramonet, M., Riley, W. J., Rocher-Ros, G., Rosentreter, J. A., Sasakawa, M., Segers, A., Smith, S. J., Stanley, E. H., Thanwerdas, J., Tian, H., Tsuruta, A., Tubiello, F. N., Weber, T. S., van der Werf, G., Worthy, D. E., Xi, Y., Yoshida, Y., Zhang, W., Zheng, B., Zhu, Q., Zhu, Q., and Zhuang, Q.: Global Methane Budget 2000–2020, *Earth System Science Data Discussions*, <https://doi.org/10.5194/essd-2024-115>, 2024.
- 1625 Schrier-Uijl, A. P., Kroon, P. S., Hensen, A., Leffelaar, P. A., Berendse, F., and Veenendaal, E. M.: Comparison of chamber and eddy covariance-based CO<sub>2</sub> and CH<sub>4</sub> emission estimates in a heterogeneous grass ecosystem on peat, *Agric. For. Meteorol.*, **150**, 825–831, <https://doi.org/10.1016/j.agrformet.2009.11.007>, 2010.
- Sha, C., Mitsch, W. J., Mander, Ü., Lu, J., Batson, J., Zhang, L., and He, W.: Methane emissions from freshwater riverine wetlands, *Ecol. Eng.*, **37**, 16–24, <https://doi.org/10.1016/j.ecoleng.2010.07.022>, 2011.
- 1630 Smeets, C. J. P. P., Holzinger, R., Vigano, I., Goldstein, A. H., and Röckmann, T.: Eddy covariance methane measurements at a Ponderosa pine plantation in California, *Atmos. Chem. Phys.*, **9**, 8365–8375, <https://doi.org/10.5194/acp-9-8365-2009>, 2009.
- Stewart, G. A., Sharp, S. J., Taylor, A. K., Williams, M. R., and Palmer, M. A.: High spatial variability in wetland methane fluxes is tied to vegetation patch types, *Biogeochemistry*, <https://doi.org/10.1007/s10533-024-01188-2>, 2024.
- 1635 Subke, J.-A., Kutzbach, L., and Risk, D.: Soil chamber measurements, in: *Springer Handbook of Atmospheric Measurements*, Springer International Publishing, Cham, 1603–1624, [https://doi.org/10.1007/978-3-030-52171-4\\_60](https://doi.org/10.1007/978-3-030-52171-4_60), 2021.
- Tokida, T., Miyazaki, T., Mizoguchi, M., Nagata, O., Takakai, F., Kagemoto, A., and Hatano, R.: Falling atmospheric pressure as a trigger for methane ebullition from peatland, *Global Biogeochem. Cycles*, **21**, <https://doi.org/10.1029/2006GB002790>, 2007.
- 1640 Treat, C. C., Bloom, A. A., and Marushchak, M. E.: Nongrowing season methane emissions – a significant component of annual emissions across northern ecosystems, *Glob. Change Biol.*, **24**, 3331–3343, <https://doi.org/10.1111/gcb.14137>, 2018.
- Tuovinen, J.-P., Aurela, M., Hatakka, J., Räsänen, A., Virtanen, T., Mikola, J., Ivakhov, V., Kondratyev, V., and Laurila, T.: Interpreting eddy covariance data from heterogeneous Siberian tundra: land-cover-specific methane fluxes and spatial representativeness, *Biogeosciences*, **16**, 255–274, <https://doi.org/10.5194/bg-16-255-2019>, 2019.
- 1645 Turetsky, M. R., Kotowska, A., Bubier, J., Dise, N. B., Crill, P., Hornibrook, E. R. C., Minkinen, K., Moore, T. R., Myers-Smith, I. H., Nykänen, H., Olefeldt, D., Rinne, J., Saarnio, S., Shurpali, N., Tuittila, E.-S., Waddington, J. M., White, J. R., Wickland, K. P., and Wilmking, M.: A synthesis of methane emissions from 71 northern, temperate, and subtropical wetlands, *Glob. Chang. Biol.*, **20**, 2183–2197, <https://doi.org/10.1111/gcb.12580>, 2014.
- 1650 Ueyama, M., Iwata, H., and Harazono, Y.: CO<sub>2</sub> and CH<sub>4</sub> fluxes data based on an automated-closed chamber system for a black spruce forest on permafrost in Fairbanks, Alaska, <https://doi.org/10.17592/001.2021093001>, 2022.
- Ueyama, M., Iwata, H., Endo, R., and Harazono, Y.: Methane and carbon dioxide emissions from the forest floor of a black spruce forest on permafrost in interior Alaska, *Polar Sci.*, **35**, 100921, <https://doi.org/10.1016/j.polar.2022.100921>, 2023a.
- 1655 Ueyama, M., Knox, S. H., Delwiche, K. B., Bansal, S., Riley, W. J., Baldocchi, D., Hirano, T., McNicol, G., Schafer, K., Windham-Myers, L., Poulter, B., Jackson, R. B., Chang, K.-Y., Chen, J., Chu, H., Desai, A. R., Gogo, S., Iwata, H., Kang, M., Mammarella, I., Pechl, M., Sonnentag, O., Tuittila, E.-S., Ryu, Y., Euskirchen, E. S., Göckede, M., Jacotot,

- 1660 A., Nilsson, M. B., and Sachs, T.: Modeled production, oxidation, and transport processes of wetland methane emissions in temperate, boreal, and Arctic regions, *Glob. Chang. Biol.*, 29, 2313–2334, <https://doi.org/10.1111/gcb.16594>, 2023b.
- Vargas, R. and Le, V. H.: The paradox of assessing greenhouse gases from soils for nature-based solutions, *Biogeosciences*, 20, 15–26, <https://doi.org/10.5194/bg-20-15-2023>, 2023.
- Vázquez-Lule, A. and Vargas, R.: Biophysical drivers of net ecosystem and methane exchange across phenological phases in a tidal salt marsh, *Agric. For. Meteorol.*, 300, 108309, <https://doi.org/10.1016/j.agrformet.2020.108309>, 2021.
- 1665 Venterea, R. T., Spokas, K. A., and Baker, J. M.: Accuracy and precision analysis of chamber-based nitrous oxide gas flux estimates, *Soil Sci. Soc. Am. J.*, 73, 1087–1093, <https://doi.org/10.2136/sssaj2008.0307>, 2009.
- Vesala, T., Kljun, N., Rannik, U., Rinne, J., Sogachev, A., Markkanen, T., Sabelfeld, K., Foken, T., and Leclerc, M. Y.: Flux and concentration footprint modelling: state of the art, *Environ. Pollut.*, 152, 653–666, <https://doi.org/10.1016/j.envpol.2007.06.070>, 2008.
- 1670 Vesala, T., Tuittila, E.-S., Mammarella, I., and Alekseychik, P.: FLUXNET-CH4 FI-Si2 Siikaneva-2 Bog, <https://doi.org/10.18140/FLX/1669639>, 2020.
- Villa, J. A., Ju, Y., Stephen, T., Rey-Sanchez, C., Wrighton, K. C., and Bohrer, G.: Plant-mediated methane transport in emergent and floating-leaved species of a temperate freshwater mineral-soil wetland, *Limnol. Oceanogr.*, 65, 1635–1650, 2020.
- 1675 Villa, J. A., Ju, Y., Yazbeck, T., Waldo, S., Wrighton, K. C., and Bohrer, G.: Ebullition dominates methane fluxes from the water surface across different ecohydrological patches in a temperate freshwater marsh at the end of the growing season, *Sci. Total Environ.*, 767, 144498, <https://doi.org/10.1016/j.scitotenv.2020.144498>, 2021.
- 1680 Virkkala, A.-M., Virtanen, T., Lehtonen, A., Rinne, J., and Luoto, M.: The current state of CO<sub>2</sub> flux chamber studies in the Arctic tundra: A review, *Progress in Physical Geography: Earth and Environment*, 42, 162–184, <https://doi.org/10.1177/0309133317745784>, 2018.
- 1685 Voigt, C., Virkkala, A.-M., Hould Gosselin, G., Bennett, K. A., Black, T. A., Detto, M., Chevrier-Dion, C., Guggenberger, G., Hashmi, W., Kohl, L., Kou, D., Marquis, C., Marsh, P., Marushchak, M. E., Nesic, Z., Nykänen, H., Saarela, T., Sauheitl, L., Walker, B., Weiss, N., Wilcox, E. J., and Sonntag, O.: Arctic soil methane sink increases with drier conditions and higher ecosystem respiration, *Nat. Clim. Chang.*, 13, 1095–1104, <https://doi.org/10.1038/s41558-023-01785-3>, 2023.
- Vroom, R. J. E., van den Berg, M., Pangala, S. R., van der Scheer, O. E., and Sorrell, B. K.: Physiological processes affecting methane transport by wetland vegetation – A review, *Aquat. Bot.*, 182, 103547, <https://doi.org/10.1016/j.aquabot.2022.103547>, 2022.
- 1690 Waddington, J. M. and Roulet, N. T.: Carbon balance of a boreal patterned peatland, *Glob. Change Biol.*, 6, 87–97, <https://doi.org/10.1046/j.1365-2486.2000.00283.x>, 2000.
- Wang, J., Luo, Y., Quan, Q., Ma, F., Tian, D., Chen, W., Wang, S., Yang, L., Meng, C., and Niu, S.: Effects of warming and clipping on CH<sub>4</sub> and N<sub>2</sub>O fluxes in an alpine meadow, *Agric. For. Meteorol.*, 297, 108278, <https://doi.org/10.1016/j.agrformet.2020.108278>, 2021.
- Wang, J. M., Murphy, J. G., Geddes, J. A., Winsborough, C. L., Basiliko, N., and Thomas, S. C.: Methane fluxes measured by

- 1695 eddy covariance and static chamber techniques at a temperate forest in central Ontario, Canada, *Biogeosciences*, 10, 4371–4382, <https://doi.org/10.5194/bg-10-4371-2013>, 2013.
- Wang, P., Wang, J., Elberling, B., Yang, L., Chen, W., Song, L., Yan, Y., Wang, S., Pan, J., He, Y., and Niu, S.: Increased annual methane uptake driven by warmer winters in an alpine meadow, *Glob. Chang. Biol.*, 28, 3246–3259, <https://doi.org/10.1111/gcb.16120>, 2022.
- 1700 Whiting, G. J. and Chanton, J. P.: Control of the diurnal pattern of methane emission from emergent aquatic macrophytes by gas transport mechanisms, *Aquat. Bot.*, 54, 237–253, [https://doi.org/10.1016/0304-3770\(96\)01048-0](https://doi.org/10.1016/0304-3770(96)01048-0), 1996.
- Wille, C., Kutzbach, L., Sachs, T., Wagner, D., and Pfeiffer, E.-M.: Methane emission from Siberian arctic polygonal tundra: eddy covariance measurements and modeling: methane emission from Siberian arctic tundra. *Glob. Chang. Biol.*, 14, 1395–1408, <https://doi.org/10.1111/j.1365-2486.2008.01586.x>, 2008.
- 1705 Xu, K., Metzger, S., and Desai, A. R.: Surface-atmosphere exchange in a box: Space-time resolved storage and net vertical fluxes from tower-based eddy covariance, *Agric. For. Meteorol.*, 255, 81–91, <https://doi.org/10.1016/j.agrformet.2017.10.011>, 2018.
- Yeo, I. and Johnson, R. A.: A new family of power transformations to improve normality or symmetry, *Biometrika*, 87, 954–959, <https://doi.org/10.1093/BIOMET/87.4.954>, 2000.
- 1710 Yuan, K., Li, F., McNicol, G., Chen, M., Hoyt, A., Knox, S., Riley, W. J., Jackson, R., and Zhu, Q.: Boreal-Arctic wetland methane emissions modulated by warming and vegetation activity, *Nat. Clim. Chang.*, 14, 282–288, <https://doi.org/10.1038/s41558-024-01933-3>, 2024.
- Yu, L., Wang, H., Wang, G., Song, W., Huang, Y., Li, S.-G., Liang, N., Tang, Y., and He, J.-S.: A comparison of methane emission measurements using Eddy Covariance and manual and automated chamber-based techniques in Tibetan Plateau alpine wetland, *Environ. Pollut.*, 181, 81–90, <https://doi.org/10.1016/j.envpol.2013.06.018>, 2013.
- 1715 Zhang, Y., Sachs, T., Li, C., and Boike, J.: Upscaling methane fluxes from closed chambers to eddy covariance based on a permafrost biogeochemistry integrated model, *Glob. Chang. Biol.*, 18, 1428–1440, <https://doi.org/10.1111/j.1365-2486.2011.02587.x>, 2012.
- Zhao, K., Ma, B., Xu, Y., Stirling, E., and Xu, J.: Light exposure mediates circadian rhythms of rhizosphere microbial communities, *ISME J.*, 15, 2655–2664, <https://doi.org/10.1038/s41396-021-00957-3>, 2021.
- 1720 Zhu, Q., Yuan, K., Li, F., Riley, W. J., Hoyt, A., Jackson, R., McNicol, G., Chen, M., Knox, S. H., Briner, O., Beerling, D., Gedney, N., Hopcroft, P. O., Ito, A., Jain, A. K., Jensen, K., Kleinen, T., Li, T., Liu, X., McDonald, K. C., Melton, J. R., Miller, P. A., Müller, J., Peng, C., Poulter, B., Qin, Z., Peng, S., Tian, H., Xu, X., Yao, Y., Xi, Y., Zhang, Z., Zhang, W., Zhu, Q., and Zhuang, Q.: Critical needs to close monitoring gaps in pan-tropical wetland CH<sub>4</sub> emissions, *Environ. Res. Lett.*, 19, 114046, <https://doi.org/10.1088/1748-9326/ad8019>, 2024.
- 1725